

**CHEMISTRY OF CYCLOPENTADIENYLCHROMIUM
COMPLEXES CONTAINING C-, N- AND S- ORGANIC
LIGANDS**

**NG WEE LIN, VICTOR
(B. Sc. (Hons.), NUS)**

NATIONAL UNIVERSITY OF SINGAPORE

2004

**CHEMISTRY OF CYCLOPENTADIENYLCHROMIUM
COMPLEXES CONTAINING C-, N- AND S- ORGANIC
LIGANDS**

**NG WEE LIN, VICTOR
(B. Sc. (Hons.), NUS)**

**A THESIS SUBMITTED FOR THE DEGREE OF MASTER
OF SCIENCE
DEPARTMENT OF CHEMISTRY
NATIONAL UNIVERSITY OF SINGAPORE
2004**

Contents

Acknowledgements	v
Abstract.....	vi
Chart 1. Compounds encountered in this thesis.....	viii
List of abbreviations	x
List of figures	xi
List of tables.....	xii

Chapter 1. Introduction

1.1 Chemistry of the tricarbonylcyclopentadienyl chromium dimer.....	1
1.2 2,5-Dimercapto-1,3,4-thiadiazolate complexes.....	14
1.3 Tetrazole complexes.....	21
1.4 2-Mercaptopyridine complexes.....	31
1.5 Cyclopentadienylchromium(III) complexes.....	39
1.6 Objectives.....	43

Chapter 2. Results and discussion

2.1 The reaction of $[\text{CpCr}(\text{CO})_3]_2$ with 2,5-dimercapto-1,3,4-thiadiazole (DMcTH ₂).....	44
2.1.1 Products and reaction pathway.....	44
2.1.2 Crystallographic studies.....	47
2.1.3 Conclusion.....	49
2.2 The reaction of $[\text{CpCr}(\text{CO})_3]_2$ with 5,5'-dithiobis(1-phenyl-1H-tetrazole) (STz) ₂	50
2.2.1 Products and reaction pathways.....	50
2.2.2 Mechanistic Considerations.....	52
2.2.3 Spectral features.....	54

2.2.4	Crystallographic studies.....	55
2.2.5	Conclusion.....	59
2.3	Reactions of $\text{CpCr}(\text{CO})_3(\eta^1\text{-STz})$ (4).....	60
2.3.1	Reactions with methylating agents.....	60
2.3.1.1	Products and reaction pathways.....	61
2.3.1.2	Product Characterization.....	64
2.3.1.2	Conclusion.....	69
2.3.2	Reaction with hydrochloric acid.....	69
2.3.2.1	Products and reaction pathways.....	69
2.3.2.2	Conclusion.....	71
2.3.3	Reaction with iodine (oxidant).....	71
2.3.3.1	Products and reaction pathways.....	72
2.3.3.2	Conclusion.....	75
2.3.4	Reaction with iron pentacarbonyl.....	75
2.4	The reaction of $[\text{CpFe}(\text{CO})_2]_2$ with 5,5'-dithiobis(1-phenyl-1H-tetrazole) (STz) ₂	78
2.4.1	Products and reaction pathways.....	78
2.4.2	Crystallographic studies.....	78
2.4.3	Conclusion.....	80
2.5	The reaction of $[\text{CpCr}(\text{CO})_3]_2$ with 2,2'-dithiodipyridine (SPy) ₂	82
2.5.1	Products and reaction pathways.....	82
2.5.2	Crystallographic studies.....	84
2.5.3	Conclusion.....	85
2.6	Reactions of $\text{CpCr}(\text{CO})_2(\eta^2\text{-SPy})$ (16)	86
2.6.1	Reaction With HX (X = F, Cl, I).....	86
2.6.1.1	Products and reaction pathways.....	87
2.6.1.2	Product Characterization.....	89
2.6.1.2	Conclusion.....	91
2.6.2	Reaction with iodine (oxidant).....	92
2.6.2.1	Products and reaction pathways.....	92

2.6.2.2 Conclusion	93
2.6.3 With hexafluorophosphoric acid and triflic acid.....	93
2.6.3.1 Products and reaction pathways.....	99
2.6.3.1 Spectra characteristics	94
2.6.3.3 Conclusion	95
2.6.4 Reaction with dicyclopentadienylzirconium dichloride.....	95
2.6.4.1 Products and reaction pathways.....	96
2.6.4.2 Properties and spectra characteristics	97
2.6.4.3 Conclusion	98
Chapter 3. Experimental	
3.1 General procedures.....	99
3.2 The reaction of $[\text{CpCr}(\text{CO})_3]_2$ with 2,5-dimercapto-1,3,4-thiadiazole (DMcTH ₂).....	101
3.2.1 At ambient temperature.....	101
3.2.2 At 90 °C.....	102
3.2.3 NMR tube reactions.....	102
3.2.4 Crystal structure analyses.....	103
3.3 The reaction of $[\text{CpCr}(\text{CO})_3]_2$ with 5,5'-dithiobis(1-phenyl-1H-tetrazole) (STz) ₂	104
3.3.1 At -30 °C.....	104
3.3.2 At ambient temperature.....	104
3.3.3 Cothermolysis of $\text{CpCr}(\text{CO})_3(\text{SCN}_4\text{Ph})$ with $[\text{CpCr}(\text{CO})_3]_2$ at 90 °C....	105
3.3.4 Crystal structure analyses.....	107
3.4 Reactions of $\text{CpCr}(\text{CO})_3(\eta^1\text{-STz})$ (4).....	108
3.4.1 Reaction with trimethyloxonium tetrafluoroborate.....	108
3.4.2 Reaction with dimethylsulfate.....	108
3.4.3 Reaction with hydrochloric acid.....	109
3.4.4 Reaction with iodine.....	110
3.4.5 Reaction with iron pentacarbonyl.....	111

3.4.6 Crystal structure analyses.....	111
3.5 The reaction of [CpFe(CO) ₂] ₂ with 5,5'-dithiobis(1-phenyl-1H-tetrazole) (STz) ₂	113
3.5.1 At ambient temperature.....	113
3.5.2 Crystal structure analyses.	114
3.6 The reaction of [CpCr(CO) ₃] ₂ with 2,2'-dithiodipyridine (SPy) ₂	115
3.6.1 At ambient temperature.....	115
3.6.2 Crystal structure analyses.....	116
3.7 Reactions of CpCr(CO) ₂ (η ² -SPy) (16).....	117
3.7.1 Reactions With HX (X = F, Cl, I).....	117
3.7.2 Reaction with iodine.....	119
3.7.3 Reactions with hexafluorophosphoric acid and triflic acid.....	119
3.7.4 Reaction with dicyclopentadienylzirconium dichloride.....	121
3.7.5 Crystal structure analyses.....	122
 Chapter 4. References.....	 123
 Chapter 5. Conclusion.....	 132
5.1 Conclusion.....	132
 Appendix	
Appendix 1. Data collection and processing parameters.....	134
Appendix 2. Selected listing of crystallographic data.....	...in CD-ROM

ACKNOWLEDGEMENTS

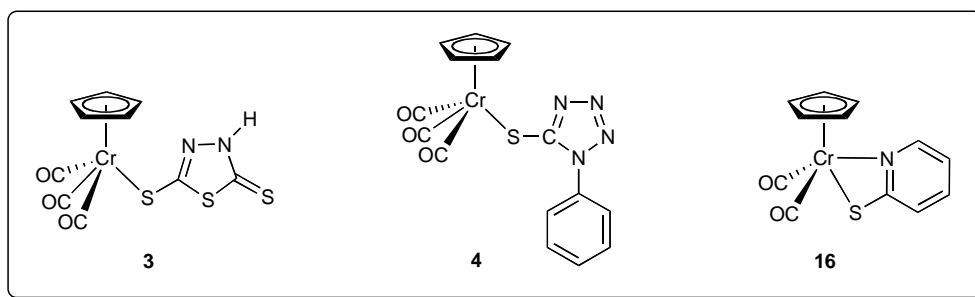
I would like to thank my supervisor Dr. Goh Lai Yoong for her patience, guidance and advice during the course of the project. In addition, special mention must be made to Dr. Goh's postgraduate, Mr. Weng Zhiqiang, for his invaluable knowledge and help throughout the project.

I would also like to thank Associate Professors J. J. Vittal and W. K. Leong, Dr. Koh, L. L. and Miss Tan G. K. for the various X-ray structured analyses. Thanks are also due to members in the teaching and technical laboratories for their help with the facilities.

Last but not least, my sincere thanks to my family, members in my research group including Richard Shin, Ng Sin Yee and Kuan Seah Ling, and friends, especially Mr. Adrian Soo, Elaine Chan and Justin Loh for their kind support.

Abstract

The reactivity of $[\text{CpCr}(\text{CO})_3]_2$ ($\text{Cp} = \text{C}_5\text{H}_5$) (**1**) towards several classes of organo-C-, N- and S- compounds have been studied. The organic substrates include: (i) 2,5-dimercapto-1,3,4-thiadiazole, (DMcTH_2), $\text{HS}(\text{CN}_2\text{SC})\text{SH}$; (ii) 5,5'-dithiobis(1-phenyl-1H-tetrazole), (STz)₂, $(\text{C}_6\text{H}_5\text{N}_4\text{CS})_2$ and (iii) 2,2'-dithiodipyridine, (SPy)₂, $(\text{C}_5\text{H}_5\text{NS})_2$. The primary products from these reactions were $\text{CpCr}(\text{CO})_3(\text{DMcTH})$ (**3**), $\text{CpCr}(\text{CO})_3(\text{STz})$ (**4**) and $\text{CpCr}(\text{CO})_2(\text{SPy})$ (**16**) respectively.



The cothermolysis of **4** with **1** at 90 °C led to the isolation of the aminocarbene-cubane complex $\text{Cp}_4\text{Cr}_4\text{S}_3(\text{N}_3\text{Ph})(\text{CpCr}(\text{CO})_2\text{CN})$ (**5**), the triazenido-cubane complex $\text{Cp}_4\text{Cr}_4\text{S}_3(\text{N}_3\text{Ph})$ (**6**) and the coordination complex $\text{Cr}(\text{SCN}_4\text{Ph})_3$ (**7**).

$\text{CpCr}(\text{CO})_3(\text{STz})$ (**4**) and $\text{CpCr}(\text{CO})_2(\text{SPy})$ (**16**) were reacted with acids, oxidizing reagents and coordinating metal fragments.

The reaction of **4** with hydrochloric acid or iodine resulted in redox reactions, which gave complexes $\text{CpCrCl}_2(\text{CH}_3\text{CN})$ (**12**) and $\text{CpCrI}_2(\text{CH}_3\text{CN})$ (**13**) respectively. The organic thiolate fragments were either protonated (by HCl) or oxidized to the disulfide (by I_2). The reaction of **4** with methylating agents such as trimethyloxonium tetrafluoroborate, Me_3OBF_4 and dimethylsulfate, $(\text{MeO})_2\text{SO}_2$ give binuclear complex,

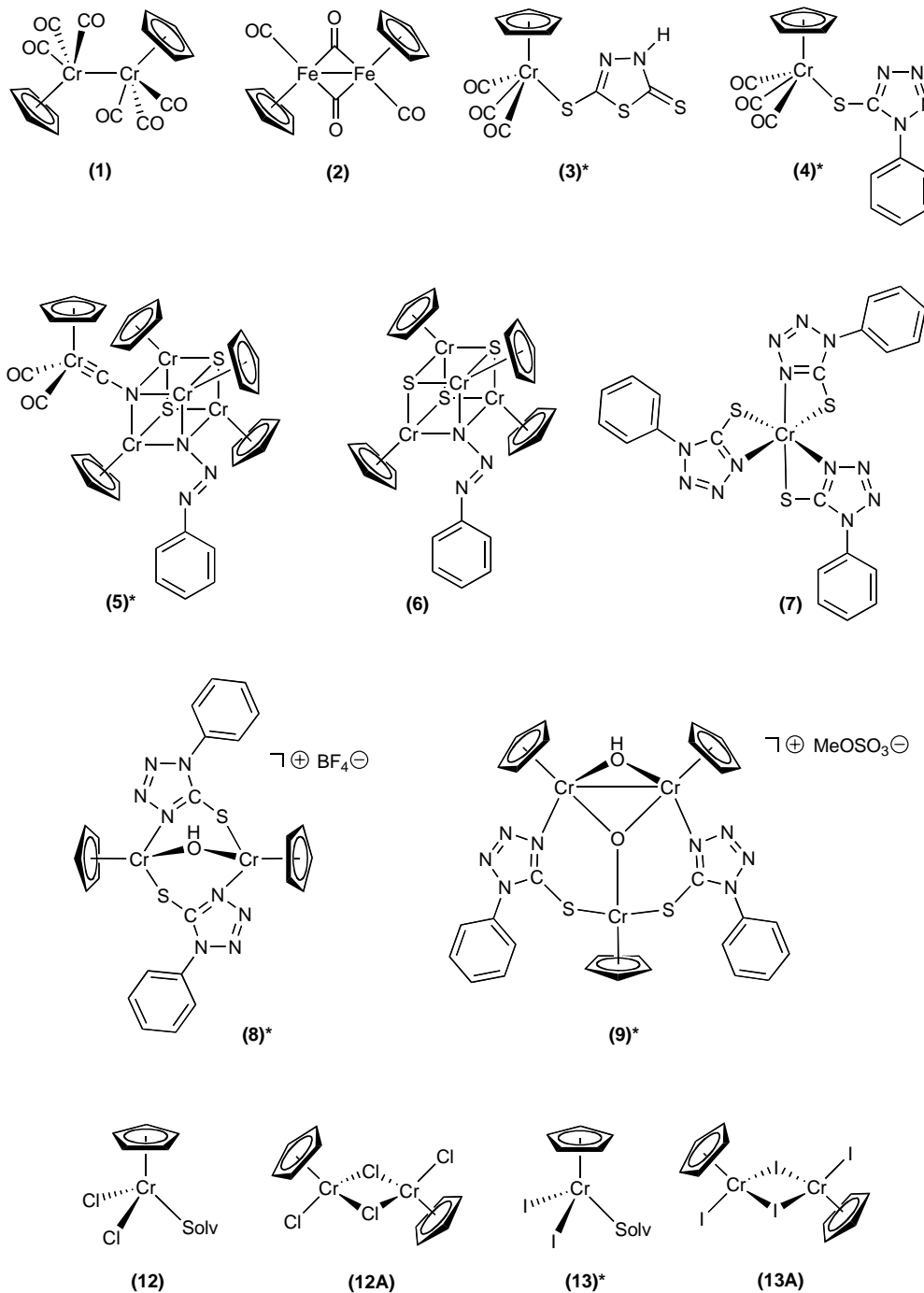
$\text{Cp}_2\text{Cr}_2(\mu\text{-OH})(\mu\text{-}\eta^2\text{-SCN}_4\text{Ph})_2\text{BF}_4$ (**8**) and trinuclear complex $\text{Cp}_3\text{Cr}_3(\mu_2\text{-OH})(\mu_3\text{-O})(\mu_2\text{-}\eta^2\text{-SCN}_4\text{Ph})_2(\text{CH}_3\text{OSO}_3)$ (**9**) respectively. These are the first examples of the 5-mercapto(1-phenyl-1H-tetrazole) ligand bridging via the exocyclic thiolate sulfur and the proximal endocyclic nitrogen.

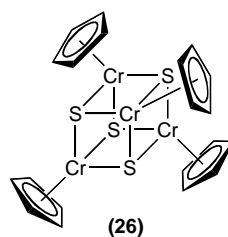
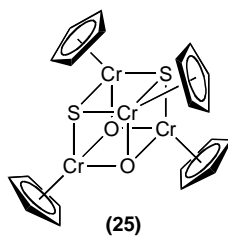
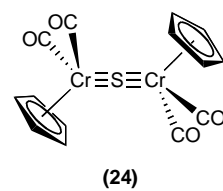
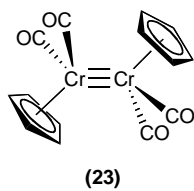
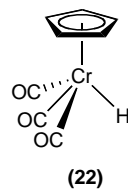
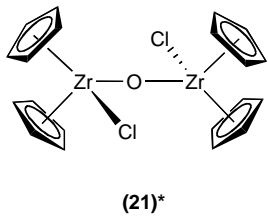
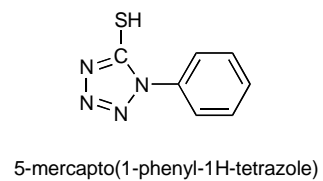
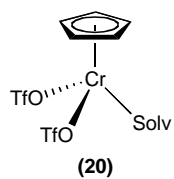
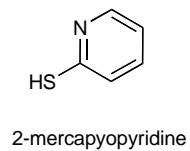
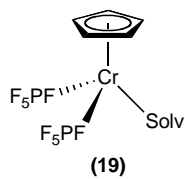
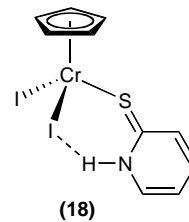
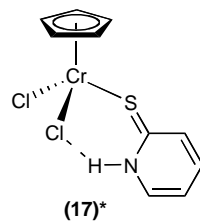
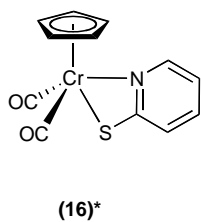
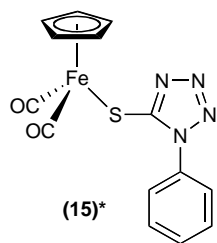
The reaction of **16** with haloacids, namely HCl and HI also resulted in redox reactions, which gave complexes $\text{CpCrCl}_2(\text{SPyH})$ (**17**) and $\text{CpCrI}_2(\text{SPyH})$ (**18**) respectively. The organic thiolate fragments was protonated to 2-mercaptopyridine. The reaction of **16** with iodine yielded $\text{CpCrI}_2(\text{CH}_3\text{CN})$ (**13**) together with the oxidized 2,2'-dithiodipyridine. In addition, the reaction of **16** with dicyclopentadienylzirconium dichloride, Cp_2ZrCl_2 , also gave $\text{CpCrCl}_2(\text{SPyH})$ (**17**) together with $[\text{Cp}_2\text{ZrCl}]_2\text{O}$ (**21**).

The reactivity of $[\text{CpFe}(\text{CO})_2]_2$ ($\text{Cp} = \text{C}_5\text{H}_5$) (**2**) towards $(\text{STz})_2$ was also investigated. The reaction yielded the mercaptotetrazole complex $\text{CpFe}(\text{CO})_2(\eta^1\text{-STz})$ (**15**), a close analogue of **4**.

Some of the isolated compounds were structurally characterized by X-ray diffraction. The structures are illustrated in Chart 1.

Chart 1. Compounds encountered in this thesis. (Structurally characterized complexes are marked with an asterisk after its numbering, e.g. (X)^{*})





List of abbreviations

Cp	η^5 -cyclopentadienyl
Cp*	η^5 -pentamethylcyclopentadienyl
br	broad
Bu	butyl
calc.	calculated
CCD	cold cathode-ray detector
d	doublet
ESI	Electrospray Ionisation
Et	ethyl
FAB-MS	Fast Atom Bombardment Mass Spectrometry
h	hour
ⁱ Pr	isopropyl
KBr	potassium bromide
m	medium
<i>m/z</i>	mass to charge ratio
M ⁺	parent ion peak (mass spectrometry)
Me	methyl
min	minute
mg	milligram
Ph	phenyl
ppm	parts per million
q	quartet
RT	room temperature
s	strong (IR) / singlet (NMR)
sh	shoulder
THF	tetrahydrofuran
UV-VIS	Ultraviolet-Visible
VT	variable temperature
w	weak
<i>ca.</i>	about (Latin <i>circa</i>)
<i>et al.</i>	and other (Latin <i>et alii</i>)
<i>i.e.</i>	this is (Latin <i>id est</i>)
Hz	Hertz
Å	angstrom
δ	NMR chemical shift in ppm

List of figures

Figure 1.3.1. The first tetrazole derivative, 2-phenyl-1,2,3,4-tetrazole-5 carbonitrile.....	21
Figure 2.1.1. Molecular structure of CpCr(CO) ₃ (DMcTH) (3).....	48
Figure 2.2.1. Molecular structure of CpCr(CO) ₃ (STz) (4).....	56
Figure 2.2.2. Molecular structure of Cp ₄ Cr ₄ S ₃ (N ₃ Ph)(CpCr(CO) ₂ ≡CN) (5).....	57
Figure 2.3.1. Molecular structure of Cp ₂ Cr ₂ (μ-OH)(μ-η ² -STz) ₂ BF ₄ (8).....	65
Figure 2.3.2. Molecular structure of Cp ₃ Cr ₃ (μ ₂ -OH)(μ ₃ -O)(μ ₂ -η ² -STz) ₂ (CH ₃ OSO ₃) (9).....	67
Figure 2.3.3. Molecular structure of CpCrI ₂ (CH ₃ CN) (12) and CpCrCl ₂ (CH ₃ CN) (13).....	75
Figure 2.4.1. Molecular structure of CpFe(CO) ₂ (STz) (15).....	79
Figure 2.5.1. Molecular structure of CpCr(CO) ₂ (SPy) (16).....	85
Figure 2.6.1. Molecular structure of CpCrCl ₂ SPyH (17).....	90
Figure 2.6.2 Molecular structure of [Cp ₂ ZrCl] ₂ O (21).....	97

List of tables

Table 1.2.1. Bonding modes of DMcTH complexes.....	15
Table 1.3.1. Bonding modes of tetrazole and 5-mercaptotetrazole complexes.....	23
Table 1.4.1. Bonding modes of 2-mercaptopyridine complexes.....	32
Table 2.1.1. Selected bond lengths (Å) and angles (deg) for 3	48
Table 2.2.1. Selected bond lengths (Å) and angles (deg) for 4	56
Table 2.2.2. Selected bond lengths (Å) and angles (deg) for 5	58
Table 2.3.1. Selected bond lengths (Å) and angles (deg) for 8	66
Table 2.3.2. Selected bond lengths (Å) and angles (deg) for 9	68
Table 2.3.3. Comparison of selected bond lengths (Å) and angles (deg) for 12 and 1	74
Table 2.4.1. Selected bond lengths (Å) and angles (deg) for 15	79
Table 2.5.1. Selected bond lengths (Å) and angles (deg) for 16	84
Table 2.6.1. Selected bond lengths (Å) and angles (deg) for 17	91
Table 2.6.2. Selected bond lengths (Å) and angles (deg) for 21	98

Chapter 1 Introduction

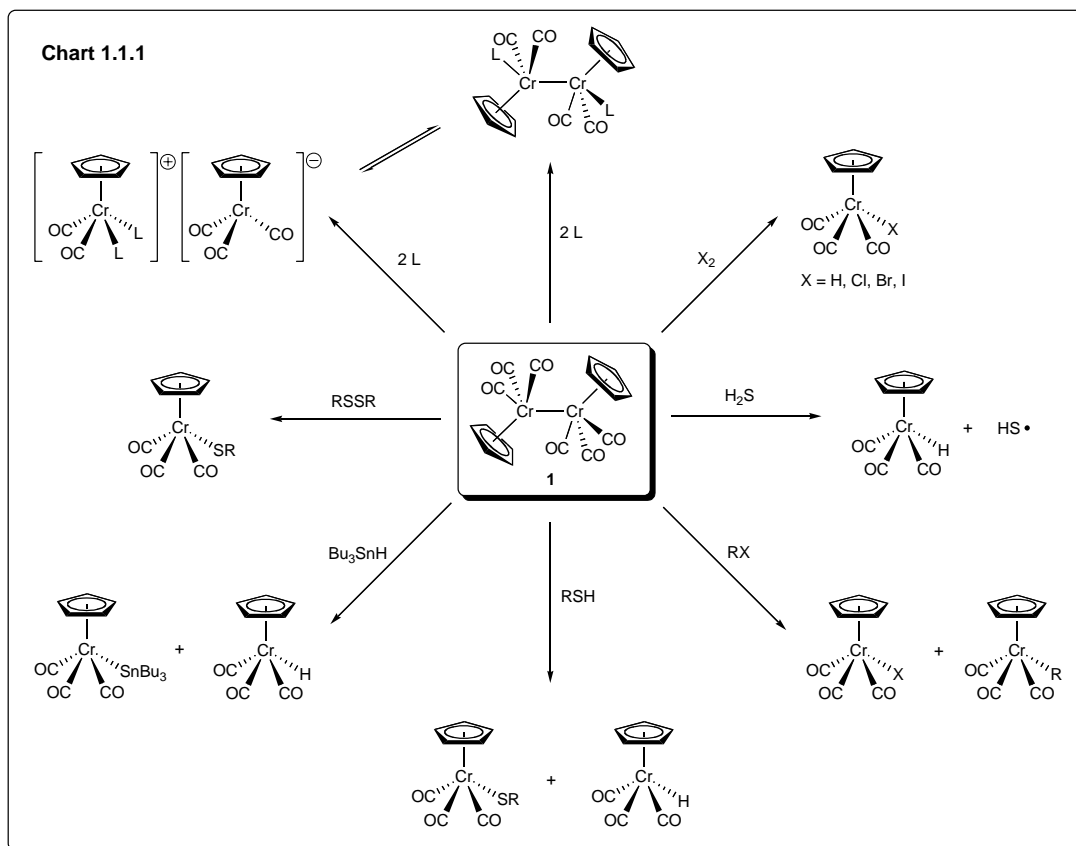
1.1 Chemistry of the tricarbonylcyclopentadienyl chromium

While the majority of organometallic complexes satisfy the 18-electron rule, there exists a few well-characterised 17-electron species and these have attracted intense research interest on account of their high reactivity.¹ These species are commonly prepared by the scission of the metal-metal bonds via thermolysis or photolysis of their corresponding 18-electron dimers,² e.g. the tricarbonylcyclopentadienyl chromium dimer, $[\text{CpCr}(\text{CO})_3]_2$ (**1**) ($\text{Cp} = \text{C}_5\text{H}_5$) which is of particular interest in this research project.³ **1** was synthesized in the late 1950's and reactivity studies in the 1960's by various research groups point to radical processes.⁴ The X-ray crystal structure analysis by Adams, Collins, and Cotton in 1974 showed the presence of an unusually long Cr–Cr bond (3.281(1) Å),⁵ which is much longer than that of its heavier congener molybdenum and tungsten analogues. This difference was attributed to steric repulsion between ligands in the two halves of the molecule.



Cotton suggested that the dimer should readily dissociate into 17-electron $\text{CpCr}(\text{CO})_3\cdot$ (**1A**) radicals (Scheme 1.1.1) and this was later established by (i) UV-VIS

studies by McLain, which showed 10% dissociation to monomer radical **1A** in room-temperature in a 10 mM solution;⁶ (ii) ESR, UV-VIS and IR studies by Vahrenkamp;⁷ and (iii) ESR and NMR studies by Goh *et al.*⁸

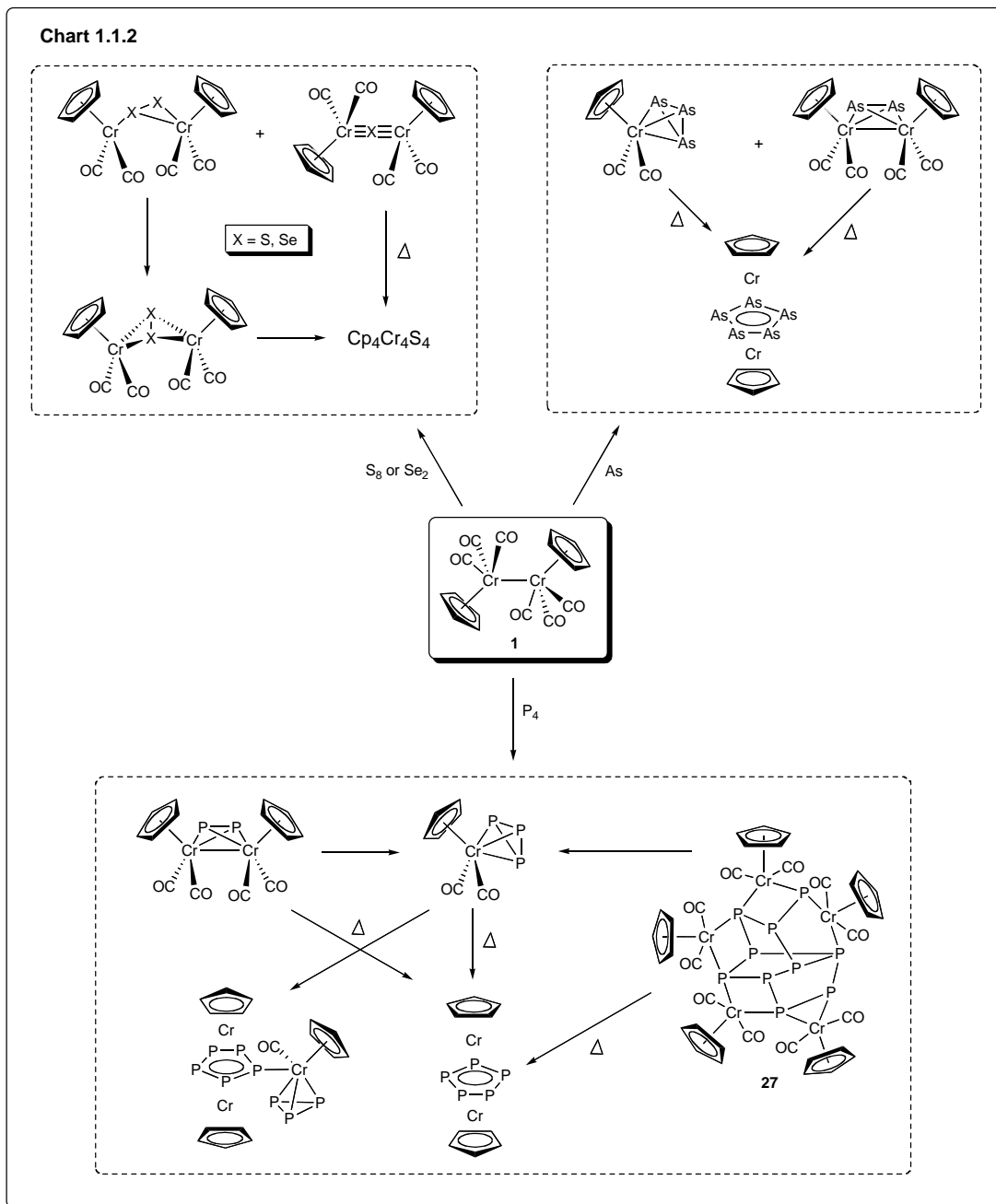


The wide range of reactions of **1** include, recombination, atom abstraction, electron transfer, ligand association and rearrangement, which resembles intimately those of organic radicals.⁹ Some of these reactions such as halogen abstraction, hydrogenation and acyl migratory insertion are important elementary steps in catalytic cycles. The high reactivity of **1** derives from the homolytic attack of **1A** on hydrogen,¹⁰ halogens and organic substrates eg, thiols,¹¹ hydrogen sulfide,¹² disulfides,¹³ organic halides,^{3a,3c} and

trialkyltin hydrides.¹⁴ In addition, substitution¹⁵ and disproportionation¹⁶ reactions of **1** are also well documented. Some of these reactions are highlighted in Chart 1.1.1.

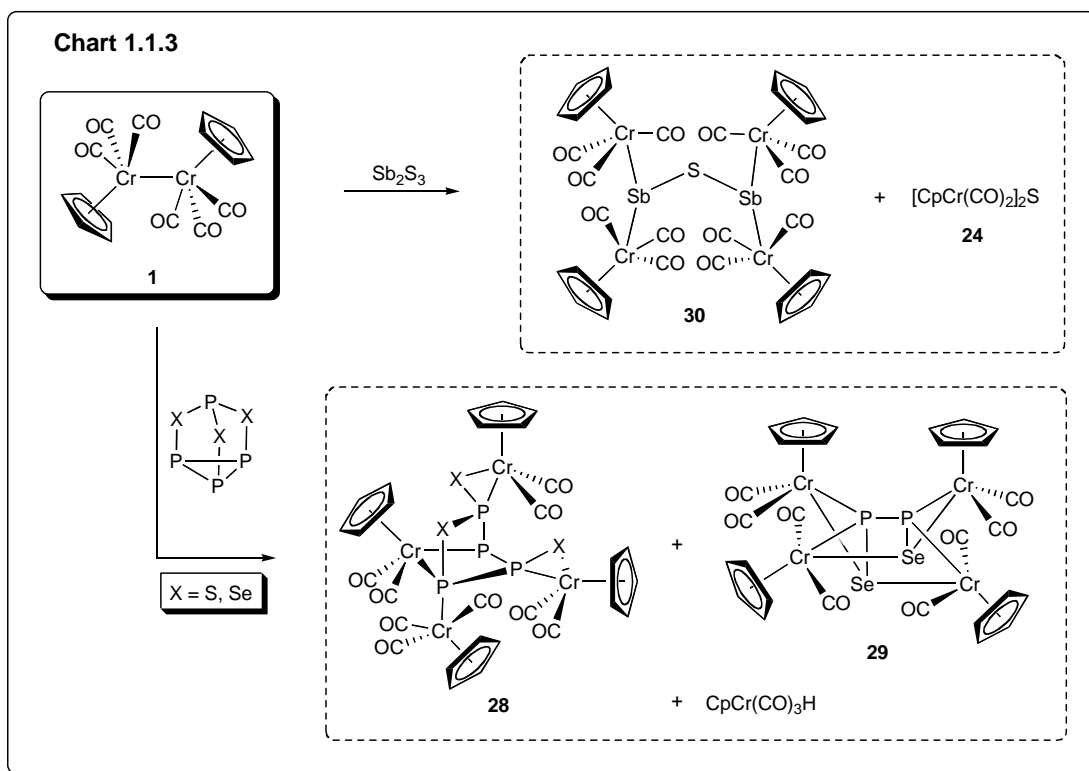
The reactions of $[\text{CpCr}(\text{CO})_3]_2$ with the homo- and hetero-polyatomic molecules of Groups 15 and 16 and diaryl dichalcogenides via a homolytic cleavage and aggregation pathways have been reviewed by Goh *et al.* These are illustrated in Chart 1.1.2 for the homonuclear chalcogenides and pnictogens, in Chart 1.1.3 for the heteronuclear polyatomic group 15 and 16 molecules and in Chart 1.1.4 for organic dichalcogen.^{17,18}

The facile reaction of **1** with elemental sulfur and selenium giving the corresponding sulfido- and seleno- complexes is an indication of the capability of **1** as a sulfur and selenide abstractor, and its preference for these soft atoms (“chalcophilic”). The polycyclophosphidochromium cluster $[\text{CpCr}(\text{CO})_2]_5\text{P}_{10}$ (**27**), obtained from the reaction of **1** with elemental yellow P_4 was perhaps one of the most outstanding products.¹⁹ The molecule consists of five $\text{CpCr}(\text{CO})_2$ fragments linked to the polyphosphorus P_{10} core with each chromium joined to two P atoms (Scheme 1.1.2). Till date, there has not been a report on an identical molecule consisting of the P_{10} moiety.

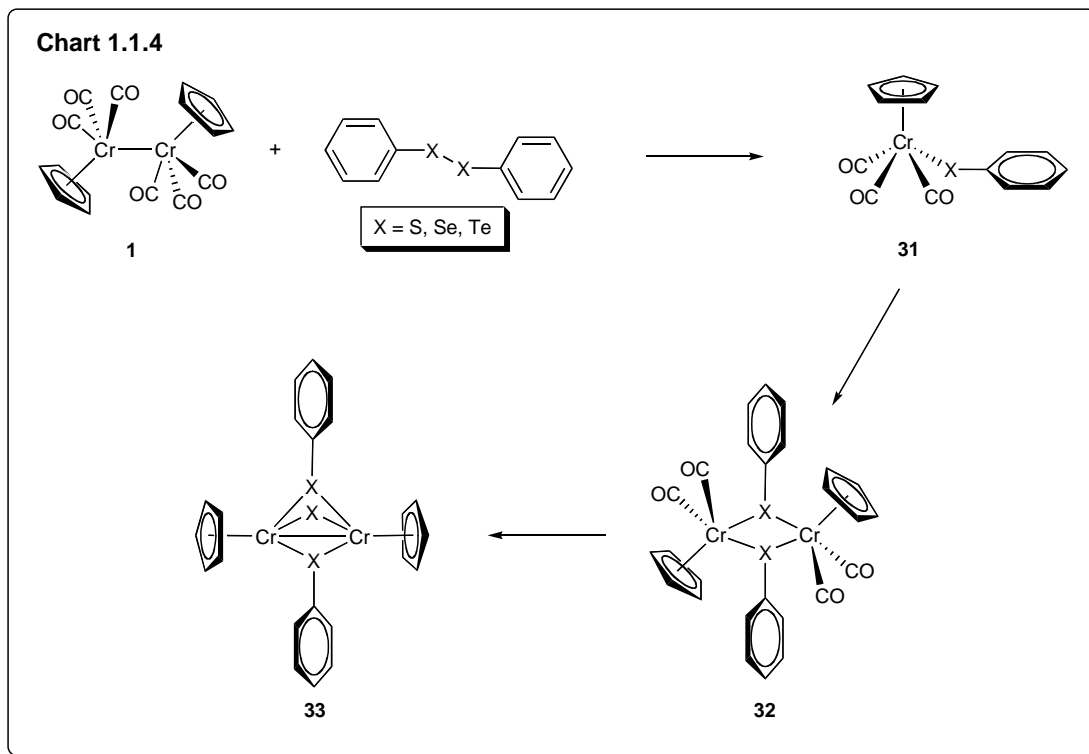


The reaction of $[\text{CpCr}(\text{CO})_3]_2$ (**1**) with P_4X_3 ($\text{X} = \text{S}, \text{Se}$) at ambient temperature led to the isolation of $\text{Cp}_4\text{Cr}_4(\text{CO})_9(\text{P}_4\text{X}_3)$ (**28**),²⁰ in which the molecular structure revealed that the initial P_4X_3 cage had undergone multiple P–P and P–S bond cleavage without fragmentation (Scheme 1.1.3). With $\text{X} = \text{Se}$, an additional product,

$\text{Cp}_4\text{Cr}_4(\text{CO})_8(\text{P}_2\text{Se}_2)$ (**29**), was also isolated in which it contains a rare case of the P_2Se_2 moiety. The reaction of **1** with excess Sb_2S_3 gave the tetranuclear complex, $\text{Cp}_4\text{Cr}_4(\text{CO})_{12}(\text{Sb}_2\text{S})$ (**30**), which contains four $\text{CpCr}(\text{CO})_3$ units linked by a Sb_2S unit (Scheme 1.1.3).^{17d}

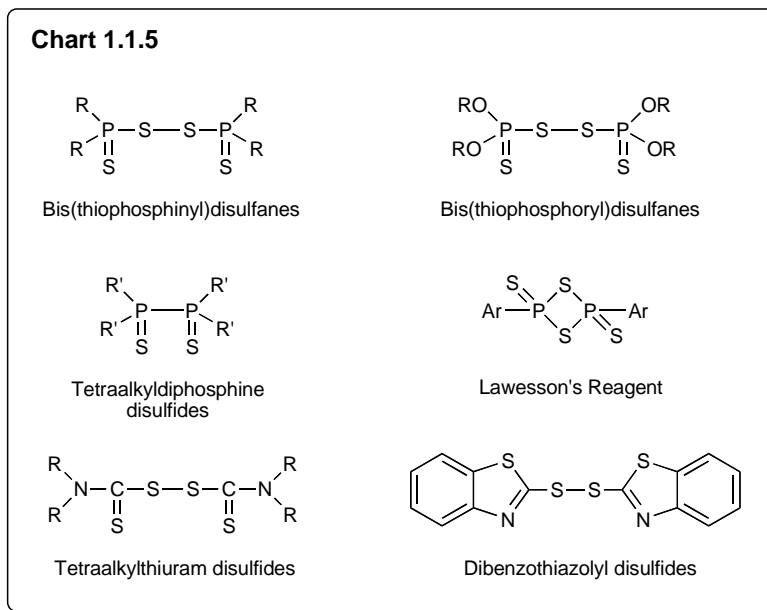


The reaction of **1** with PhXXPh ($\text{X} = \text{S}, \text{Se}, \text{Te}$) led to the isolation of $\text{CpCr}(\text{CO})_3(\text{XPh})$ (**31**) which subsequently converts to $[\text{CpCr}(\text{CO})_2(\text{XPh})]_2$ (**32**) and $[\text{CpCr}(\text{XPh})]_2\text{S}$ (**33**) under thermolytic conditions (Chart 1.1.4).¹⁸

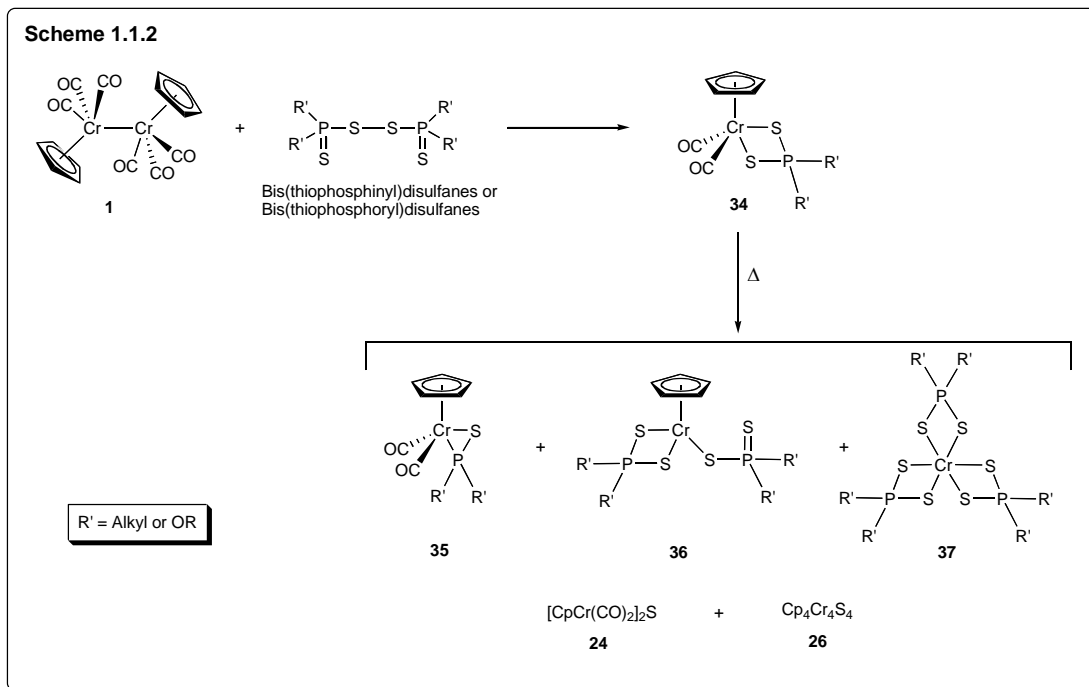


These studies demonstrated that the tricarbonylcyclopentadienyl chromium radical species has effectively and efficiently cleaved the S–S, P–P and S–P bond in polyatomic molecules of Group 15 and 16 molecules, generating a series of remarkable complexes having atypical bonding and structures.

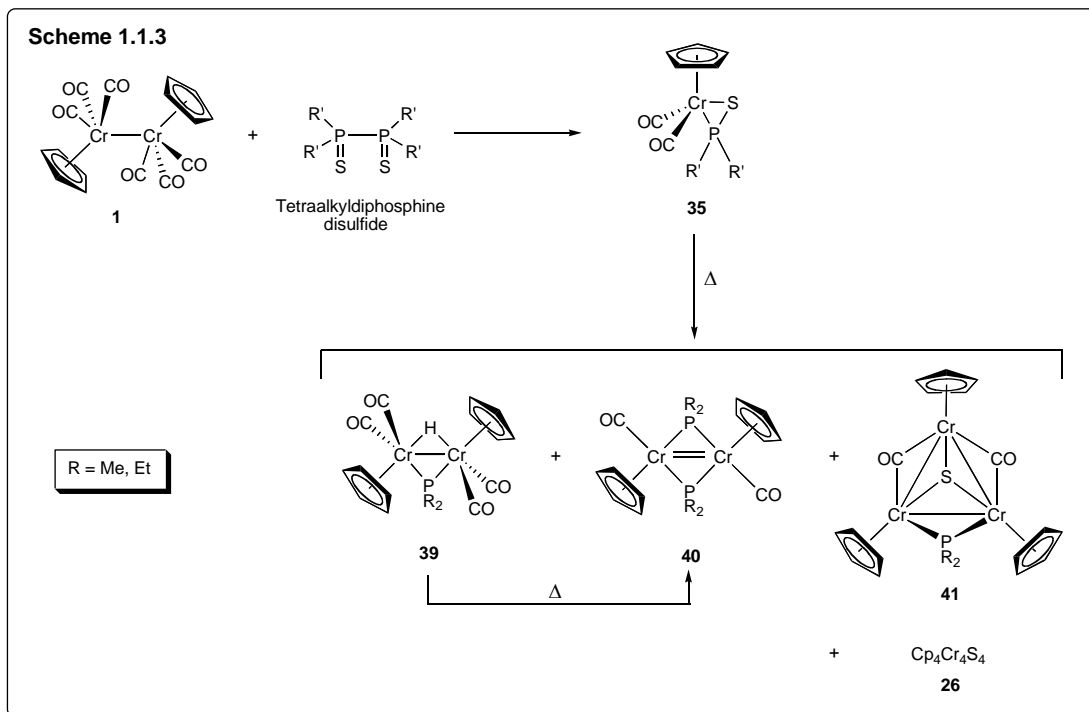
Investigations of the reaction of $[\text{CpCr}(\text{CO})_3]_2$ (1) with organic compounds, containing S–S, P–P and S–P bonds (Chart 1.1.5), viz bis(thiophosphinyl)disulfanes,²¹ bis(thiophosphoryl)disulfanes,²¹ tetraalkyldiphosphine disulfides,²² Lawesson's reagent,²³ tetraalkylthiuram disulfides²⁴ and dibenzothiazolyl disulfide,²⁵ including the reactivity of 1 towards various Cr-E (E = C, N, P, S) bonds were carried out by Goh *et al.*²⁶



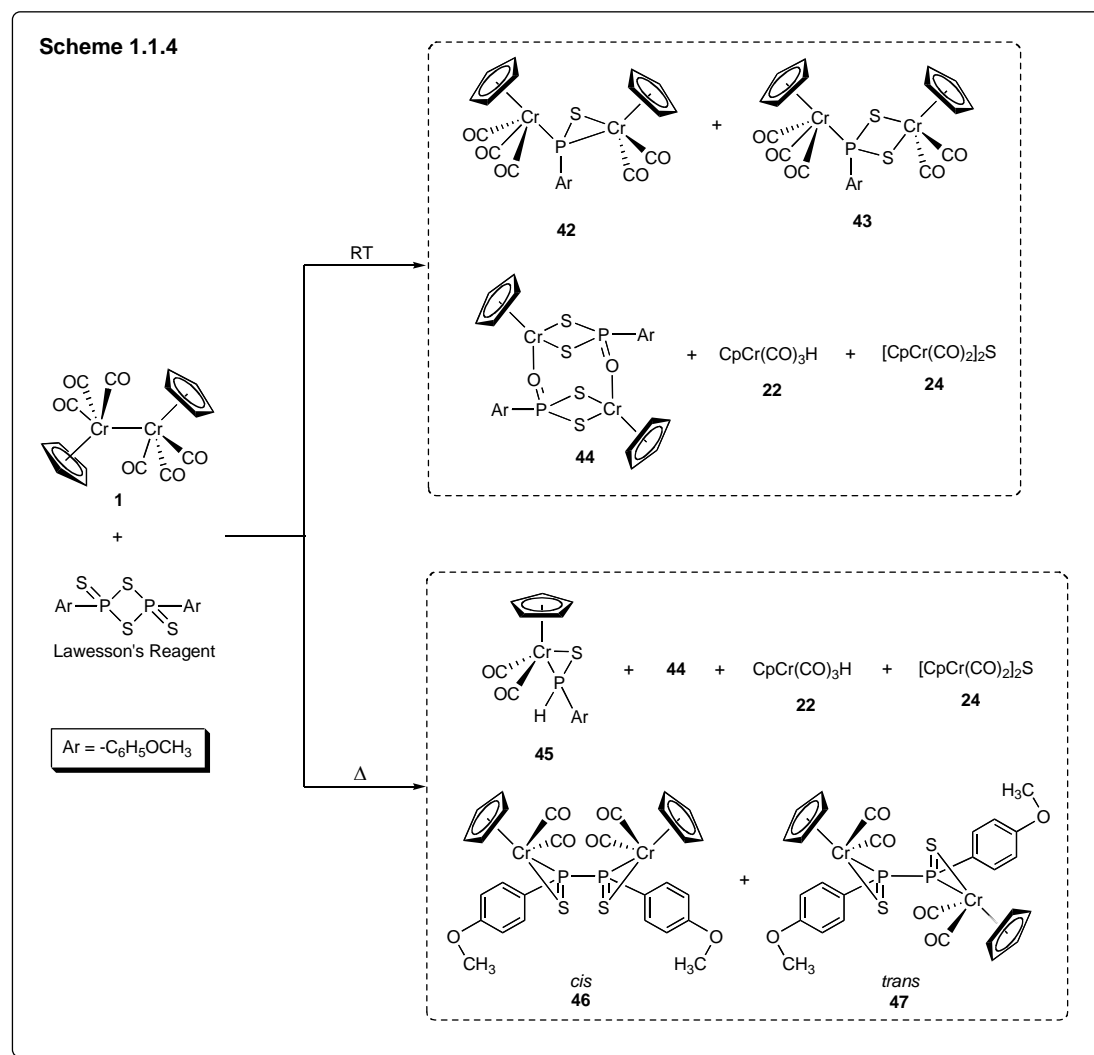
The reaction of bis(thiophosphinyl)disulfanes and bis(thiophosphoryl)disulfanes yielded very similar products, indicating that the auxiliary substituents on the phosphorus do not significantly modify its reactivity towards **1** (Scheme 1.1.2). The formation of $\text{CpCr}(\text{CO})_2(\text{S}_2\text{PR}_2)$ (**34**) is not unexpected, however, the formation of the Cr(III) species, $\text{Cr}(\text{S}_2\text{PR}_2)_3$ (**37**), involving the loss of a Cp ligand was a rare phenomenon.^{21,26}

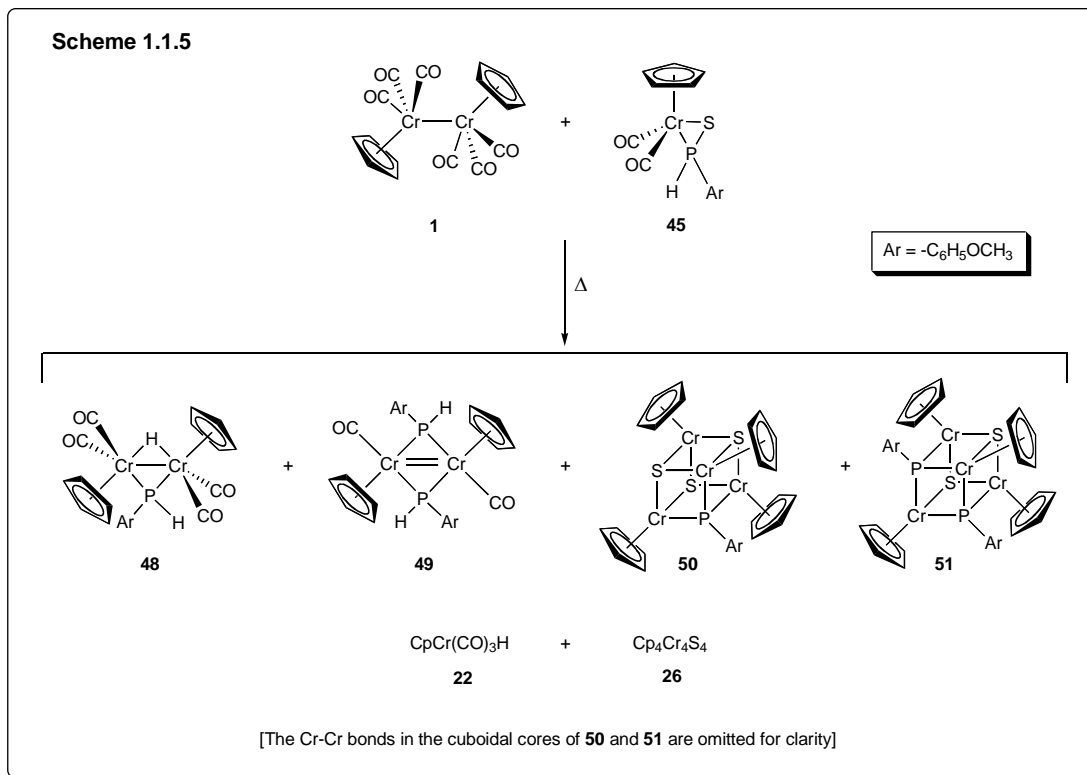


The cleavage of P-P bonds in tetraalkyldiphosphine disulfides by **1** was reported to require thermal activation. A series of di- and tri-nuclear complexes was obtained, all having a bridging phosphido $\mu_2\text{-PR}_2$ fragment. The tri-nuclear chromium complex (**41**) contains a bridging sulfido $\mu_3\text{-S}$ fragment, which adds to a family of such species of which the butoxide- and nitrene-bridged analogues have been reported (Scheme 1.1.3).^{22,26}

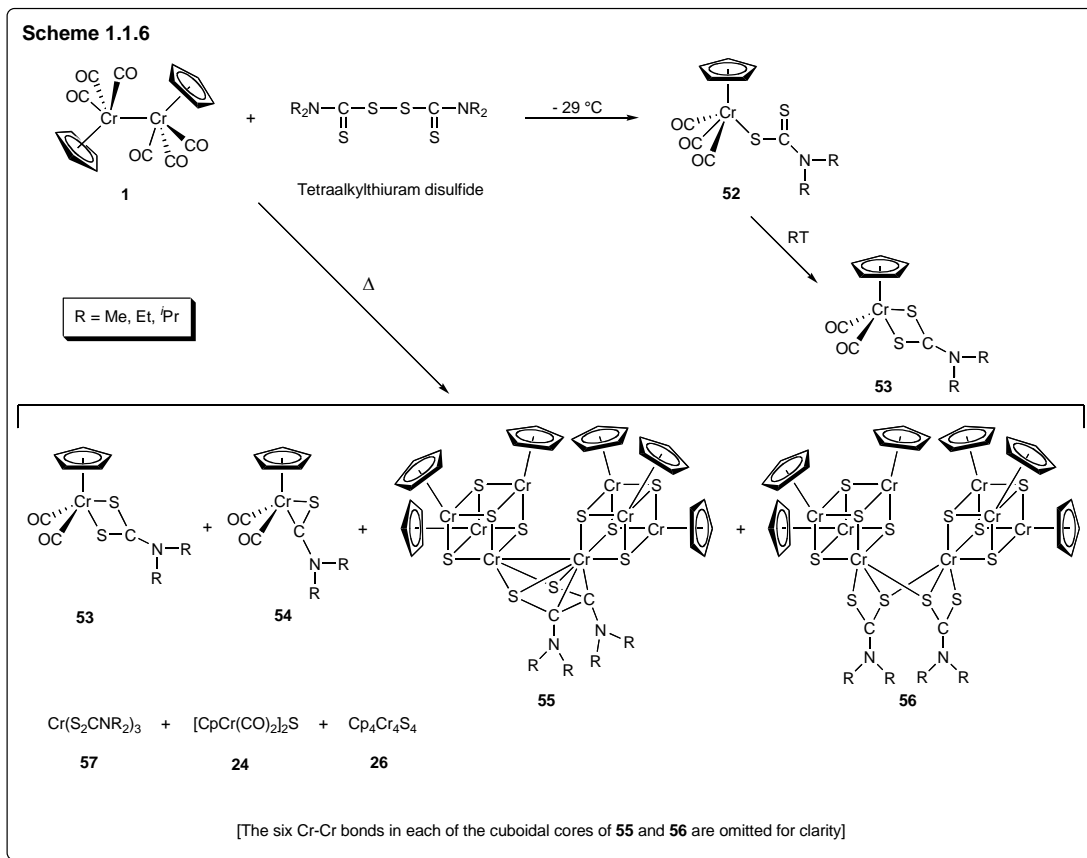


The four-membered P_2S_2 ring with two $\text{P}=\text{S}$ in the Lawesson's reagent was cleaved efficiently by **1**. At ambient and elevated temperatures, two different series of products were obtained (Scheme 1.1.4). In addition, the interaction of the primary product obtained at elevated temperature, $\text{CpCr}(\text{CO})_2(\text{SPHAr})$ (**45**), with **1** was also investigated. Surprisingly, it gave a completely new series of aggregated products (Scheme 1.1.5). A detailed mechanism on the fragmentation and aggregation on the complex systems has been proposed and interpreted by Goh *et al.*^{23,26}

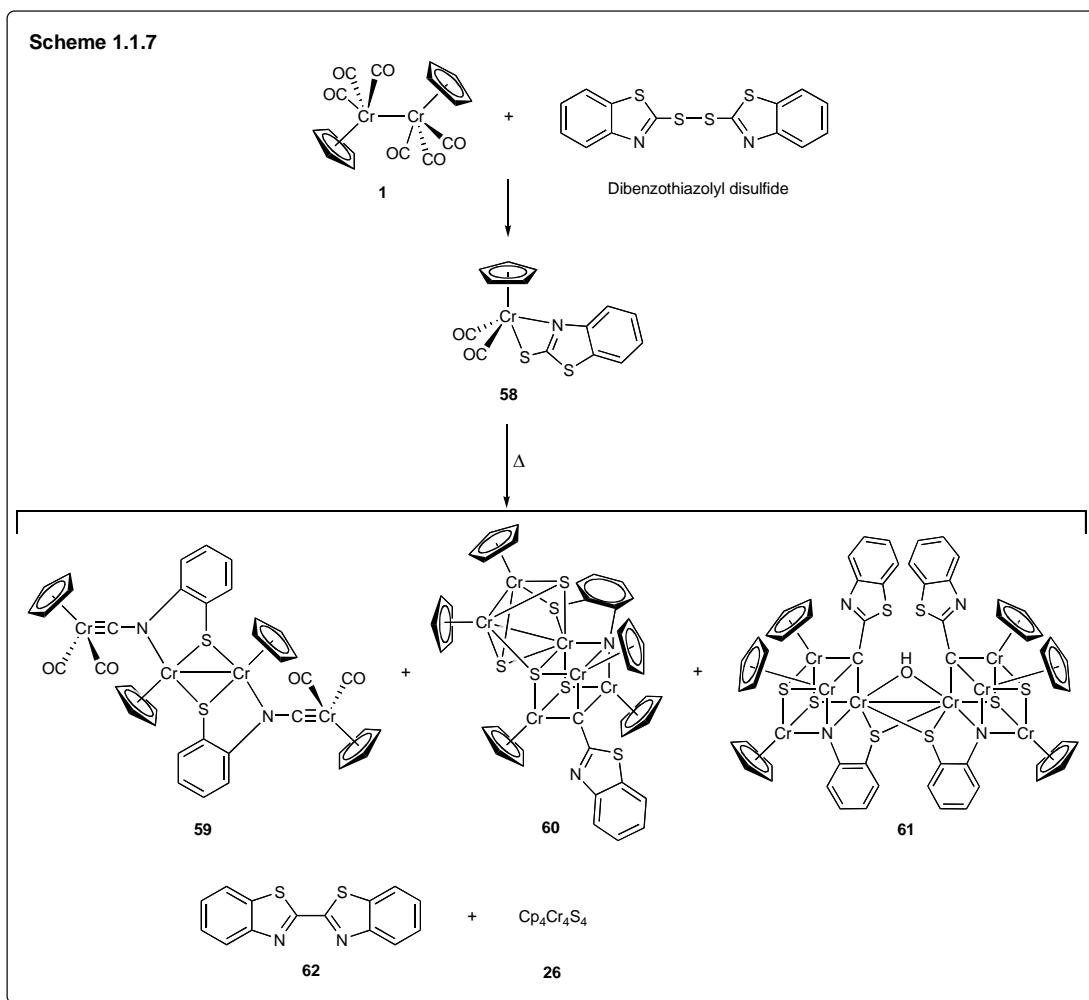




The reaction of **1** with tetraalkylthiuram disulfides gave some extraordinary results. At $-29\text{ }^{\circ}\text{C}$, the rare monodentate product $\text{CpCr}(\text{CO})_3(\eta^1\text{-S}_2\text{CNR}_2)$ (**52**) could be obtained at $-29\text{ }^{\circ}\text{C}$ in admixture with the bidentate product, $\text{CpCr}(\text{CO})_2(\eta^2\text{-S}_2\text{CNR}_2)$ (**53**), the sole product at ambient temperature. The interaction of **1** with tetraalkylthiuram disulfides at elevated temperatures yielded a series of structurally interesting complexes (Scheme 1.1.6) including a thiocarbenoid complex, $\text{CpCr}(\text{CO})_2(\eta^2\text{-SCNR}_2)$ (**54**), a thiocarboxamido dicubane-like cluster, $\text{Cp}_6\text{Cr}_8\text{S}_8(\eta^2, \eta^4\text{-SCNR}_2)_2$ (**55**), and a dithiocarbamate dicubane-like cluster, $\text{Cp}_6\text{Cr}_8\text{S}_8(\eta^2, \eta^4\text{-S}_2\text{CNR}_2)_2$ (**56**). The interaction of **1** with (**53**), (**54**), and the coordination complex, $\text{Cr}(\eta^2\text{-S}_2\text{CNR}_2)_3$ (**57**), was also investigated and reviewed.^{24,26}

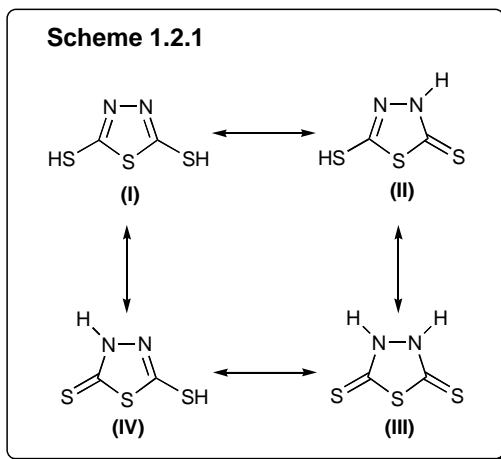


Finally, the bioactive ligand, dibenzothiazolyl disulfide was also reacted with **1**. The reaction was instantaneous at ambient temperature, which yielded $\text{CpCr}(\text{CO})_2(\text{SCSN}(\text{C}_6\text{H}_4))$ (**58**) in moderately high yields. The interaction of **1** with dibenzothiazolyl disulfide at elevated temperatures yielded a series of structurally interesting complexes (Scheme 1.1.7) including a tetranuclear bis-carbyne complex, $[\text{Cp}_2\text{Cr}_2(\text{CO})_2(\equiv\text{CNS}(\text{C}_6\text{H}_4))]_2$ (**59**), a hexanuclear chromium cluster, $\text{Cp}_5\text{Cr}_6\text{S}_4(\text{SN}(\text{C}_6\text{H}_4))(\text{SNC}_2(\text{C}_6\text{H}_4))$ (**60**), and a dicubane-like cluster with a hydroxyl bridge, $\text{Cp}_6\text{Cr}_8\text{S}_4(\mu\text{-OH})(\text{SN}(\text{C}_6\text{H}_4))_2(\text{SNC}_2(\text{C}_6\text{H}_4))_2$ (**61**).^{25,26}



1.2 2,5-dimercapto-1,3,4-thiadiazolate (DMcTH) Complexes

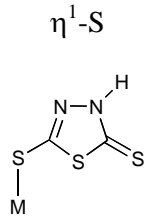
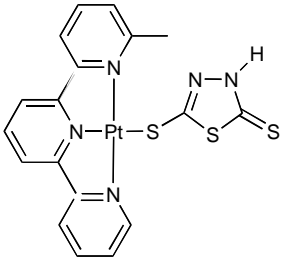
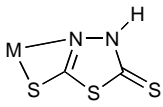
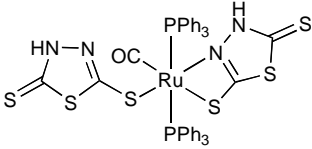
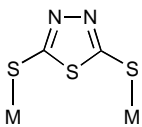
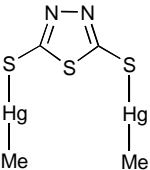
The trivial name of 2,5-dimercapto-1,3,4-thiadiazole (DMcTH₂) is known as “Bismuthiol I” because the dithiol is a specific reagent for the highly insoluble bismuth(III) salts in analytical chemistry. Although this nomenclature has been deemed obsolete under the new IUPAC naming system, many chemical suppliers still refer to it. DMcTH₂ has often been used in the detection and determination of heavy metal ions in the analytical industry.²⁷ It has also been utilized as photographic stabilizers and as anti-corrosion paint additives.²⁸

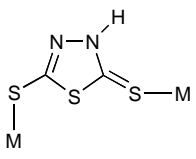
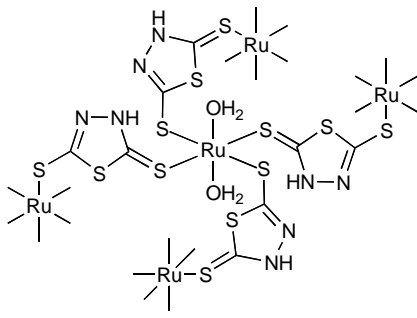
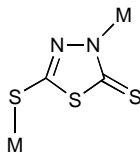
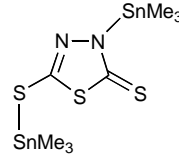
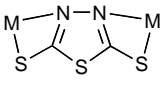
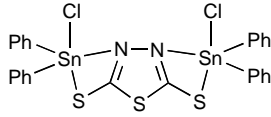
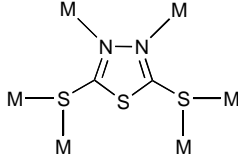
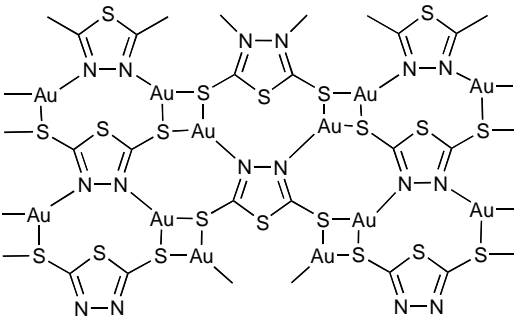


DMcTH₂ possesses numerous coordination sites, which include the endocyclic nitrogen and exocyclic sulfur atoms. The free ligand was shown to crystallize as 1,3,4-thiadiazole-2-thiol-5-thione (II) and was conjectured to exist in a mixture of tautomers in a solvent-dependent solution (Scheme 1.2.1).²⁹ The combination of these hard and soft donors could potentially give rise to a great variety of main-group and transition metal complexes. Some examples of the different bonding modes are illustrated in Table 1.2.1.

However, many of its metal complexes reported were insoluble powders and hence their x-ray structures remain elusive. Previous work relied heavily on elemental analyses, magnetic measurements and spectrometric studies for the prediction of many of the metal complexes. But unfortunately, the tautomeric forms and bonding modes of these complexes were often not conclusive. The x-ray structures of these complexes available so far are mostly of the late transition metals, including those of Ru,³⁰ Pt,³¹ Au³² and Hg,³³ and of the main-group metals, Tl³⁴ and Sn.³⁵ It is this versatility and the scarcity of organotransition metal complexes that has prompted an investigation of its reactivity with the tricarbonylcyclopentadienyl chromium dimer, [CpCr(CO)₃]₂.

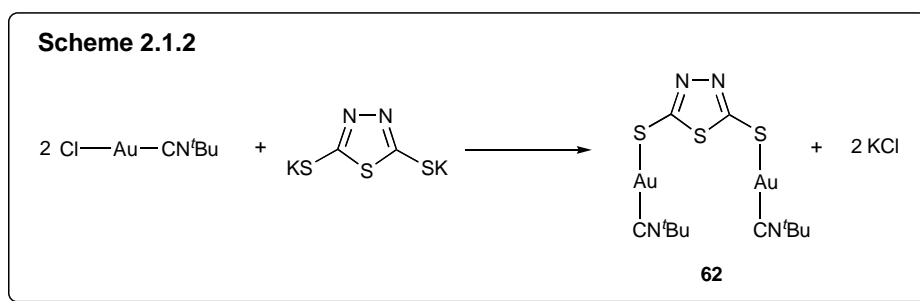
Table 1.2.1. Bonding modes of DMcTH complexes

No	Coordination Modes	Examples	Ref
1	$\eta^1\text{-S}$ 		31
2	$\eta^2\text{-S,N}$ 		30
3	$\mu\text{-}\eta^1, \eta^1(\text{S,S}')$ 		33

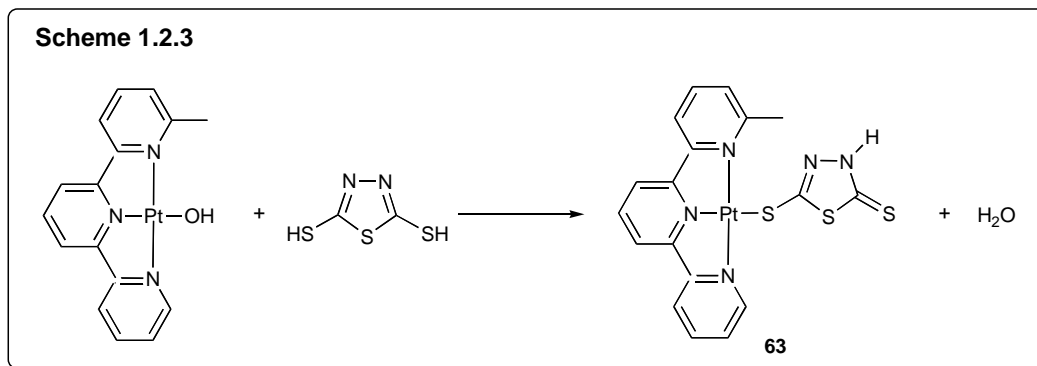
4	$\mu\text{-}\eta^1, \eta^1(\text{S}, \text{S}')$ 	 (No X-ray Structure)	36
5	$\mu\text{-}\eta^1, \eta^1(\text{S}, \text{N})$ 	 (No X-ray Structure)	37
6	$\mu\text{-}\eta^2, \eta^2[(\text{S}, \text{N}), (\text{S}', \text{N}')]]$ 		35(b)
7	$\mu_6\text{-}(\eta^1, \eta^1), \eta^1, \eta^1, (\eta^1, \eta^1)$ $[(\text{S}, \text{S}), (\text{S}', \text{S}'), \text{N}, \text{N}']$ 	 (No X-ray Structure)	32(a)

These metal complexes are generally prepared via salt elimination or promoted with the elimination of a small molecules such as water and hydrogen.

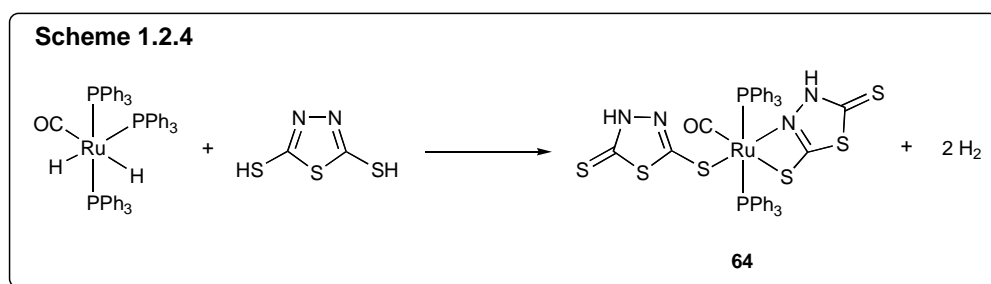
In their continuing effort of pursuing aurophilic interactions between two-coordinate gold (I) centres, Schmidbaur *et al.* have treated 2 mole equivalents of $(t\text{BuNC})\text{AuCl}$ with 1 equivalent of the dipotassium salt of DMcTH₂, K₂(DMcT) (Scheme 1.2.2). This results in the formation of the crystalline $[(t\text{BuNC})\text{Au}]_2(\text{DMcT})$ (**62**). In this complex, the two gold centres are bridged to the peripheral sulfide groups of the DMcT ligand leaving the other three heteroatoms of the heterocycle unengaged. The aurophilic interaction in this case was negligible.^{32a}



A different synthesis methodology via the direct reaction of a basic hydroxyl metal complex with 2,5-dimercapto-1,3,4-thiadiazole was reported by Tsuge *et al.*³¹ This involves the acid-base type of reaction in which the acidic thiol proton can be abstracted by a basic source e.g. metal hydroxyl group. Thus the reaction of a (terpyridine)platinum (II) hydroxyl salt with DMcTH₂ yielded the thiadiazolate complex **63** in which the ligand was bonded monodentate to the platinum metal centre via the exocyclic sulfide atom (Scheme 1.2.3). The resultant amido structure is a clear indication of the thiol-thione equilibrium in solution.

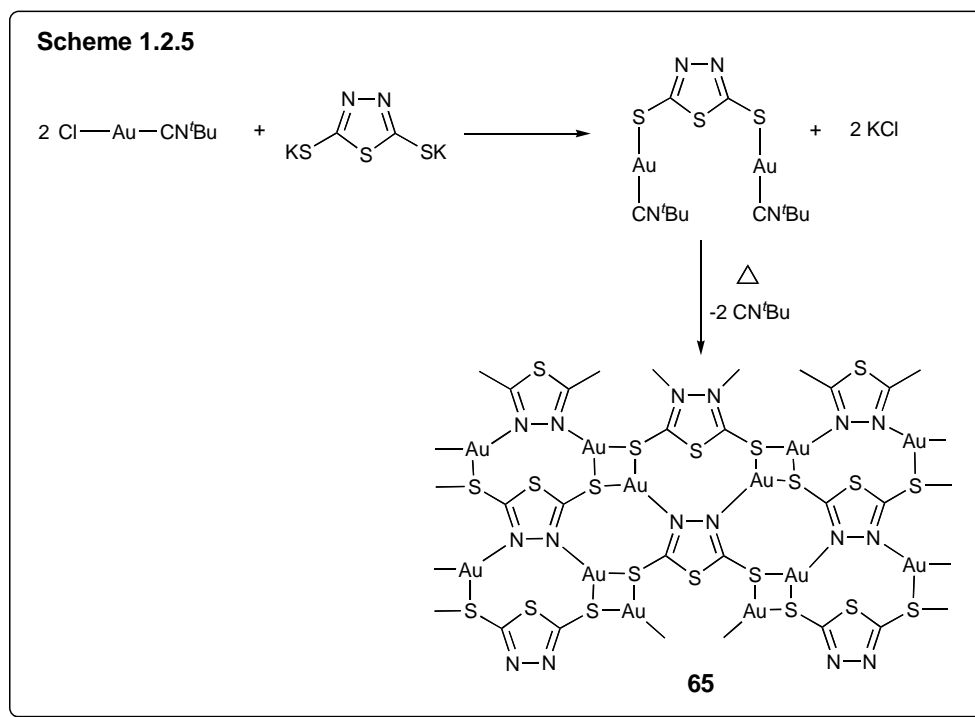


This synthetic methodology is similar to the one described above. It involves the direct reaction of a basic hydride metal complex with DMcTH_2 . This also involves the acid-base type of reaction in which the acidic thiol proton can be abstracted by a basic source e.g. metal hydrido group. The reaction of a ruthenium (II) dihydrido complex with DMcTH_2 yielded the thiadiazolate complex **64** in which there are two thiadiazolate bonded to the ruthenium metal centre, one monodentate S-bound, while the other chelating via the exocyclic S-atom and endocyclic N-atom, resultant from a $\text{Ru}\dots\text{N}$ secondary interaction (Scheme 1.2.4). There is also a clear indication of the thiol-thione equilibrium in solution as reported by Mura *et al.*³⁰

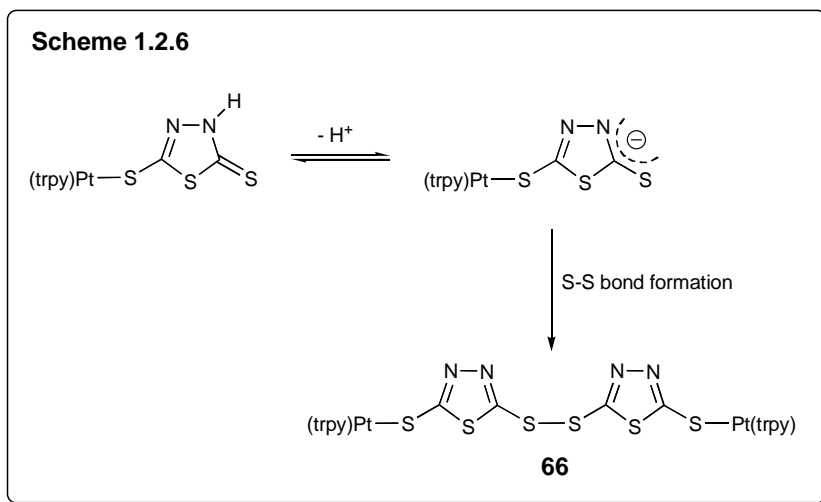


Reactivity studies of thiadiazolate complexes have been scarce, with only a couple of reports dealing with thermal transformations and oligomerization, and deprotonation coupled by redox reaction.

Owing to the multi-donor sites present in this class of versatile ligand, oligomerization can often be expected. This transformation process may be promoted generally via thermal agitation and displacement of an auxiliary ligand. As a means of designing and constructing supramolecular systems, Schmidbaur and coworkers have thermolysed $[(^t\text{BuNC})\text{Au}]_2(\text{DMcT})$ and obtained a supramolecular aggregation **65** based on aurophilic interaction, derived from the loss of the isocyanide ligand (Scheme 1.2.5).^{32a}

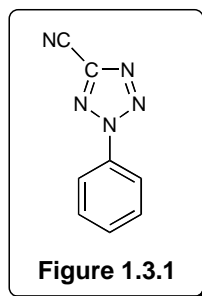


The amido tautomer of the platinum complex was investigated by Tsuge *et al.* utilizing electrochemical means. A series of cyclic voltammetry studies in the presence of base indicated that the loss of the amido-proton could cause the oxidative coupling of the free thiolate resulting in the formation of the disulfide complex **66**. The final step for the formation of the S-S coupled complex was found to be irreversible, although the deprotonation step was otherwise (Scheme 1.2.6).³¹

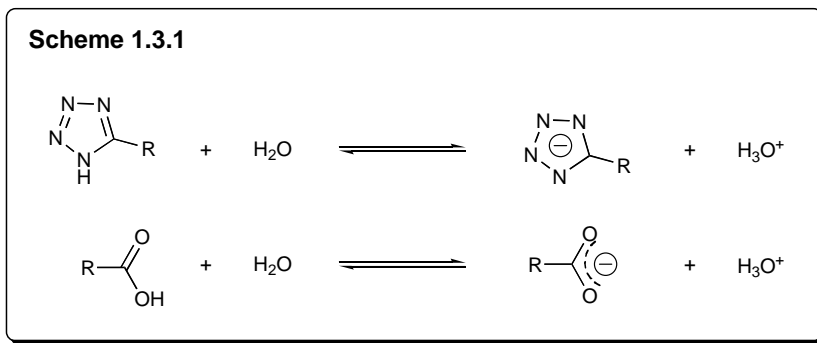


1.3 Tetrazole complexes

While the first tetrazole derivative (Figure 1) was synthesized and reported about a century ago, this class of higher azoles did not receive much attention.³⁸ It was only in the late 1940s that there was an increase in research interest in these compounds on account of their potential in the fields of explosives, photography and agriculture.³⁹

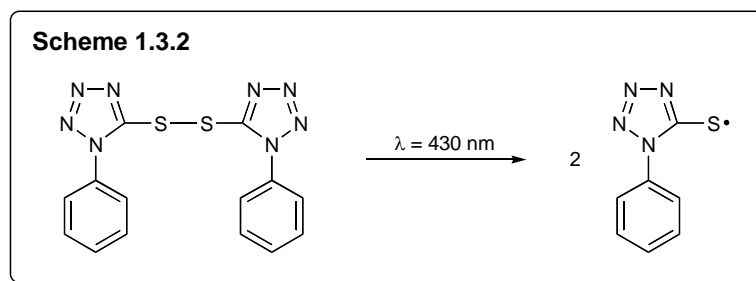


In the last couple of decades, interest in this class of compounds has increased owing to its pharmacological and biochemical properties. The tetrazole-containing drugs are not only important supramolecular complexes, but are also essential in vivo receptor binding in certain diseases. Au(I) complexes of the type $[\text{Au}(\text{N-heterocycle})\text{PPh}_3]$ (N-heterocycle = imidazole, pyrazole, and tetrazole) for example demonstrated antimicrobial activity toward Gram positive species.⁴⁰ In addition, there are many biochemical studies on the functional and structural diversity in this class of compounds as metal complexes, which may act as aromatase inhibitors and enzyme stability.⁴¹ It is also noteworthy that the 5-substituted tetrazolic acid derivatives are also the formal nitrogen analogs of their carboxylic acid counterparts (Scheme 1.3.1).



Molloy and co-workers have studied many tetrazole-coordinated complexes with main group 14 metals, especially tin. In addition to structurally interesting complexes, they had synthesized specially assembled tetrazole-linked metal polymers and supramolecules for conductivity and optical-related applications.⁴²

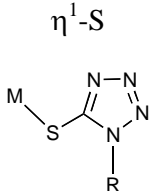
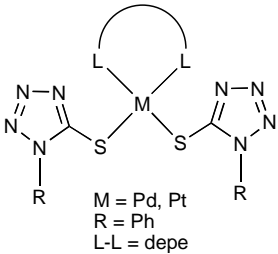
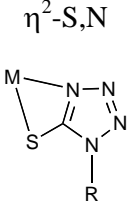
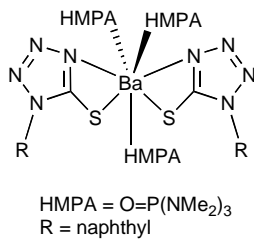
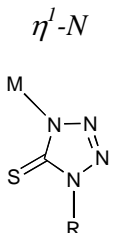
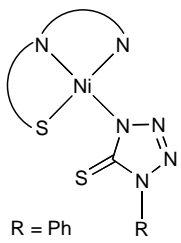
The special feature in the structure of 5,5'-dithiobis(1-phenyl-1H-tetrazole) which is of interest to us in this project is the reactivity of the S-S bond towards 1. It is known that the S-S bond of 5,5'-dithiobis(1-phenyl-1H-tetrazole) can be photochemically cleaved by nanosecond-laser flash photolysis and the transient absorption band at ca. 430 nm was attributed to the resultant thio-radicals (Scheme 1.3.2). It was found that the unpaired electron of the radical localized mainly on the sulfur atom.⁴³

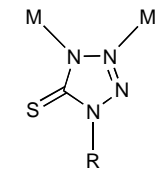
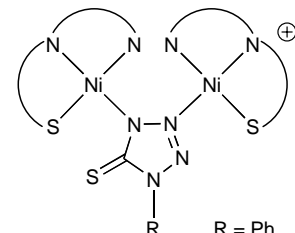
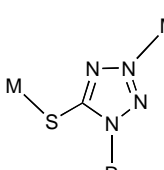
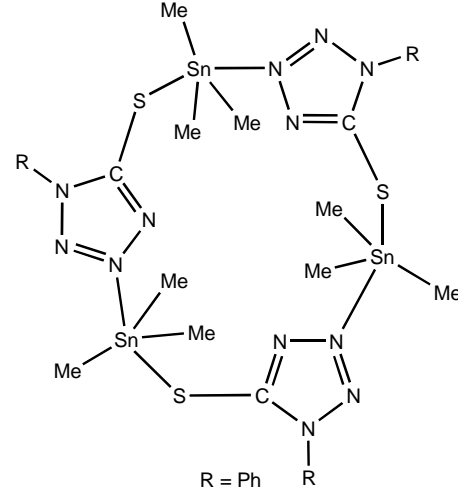
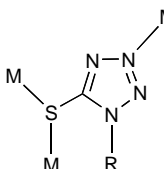
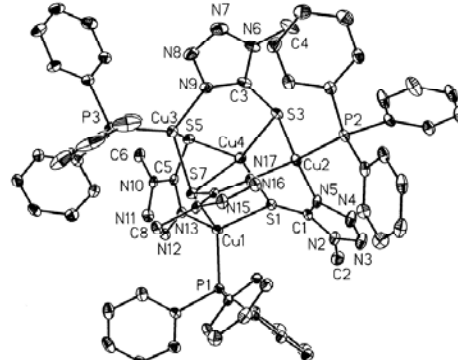


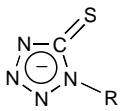
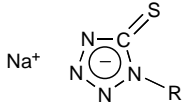
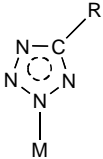
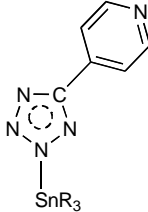
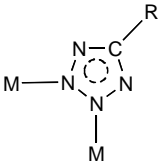
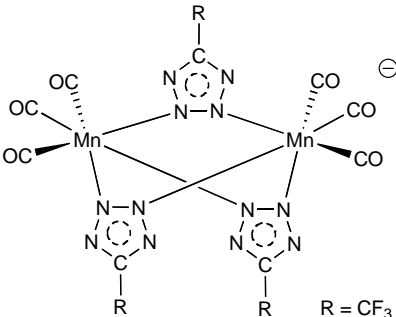
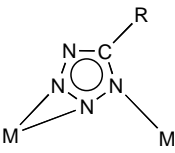
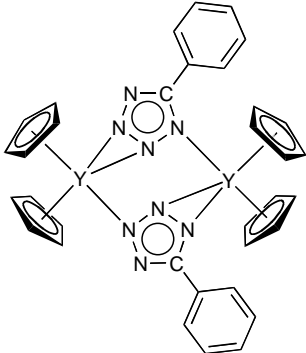
Tetrazole with various coordination sites is a coordinatively versatile and interesting ligand. The ligand may be monodentate, bidentate or bridging. When an exocyclic thiolate moiety is present on the carbon atom of the tetrazole ring, it may

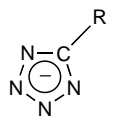
coordinate through the exocyclic sulfur atom or the two nitrogen atoms, having the lone pair of electrons, on the tetrazole ring to form dimers, trimers and even polymeric organometallic complexes. Indeed, the tetrazole and its derivatized 5-mercaptotetrazole ligands are known to exhibit at least ten different bonding modes as shown in Table 1.3.1.

Table 1.3.1. Bonding modes of tetrazole and 5-mercaptotetrazole complexes

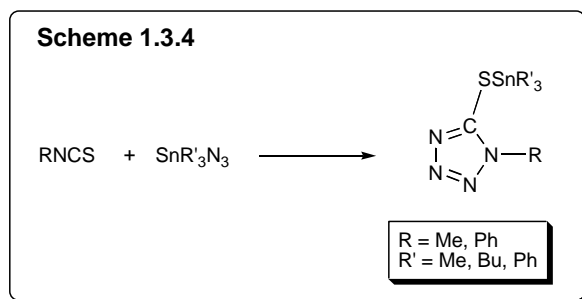
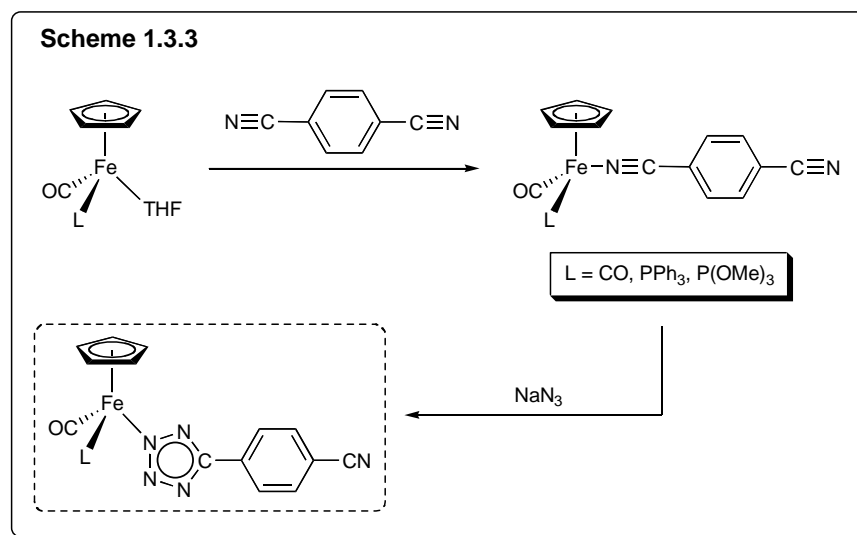
No	Coordination Modes	Examples	Ref
1	$\eta^1\text{-S}$ 	 <p>M = Pd, Pt R = Ph L-L = depe</p>	44
2	$\eta^2\text{-S,N}$ 	 <p>HMPA = O=P(NMe₂)₃ R = naphthyl</p>	45
3	$\eta^1\text{-N}$ 	 <p>R = Ph</p> <p>(No X-ray Structure)</p>	46

4	$\mu\text{-}\eta^1, \eta^1(\text{N}, \text{N}')$ 	 <p style="text-align: center;">R = Ph</p> <p style="text-align: center;">(No X-ray Structure)</p>	46
5	$\mu\text{-}\eta^1, \eta^1(\text{S}, \text{N})$ 	 <p style="text-align: center;">R = Ph</p>	47
6	$\mu\text{-}\eta^2, \eta^1[(\text{S}, \text{S}), \text{N}]$ 		48

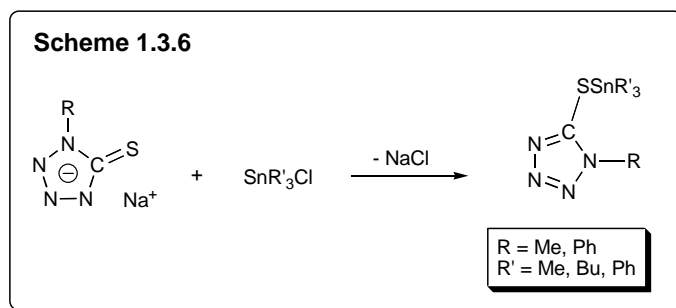
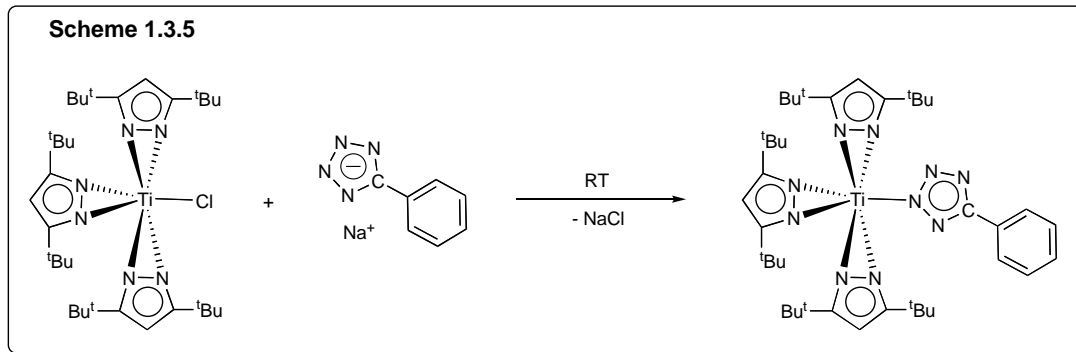
7	$\eta^5-(\text{CN}_4)$ 	 Na^+ (No X-ray Structure)	49
8	$\eta^1\text{-N}$ 	 $\text{R} = \text{Et, Bu}$	50
9	$\mu\text{-}\eta^1, \eta^1(\text{N}, \text{N}')$ 	 $\text{R} = \text{CF}_3$	51
10	$\mu\text{-}\eta^1, \eta^2(\text{N}, \text{N}', \text{N}'')$ 		52

11	$\eta^5-(\text{CN}_4)$ 	51
----	---	----

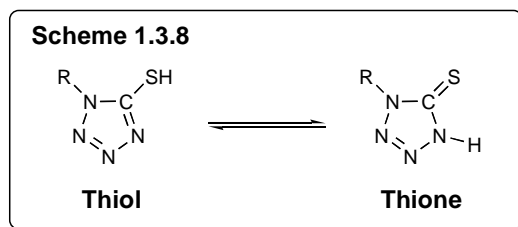
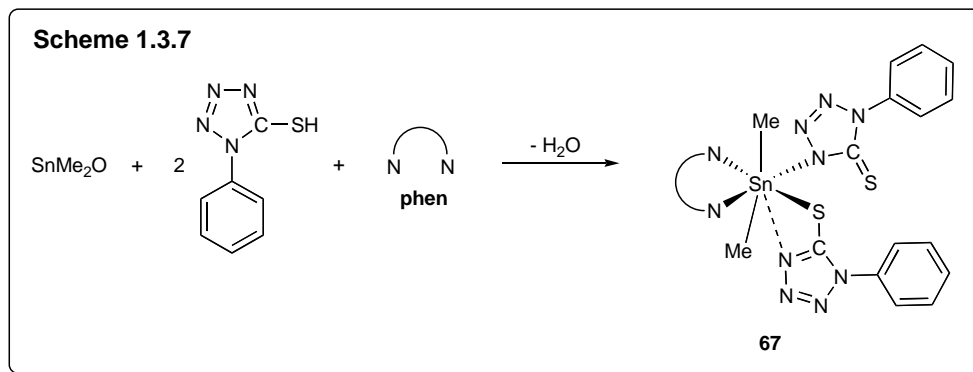
Conventional pathways to these tetrazole complexes involve cycloaddition reactions. The 1,3-dipolar addition of an azide to cyano/thiocyano-bound metal complexes or otherwise cyanide/thiocyanide to azido-bound metal complexes can, in general, be effected to produce tetrazole complexes (Schemes 1.3.3 and 1.3.4).^{53,54}



Another general method of synthesizing this class of metal complexes is via salt elimination reactions, as shown in Schemes 1.3.5 and 1.3.6.^{55,56}



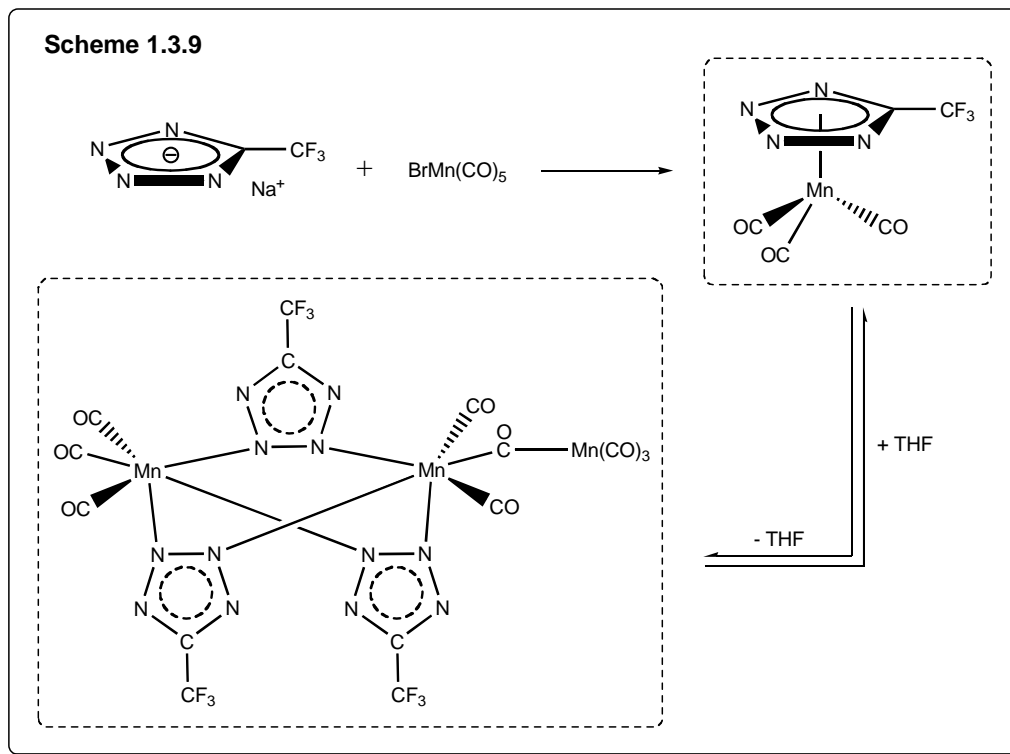
A different synthetic methodology via the reaction of a basic oxide metal complex with the thiol derivative of the tetrazole was reported by Castano *et al.*⁵⁷ This involves the acid-base type of reaction in which the acidic thiol proton can be abstracted by a basic source e.g. metal oxide. The reaction of a dimethyltin (IV) oxide with 1-phenyl-5-thione-1,2,3,4-tetrazole in the presence of phenanthroline yielded the tetrazole complex **67** in which there are two tetrazole bonded to the tin metal centre, one N- and the other S-bound, which also forms an additional Sn...N secondary interaction (Scheme 1.3.7). This is a clear indication of the thiol-thione equilibrium in solution (Scheme 1.3.8).⁵⁸



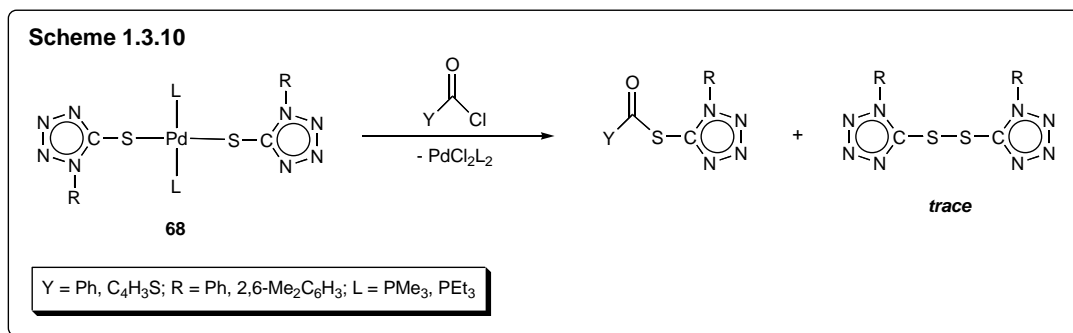
Although the coordination of the disulfide ligand (5,5'-dithiobis(1-phenyl-1H-tetrazole)) to metal complexes have been reported and the whole ligand found to be intact via spectroscopic means, no structural confirmation is available.

Reactivity studies of tetrazole complexes have been scarce, with only a few reports dealing with thermal transformations and oligomerization, electrophilic substitution, protonation and methylation reactions.

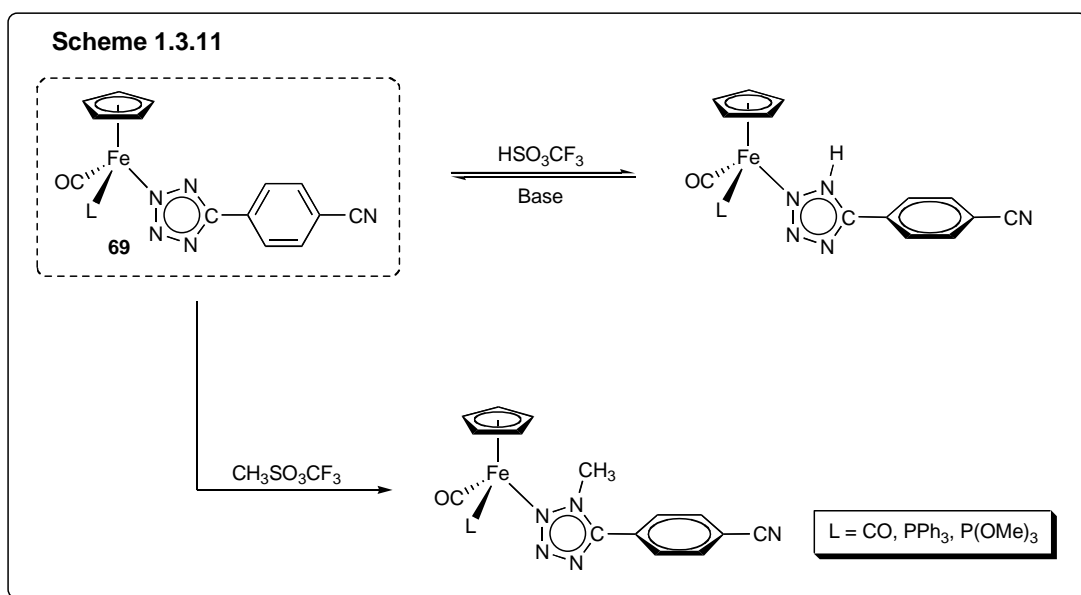
The structure of a η^5 -coordinated metal-tetrazolate complex has remained elusive till now although there were some evidence supporting its existence. Owing to the multi-donor sites present in this class of versatile ligand, oligomerization can often be expected. This transformation process may be effected generally via thermal agitation and displacement of solvent molecules (Scheme 1.3.9).⁵¹



The reactivity of some palladium (II) tetrazole-thiolate complexes **68** with electrophiles such as organic acyl halides was investigated by Kim *et al.* (Scheme 1.3.10).⁴⁴ The formation of the thioacyl organic compounds indicated the abstraction of the thiolate group from the metal complex by the electrophilic acyl halide. While on the other hand, the formation of the disulfide dimer was likely to have resulted from reductive elimination, and this result appears somewhat surprising.



Palazzi and coworkers have synthesized a series of Fe(II) 5-aryl tetrazolate complexes **69** via cycloaddition and have found interesting interannular conjugation between the phenyl and the tetrazolate moieties.⁵² In addition, protonation and methylation reactions performed on these complexes were found to be detrimental to the interannular conjugation (Scheme 1.3.11). However, the protonation process was found to be reversible.



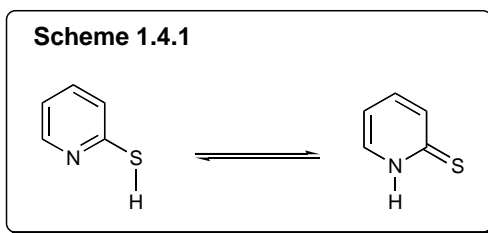
1.4 2-Mercaptopyridine Complexes

Compounds of heterocyclic thionates, in particular that of 2-mercaptopyridine, with transition and other main group metals received intense research interest because of their biological activity and many practical applications. In the field of bioorganic and bioinorganic studies, the use of 2-mercaptopyridine and its derivatives is prevalent. High-resolution mapping of nucleoprotein complexes by site-specific protein-DNA can be achieved with the aid of this class of ligand. It can be used as a non-acidic matrix for the matrix-assisted laser desorption in the analysis of bio-macromolecules and it is also commonly used as a thio-substituted pyrimidine bases for RNA-catalysed nucleotide synthesis.⁵⁹ A recent study showed that women with atherosclerotic CVD and are allergic or show contraindications when using aspirin can use other antiplatelet agents, such as newer thiopyridine derivatives, to prevent vascular events.⁶⁰

In affinity chromatography and other specialized "adsorption" technique, the column packing are supplied in their free thiol form or in oxidized form as mixed disulfides with 2-mercaptoethanol or 2-mercaptopyridine. Recent examples of Sn-S bonded compounds such as those with 2-mercaptopyridine show fungicidal activities against a range of test samples.⁶¹ In polymer science, the styrene grafts are attached to cellulose backbone with labile carbonate linkages and terminated with 2-mercaptopyridine groups generated by chain transfer.⁶² In addition, it can also increase the rigidity of polymers via higher degree of interactions such as when 2-mercaptopyridine groups replace the phenyl groups in polystyrene. A series of work on

the electronic and magnetic properties of some Fe(II)-Fe(III) complexes through a 2-mercaptopyridine bridge were also investigated by Y. Moreno and coworkers.⁶³

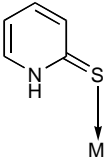
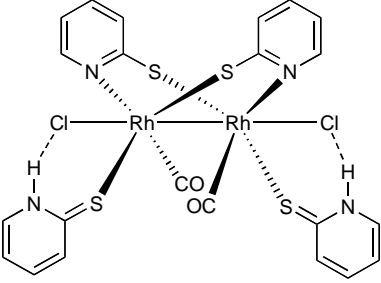
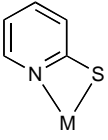
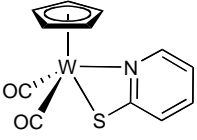
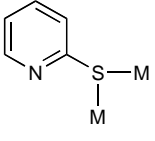
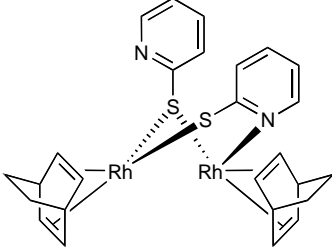
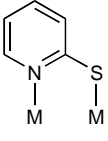
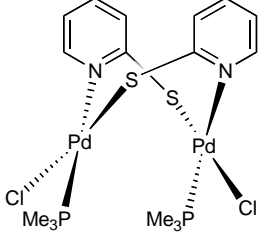
Besides the various application studies on 2-mercaptopyridine and its metal complexes, the free ligand has also been characterized by the thiol-thione tautomerism (Scheme 1.4.1).⁶⁴

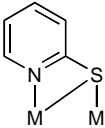
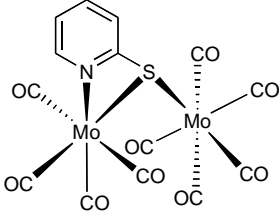
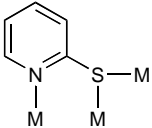
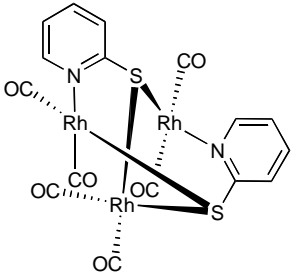
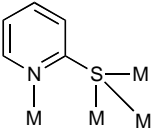
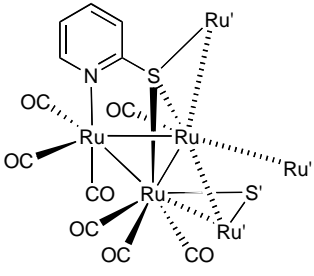


The coordination and structural diversity of metal complexes with 2-mercaptopyridine is also an established field of study. The availability of the soft thionate sulfur and the hard thioamide nitrogen atoms as coordination sites render the ligand extremely versatile, capable of coordinating to a great variety of main-group and transition metal complexes. This is shown in the wide array of metal complexes possessing different bonding modes illustrated in Table 1.4.1.

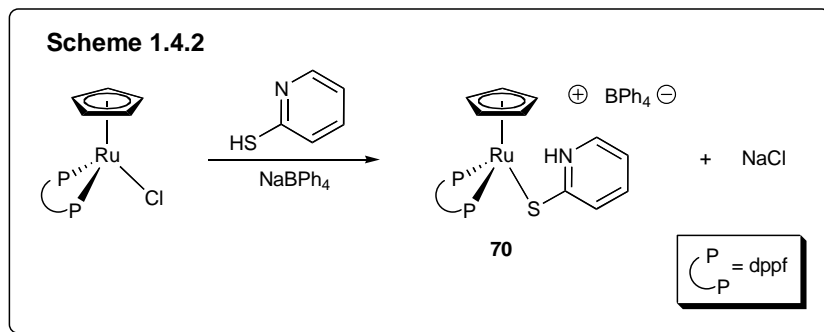
Table 1.4.1. Bonding modes of 2-mercaptopyridine complexes

No	Coordination Modes	Examples	Ref
1	η^1 -S 		65

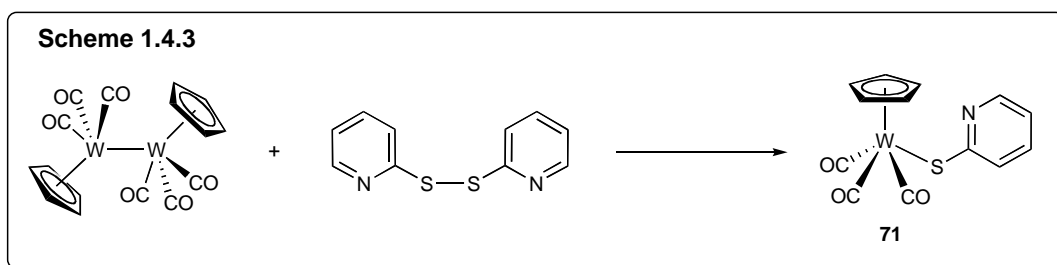
2	$\eta^1\text{-S}$ 		66
3	$\eta^2\text{-(S,N)}$ 		65
4	$\mu\text{-}\eta^1, \eta^1\text{(S,S)}$ 		67
5	$\mu\text{-}\eta^1, \eta^1\text{(S,N)}$ 		68

6	$\mu_2\text{-}\eta^2, \eta^1[(\text{S}, \text{N}), \text{S}]$ 		69
7	$\mu_3\text{-}\eta^1, \eta^1, \eta^1[\text{S}, \text{S}, \text{N}]$ 		70
8	$\mu_4\text{-}\eta^1, \eta^1, \eta^1, \eta^1[\text{S}, \text{S}, \text{S}, \text{N}]$ 		71

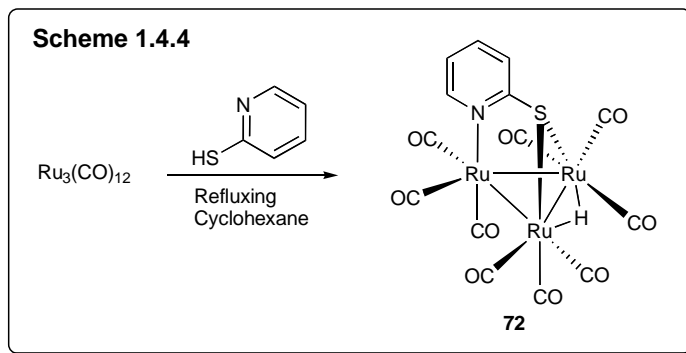
These metal complexes are generally prepared via salt elimination or promoted by small molecule elimination. The concurrent chloride abstraction by NaBPh_4 and coordination of the 2-mercaptopyridine ligand on $\text{CpRu}(\text{dppf})\text{Cl}$ facilitates the formation of the orange complex, $[\text{CpRu}(\text{dppf})(\text{SC}_5\text{H}_4\text{NH})][\text{BPh}_4]$ (**70**), as reported by Goh *et al.* (Scheme 1.4.2).⁷² The 2-mercaptopyridine on the complex was found to have undergone a tautomerism to the thione form, having a N-H proton shift at δ 9.66.



In the synthesis of CpW(CO)₃SPy (**71**), the [CpW(CO)₃]₂ was irradiated to produce the {CpW(CO)₃} radical which will subsequently attack the disulfide bond of the organic molecule (Scheme 1.4.3).⁶⁵ Since **1** readily dissociates into the radical **1A**, it is of interest to us to compare this reaction with that of **1**.

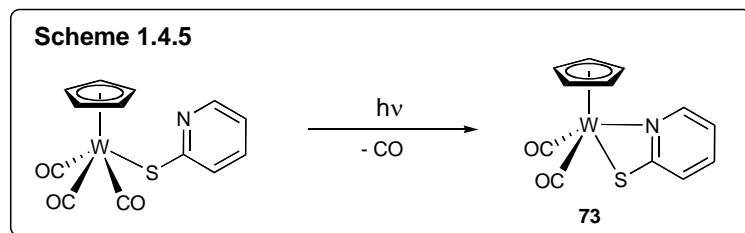


The direct reaction of the ruthenium cluster, Ru₃(CO)₁₂, with pyridine-2-thiol (PySH) was reported by Deeming *et al.*⁷¹ (Scheme 1.4.4). The formation of yellow substituted cluster (**72**) consists of a 2-mercaptopyridine ligand that bridges two ruthenium atoms through the S-atom and bonds to the third ruthenium atom through the pyridine ring. In addition, the acidic proton on the pyridine-2-thiol ligand was transferred onto the tri-ruthenium cluster as a bridging hydride.

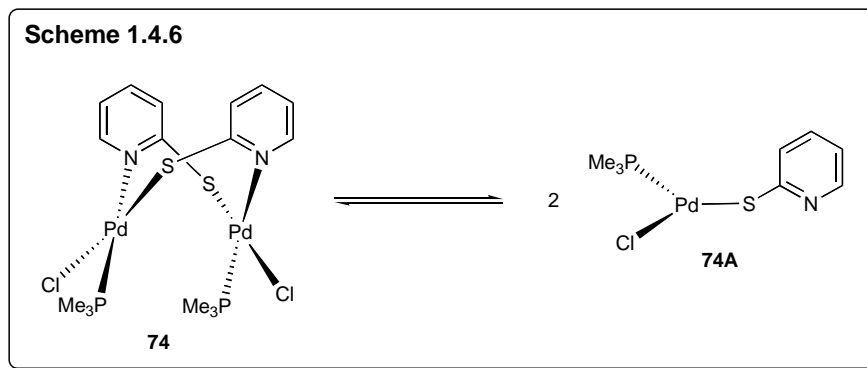


Besides the studies on the structural diversity of the 2-mercaptopyridine complexes, their chemistry and reactivity have also been investigated.

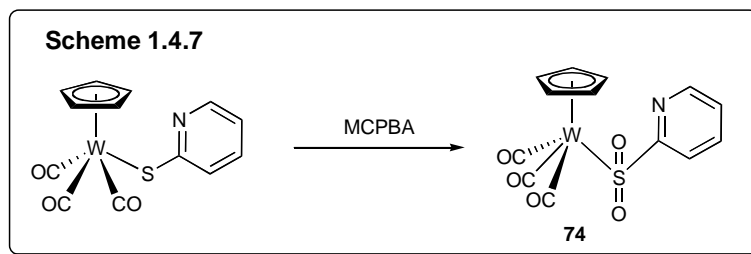
Monodentate 2-mercaptopyridine coordinated to metals can undergo thermal- or photochemical-induced chelation. In the following example, it involves the decarbonylation on the organometallic moiety by photolysis with consequential chelation via the thioamide nitrogen atom (Scheme 1.4.5).⁶⁵



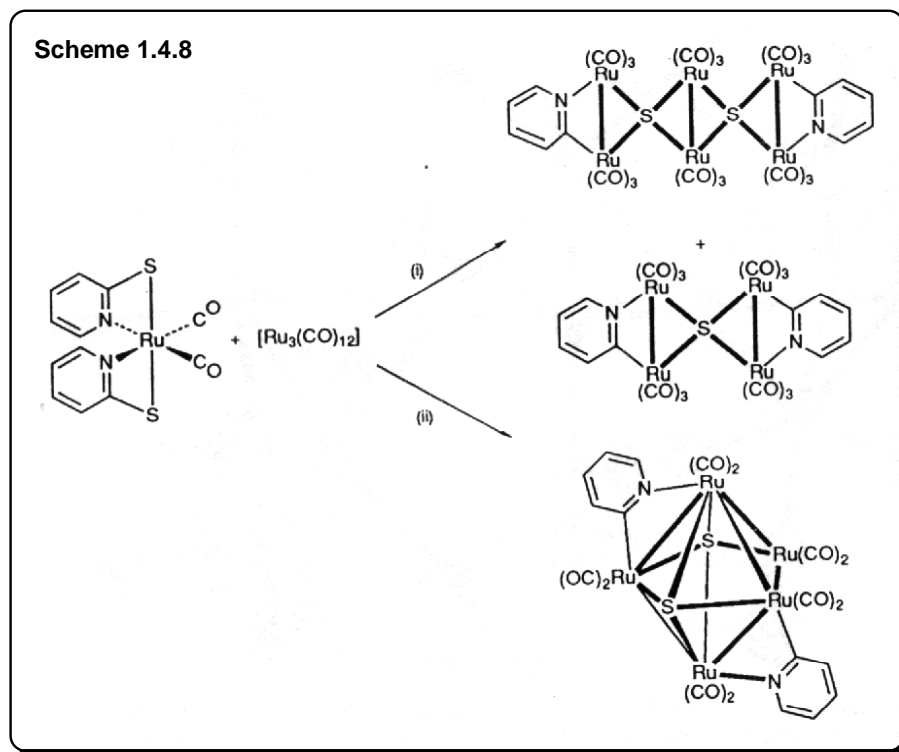
Besides photolytic reactions, bridging 2-mercaptopyridine complexes are often found to be fluxional in solution. Jensen and coworkers have postulated an unusual reversible dimerization of a $\text{Pd}_2(\mu\text{-N,S-}\eta^2\text{-SPy})_2\text{Cl}_2(\text{PMe}_3)_2$ (**74**) complex which involves the rupture of the palladium-nitrogen bond (Scheme 1.4.6).⁶⁸ It was also found that the monomeric species are more stable at higher temperatures.



The monodentate 2-mercaptopyridine ligand bonded on the metal centre can be selectively oxidized by suitable oxidizing agent such as MCPBA (m-chloroperoxybenzoic acid) under rather mild conditions (Scheme 1.4.7).⁷³



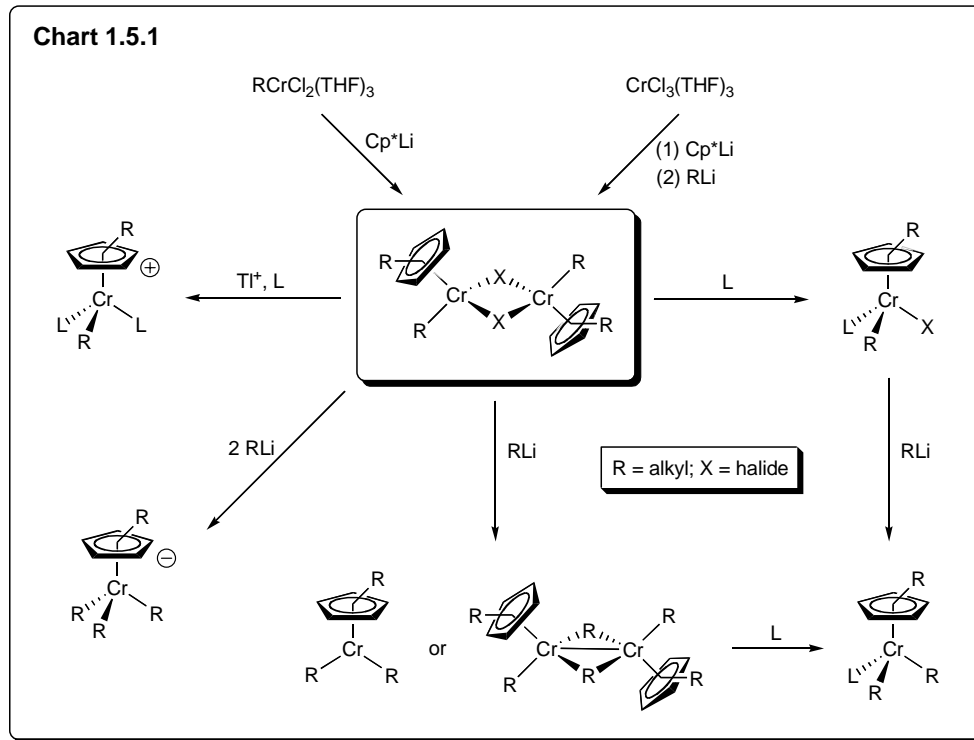
The 2-mercaptopyridine ligand bonded to metal complexes may also undergo complete desulfurisation breaking the C-S bond. This has great impact on the petrochemical industry. The following example involves the complete desulfurisation of 2-mercaptopyridine ligand coordinated to ruthenium yielding a series of ruthenium clusters (Scheme 1.4.8).⁷⁴ Such methodology is useful in the synthesis of metal clusters, which are very useful in the field of catalyst.



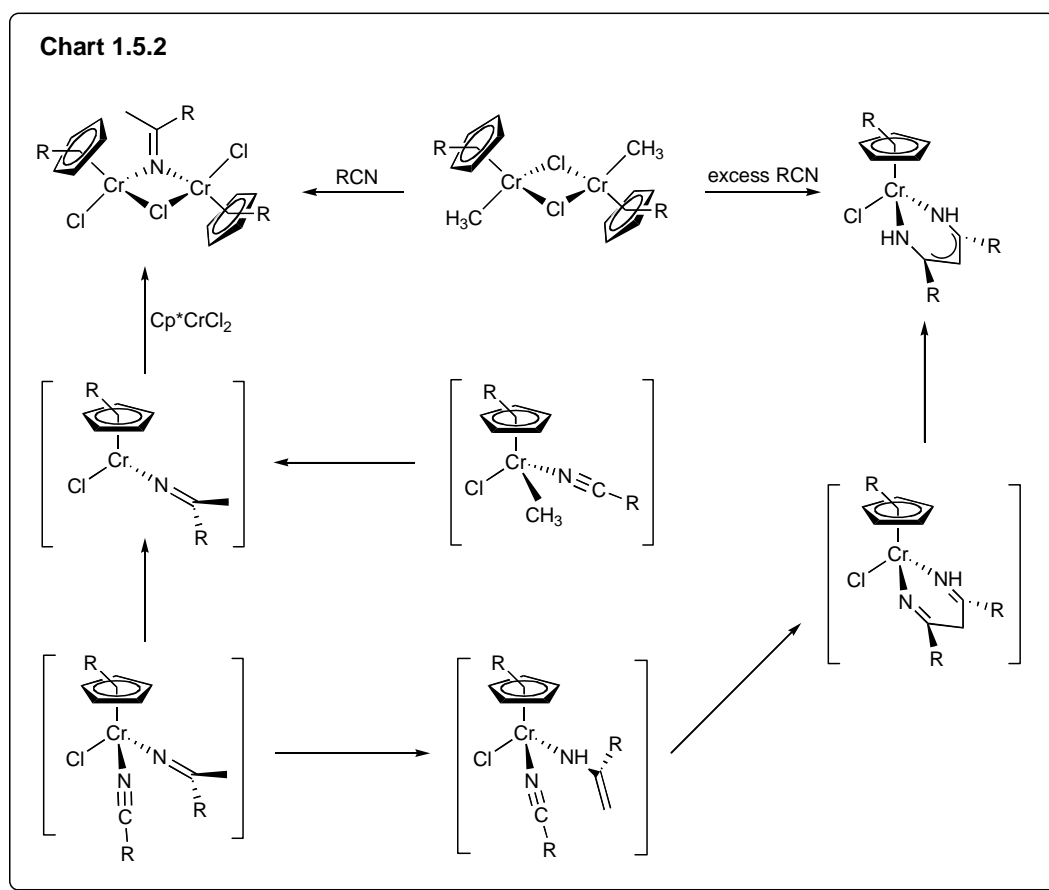
Desulfurisation; (i) Light petrolueum, 150°C, Carius-tube; (ii) Xylene, Reflux.

1.5 Cyclopentadienylchromium(III) complexes.

Unsaturated, high oxidation state, paramagnetic organotransition metal species continue to attract intense interest, on account of their high reactivity.¹ The importance of these paramagnetic compounds in catalytic and stoichiometric organometallic reactions is rapidly gaining pace. Aside from minor applications in the hydrogenation of conjugated dienes and hydrocarbon oxidation,⁷⁵ by far the most important role of chromium catalysis is in the polymerization of small olefins e.g. ethylene, propylene using heterogeneous catalysis.⁷⁶ The paramagnetic nature of these complexes renders non-feasible the use of NMR spectroscopy in their characterization. Hence, structural characterization by x-ray diffraction plays a crucial role in the development of this chemistry.

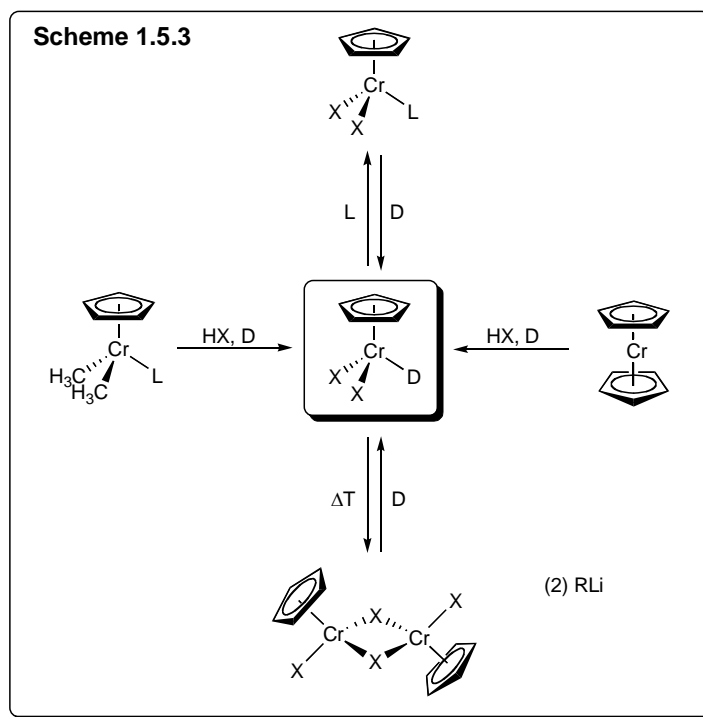


Theopold and coworkers have been the vanguard in this field of organometallic synthesis and catalysis. His work focuses on the synthesis of cyclopentadienylchromium(III) alkyl/halide complexes and their applications on olefin polymerization. Some common synthetic pathways to these complexes are summarized in Chart 1.5.1.⁷⁷ The high reactivity of these cyclopentadienylchromium(III) alkyl/halide complexes is expected since they are often electron-deficient and coordinatively unsaturated. The following example illustrates the facile insertion of an organic nitrile across such complexes (Chart 1.5.2).^{77,78}



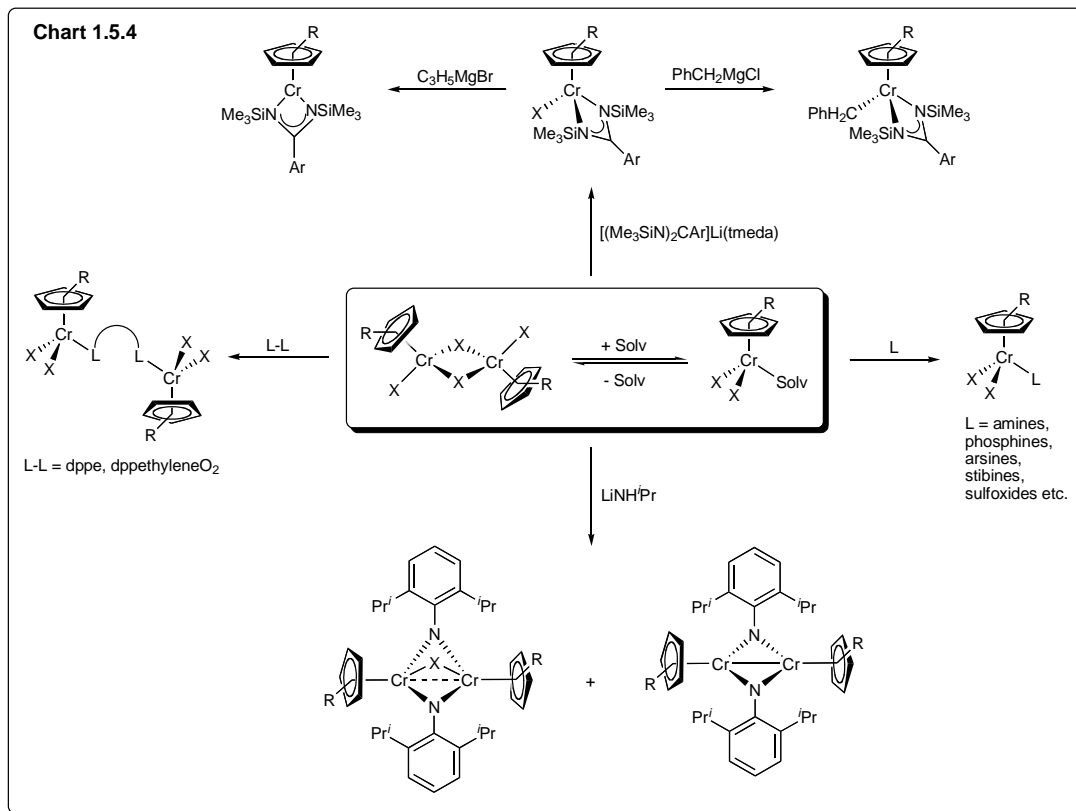
Finally, the common but versatile cyclopentadienylchromium(III) halide complexes have been much studied and reviewed. Besides being electron-deficient, there

often exist some labile ligands, which can be replaced easily. This is definitely a great advantage in the application in organo-catalysis. Given below is a brief overview of some of the common preparation of these complexes (Chart 1.5.3).⁷⁹



The high reactivity of these cyclopentadienylchromium(III) halide complexes is also expected since they are often electron-deficient and coordinatively unsaturated.

Some reactions of such complexes are summarized in Chart 1.5.4.^{79,80}

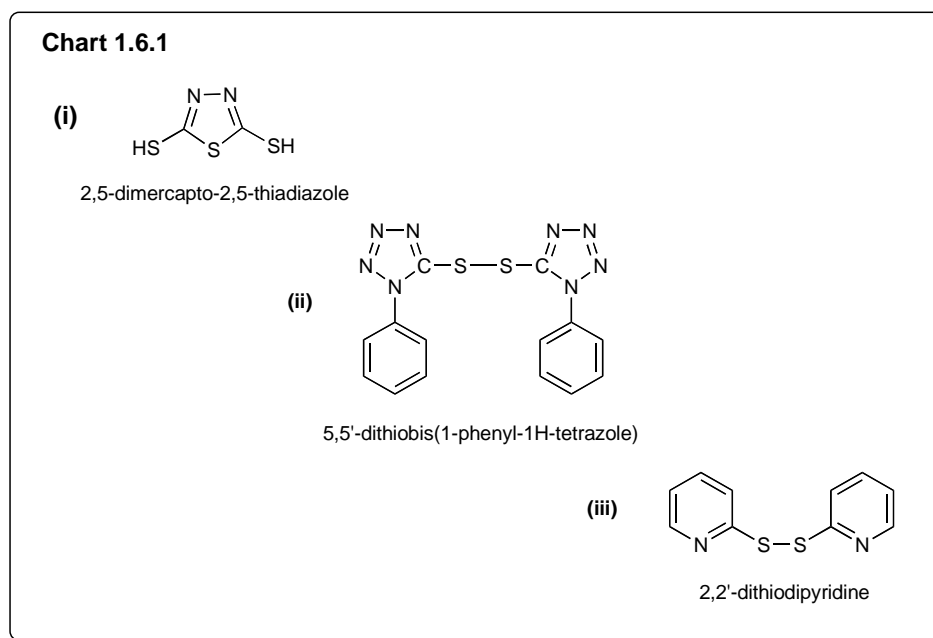


The synthesis and characterization of these paramagnetic reactive cyclopentadienylchromium(III) complexes have opened up a whole new plethora of opportunities for their application in organometallic catalysis. Further investigations into these systems will be both essential and rewarding.

1.6 Objectives.

This project was aimed at the investigation of the reactivity of $[\text{CpCr}(\text{CO})_3]_2$ (**1**) towards organic substrates, containing S-H, S-S, C-S, C-N and N-N bonds, as found in (i) 2,5-dimercapto-1,3,4-thiadiazole, (ii) 5,5'-dithiobis(1-phenyl-1H-tetrazole) and (iii) 2,2'-dithiodipyridine, as show in Chart 1.6.1.

In addition to products arising from the homolytic cleavage by **1A**, of the group 15 and 16 nonmetal–nonmetal bonds, the reactivity of the primary organochromium products towards acids, methylating reagents and metal fragments will be investigated.



2.1 The reaction of $[\text{CpCr}(\text{CO})_3]_2$ (**1**) with 2,5-dimercapto-1,3,4-thiadiazole (DMcTH₂)

2.1.1 Products and reaction pathways

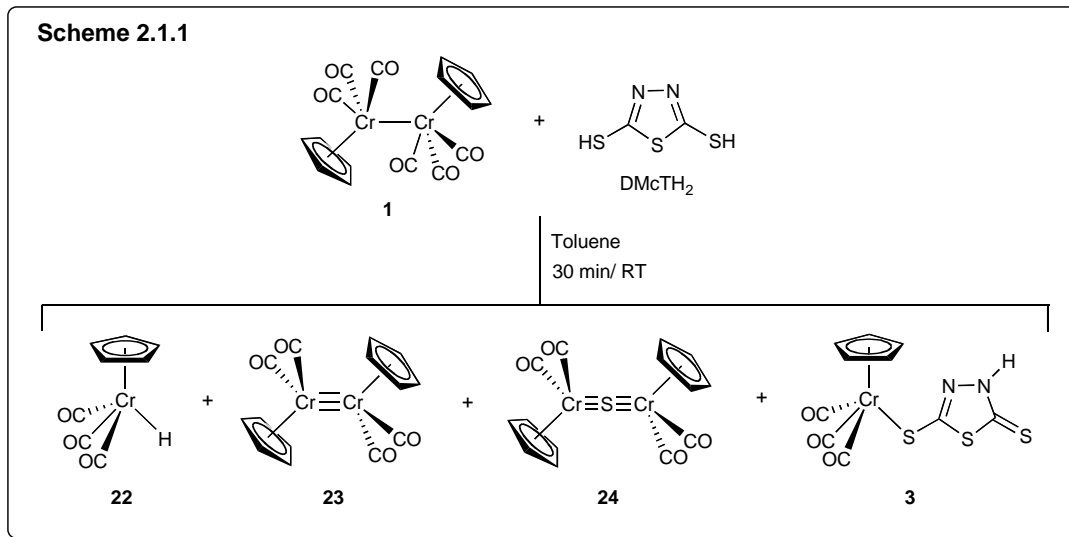
Using 1 (**1**) : 1 DMcTH₂

A facile reaction between $[\text{CpCr}(\text{CO})_3]_2$ (**1**) and one mole equivalent of DMcTH₂ in toluene at ambient temperature produced a deep red solution. From this solution, a moderate yield of $\text{CpCr}(\text{CO})_3(\eta^1\text{-DMcTH})$ (**3**) (28%) was obtained as red crystals, along with some known complexes, namely $\text{CpCr}(\text{CO})_3\text{H}$ (**22**), $[\text{CpCr}(\text{CO})_2]_2$ (**23**) and $[\text{CpCr}(\text{CO})_2]_2\text{S}$ (**24**) (Scheme 2.1.1), together with an uncharacterizable green oil (Scheme 2.1.1). The chelate derivative $\text{CpCr}(\text{CO})_2(\eta^2\text{-DMcTH})$ was not observed, probably due to incompatible orientation of the nitrogen or sulfur orbitals to match that of the central chromium metal centre, and/or a more thermodynamically favourable decomposition of **3** to an insoluble dirty green solid which was isolated.

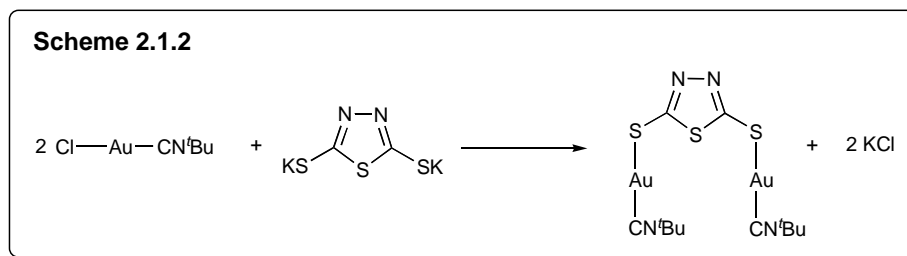
Spectral characteristics of **3**

Its infrared spectrum in KBr disc shows three CO absorption bands (2034s, 1954s, 1890s), which falls in the normal range for stretching frequency for *cis* terminal carbonyls. In addition, there is a strong N-H stretch at 3099 cm^{-1} . The ¹H NMR spectrum shows the Cp (¹H) peak at δ 4.00 (s, 5H) and NH (¹H) peaks at δ 8.93 (s, 1H). The ¹³C NMR spectrum is not available owing to the instability of the complex in solution. The FAB⁺-MS showed the molecular ion peak at m/z 351. High resolution FAB⁺-MS showed

m/z 350.9016, which is in close agreement to the calculated value of 350.9024, but elemental analysis was unsatisfactory due to its instability.

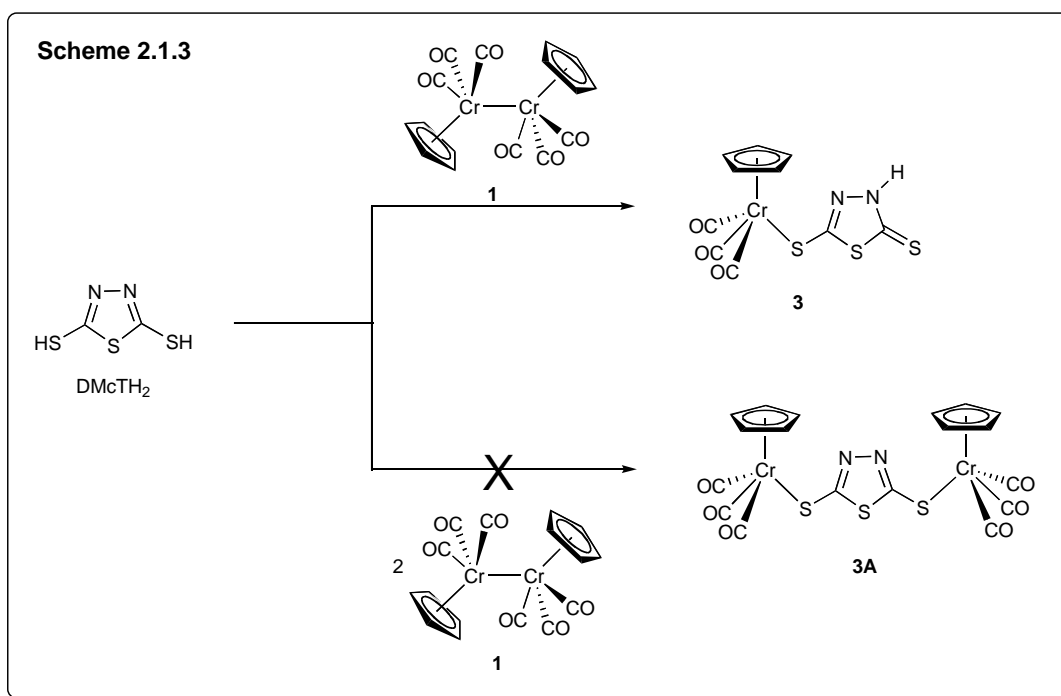


Many binuclear gold complexes were synthesized using the potassium salt of 2,5-dimercapto-1,3,4-thiadiazolate with 2 mole equivalent of chloro-gold complexes, e.g. as shown in Scheme 2.1.2.^{32a} Since the 17-electron organometallic fragment **1A** is a very efficient hydride abstractor, we thought that 2 mole equivalents of **1** could react with 1 mol equivalent of DMcTH₂ to yield a similar binuclear chromium complex with the concurrent formation of **22**.



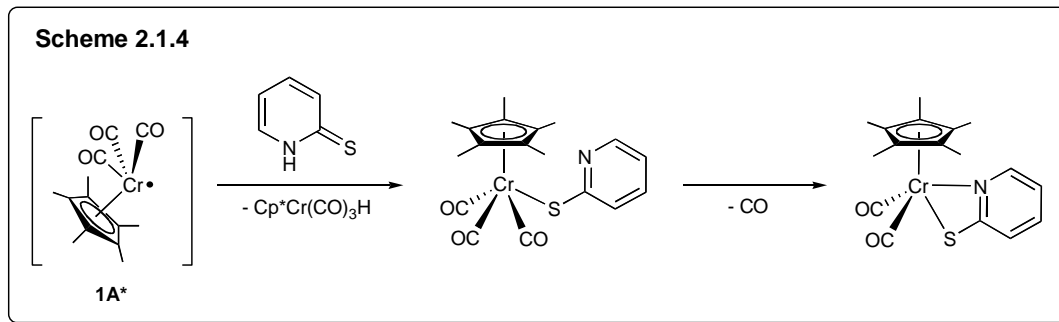
Using 2 (**1**) : 1 DMcTH₂

The reaction was hence carried out at 90 °C with 2 mol equivalents of **1** to DMcTH₂. In fact, the product composition of this particular reaction is very similar to that obtained above (Scheme 2.1.3) and the probable binuclear-chromium complex (**3A**) with a bridging 2,5-dimercapto-1,3,4-thiadiazolate (DMcT²⁻) was not observed. It appears that the excess **1** was converted to the triply bonded Cr≡Cr-dimer, [CpCr(CO)₂]₂ (**23**), and **3** degraded to an insoluble dirty green solid. Indeed, this degradation was confirmed in separate ¹H NMR tube experiments, which showed that (i) **3** prepared in situ from the reaction of **1** with DMcTH₂ degraded at extended reaction time and (ii) the degradation of **3** was faster at higher concentrations.



Hoff and coworkers had carried out a reaction between [Cp*Cr(CO)₃]₂ (**1***) and thione-amide ligands.⁸¹ It was reported that the coordination of the thione S atom to the {Cp*Cr(CO)₃} (**1A***) fragment first takes place, followed by the abstraction of the amide

proton by a second fragment of **1A*** (Scheme 2.1.4). However, in our case, a similar reaction did not take place.



2.1.2 Crystallographic studies

The ORTEP of **3** is depicted in Figure 2.1.1. The unit cell contains two independent molecules of the compound. The two molecules differ in the orientation of the heterocyclic rings. Selected bond lengths and angles are listed in Table 2.1.1. The molecule possesses a four-legged piano-stool configuration at Cr, which is coordinated to a monodentate 2,5-dimercapto-1,3,4-thiadiazolate and three CO ligands. The S(3)-C(5) bond length of 1.683(7) Å is within the range of the C=S double bond, and is slightly shorter than the other C-S bond (1.719(7) Å) in the heterocycle as indicated in Table 2.1.1. This pair of C-S and C=S bond lengths is comparable to that in complexes [Pt(trpy)₂(η¹-TDZ)](PF₆) (1.64(1) and 1.75(1) Å)³¹ and [Ru(CO)(PPh₃)₂(η¹-TDZ)((η²-TDZ)] (1.67(2) and 1.71(2) Å).³⁰ The bond length of N(1)-C(4) (1.289(8) Å) is shorter than N(2)-C(5) (1.321(8) Å) indicative of C=N double bond character versus a C-N single bonding mode, respectively. The bond length of N(1)-N(2) (1.372(7) Å) is within the range of the N-N single bond length of 1.24 - 1.40 Å.⁸² The Cr(1)-S(1)-C(4) angle is 108.0(3)° indicative of a bent geometry. In addition, the bond angles of S(2)-C(5)-S(3)

(124.6(4) Å), N(2)-C(5)-S(3) (127.5(5) Å) and N(2)-C(5)-S(2) 107.8(5) Å), indicates a distorted trigonal geometry around the C(5) atom.

Table 2.1.1. Selected bond lengths (Å) and angles (deg) for **3**

Bond lengths (Å)			
Cr(1)-S(1)	1.857(8)	S(1)-C(4)	1.719(7)
S(2)-C(5)	1.733(7)	S(2)-C(4)	1.764(7)
S(3)-C(5)	1.683(7)	N(1)-C(4)	1.289(8)
N(1)-N(2)	1.372(7)	N(2)-C(5)	1.321(8)
Bond angles (deg)			
Cr(1)-S(1)-C(4)	108.0(3)	S(2)-C(5)-S(3)	124.6(4)
N(2)-C(5)-S(3)	127.5(5)	N(2)-C(5)-S(2)	107.8(5)

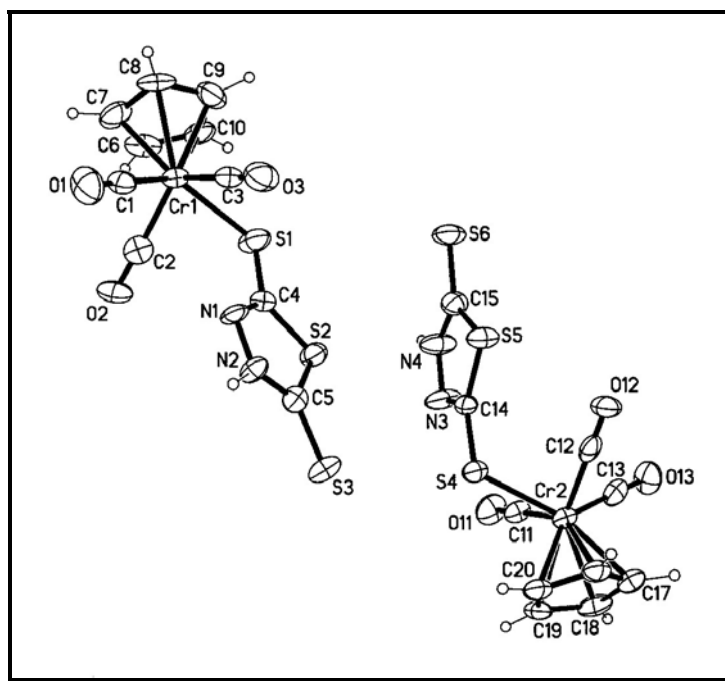


Figure 2.1.1. Molecular structure of CpCr(CO)₃(DMcTH) (**3**). Thermal ellipsoids are drawn at the 50% probability level.

2.1.3 Conclusion

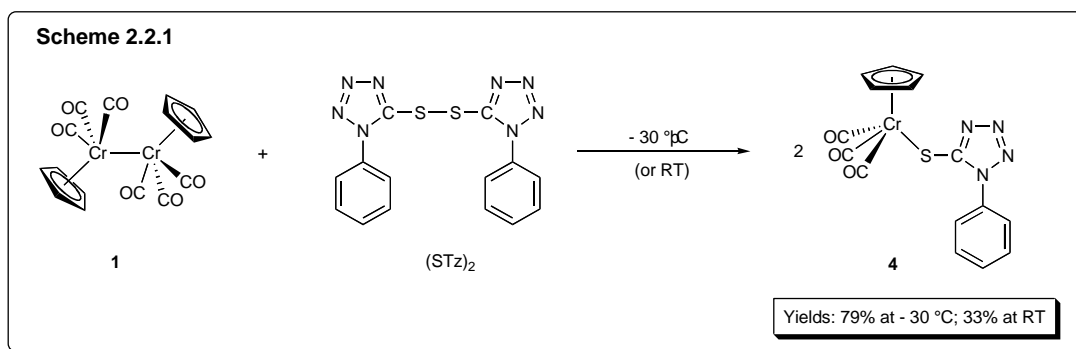
The reaction of [CpCr(CO)₃]₂ with 2,5-dimercapto-1,3,4-thiadiazole (DMcTH₂), demonstrates the facile S–H homolytic bond cleavage by the 17-electron organometallic species **1A**, providing an efficient route to the 2,5-dimercapto-1,3,4-thiadiazolate (DMcTH) cyclopentadienyl chromium complexes. This is the first example of a Cp-containing 2,5-dimercapto-1,3,4-thiadiazolate complex that has been synthesized.

The coordination of the DMcTH₂ and the Cp ligands, both of which are uninegatively charged, together with two neutral CO molecules confers a +2 oxidation state on Cr(1) atom. The organometallic complex obeys the 18-electron rule but is highly unstable even in the solid state. The reason for its high instability is probably due to the presence of other donating atoms, which may consequently result in oligomerization or even polymerization. This may be one reason why the chelated product CpCr(CO)₂(η²-DMcTH) was not formed.

2.2 The reaction of $[\text{CpCr}(\text{CO})_3]_2$ (**1**) with 5,5'-dithiobis(1-phenyl-1H-tetrazole) (**STz**)₂

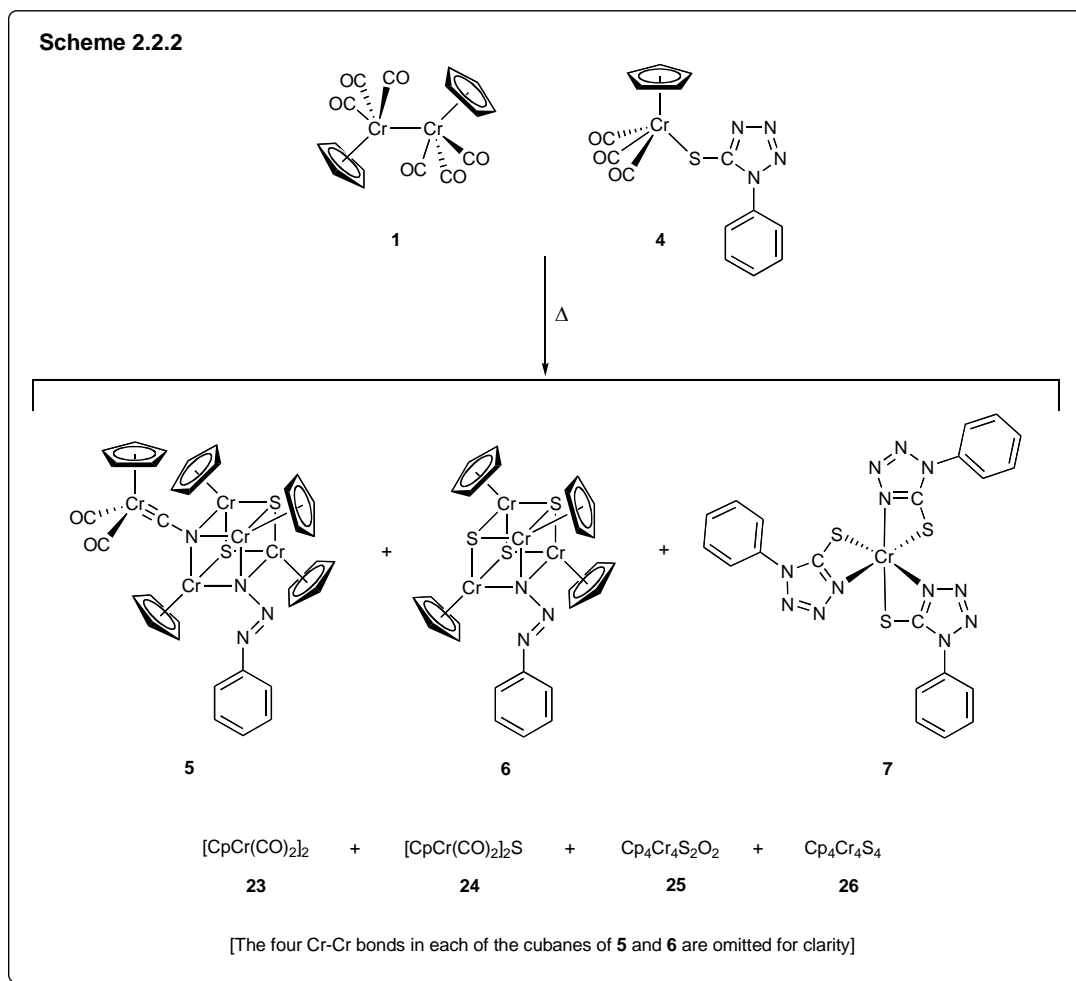
2.2.1 Products and reaction pathways

A facile reaction between $[\text{CpCr}(\text{CO})_3]_2$ (**1**) and one mole equivalent of (**STz**)₂ in toluene at ambient temperature produced a magenta solution. From this solution, moderate yield of $\text{CpCr}(\text{CO})_3(\text{STz})$ (**4**) (33%) was obtained as red crystals. When the same reaction was repeated at $-30\text{ }^\circ\text{C}$, the yield of **4** increased to 79% (Scheme 2.2.1).



When **4** was stirred at high temperatures or more than 24 h, it was found to convert quantitatively to a purple insoluble solid. This IR spectrum of the insoluble purple powder indicates the absence of $\text{C}\equiv\text{O}$ stretches. The elemental analysis could not be rationalized but showed the presence of C, H, N, S and Cr. The chelate derivative $\text{CpCr}(\text{CO})_2(\eta^2\text{-STz})$ was not observed probably due to similar reasons which was discussed in Section 2.1.1, in this case the incompatible orientation of the N-orbitals and the formation of an insoluble purple solid.

The cothermolysis of $\text{CpCr}(\text{CO})_3(\text{STz})$ (**4**) with $[\text{CpCr}(\text{CO})_3]_2$ (**1**) in refluxing toluene for 2 h led to the isolation of the $[\text{CpCr}(\text{CO})_2]_2$ (**23**) (34%) and $[\text{CpCr}(\text{CO})_2]_2\text{S}$ (**24**) (6%) as a mixture of deep green crystals, the chromium aminocarbonyne-cubane complex $\text{Cp}_4\text{Cr}_4\text{S}_3(\text{N}_3\text{Ph})(\text{CpCr}(\text{CO})_2\text{CN})$ (**5**) as brown crystalline solids (4%), the triazenido-cubane complex $\text{Cp}_4\text{Cr}_4\text{S}_3(\text{N}_3\text{Ph})$ (**6**) as brown microcrystal (7%), the μ_3 -oxo cubane complex $\text{Cp}_4\text{Cr}_4\text{S}_2\text{O}_2$ (**25**) (9%) as dark greenish crystals, the coordination complex $\text{Cr}(\text{SCN}_4\text{Ph})_3$ (**7**) (1%) as blue solids and the cubane $\text{Cp}_4\text{Cr}_4\text{S}_4$ (**26**), as presented in Scheme 2.2.2.

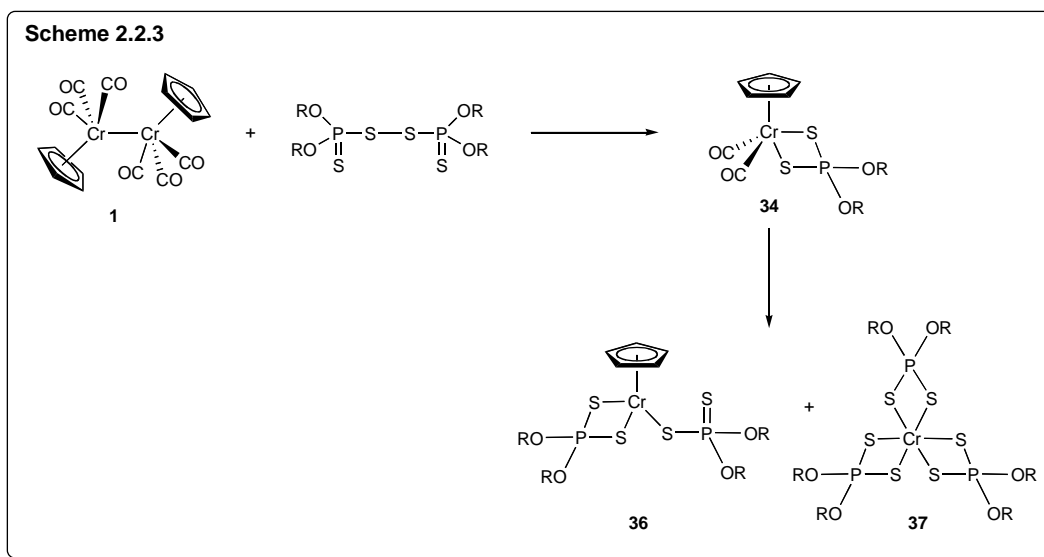
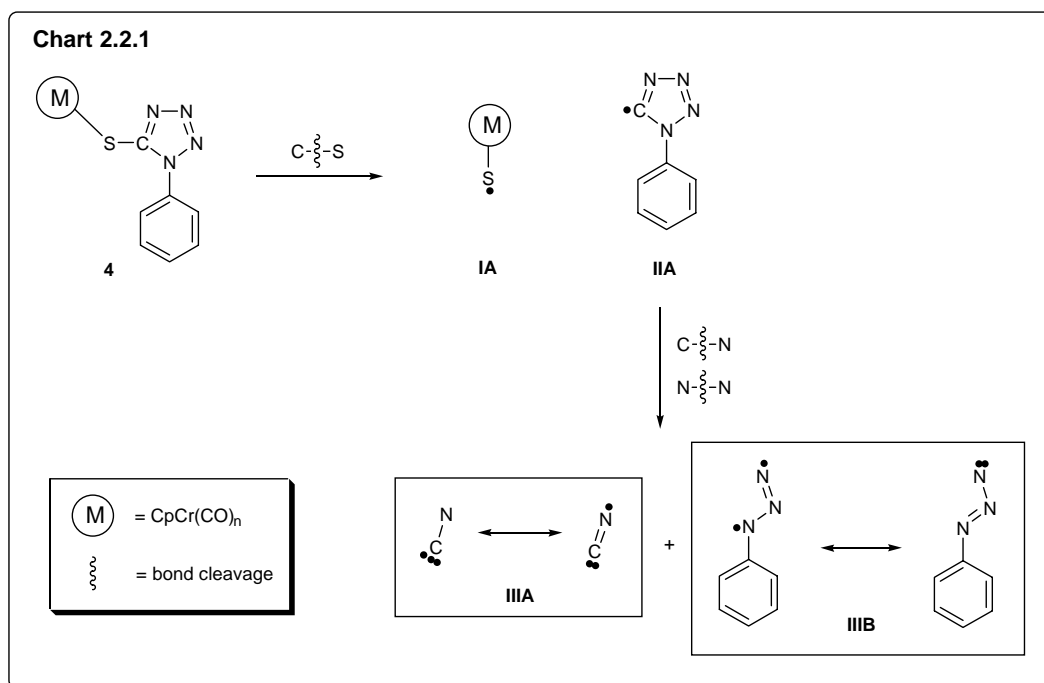


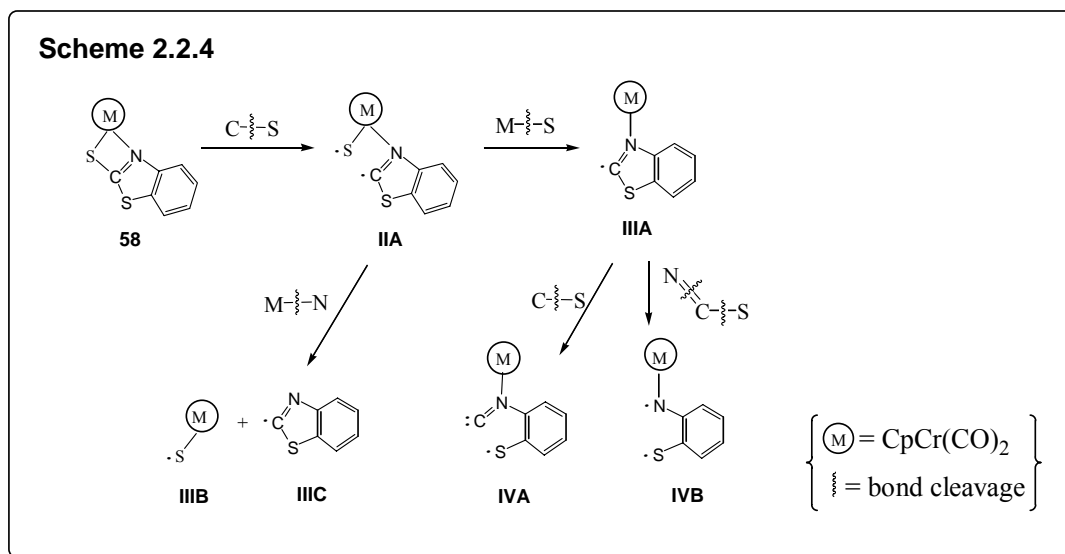
2.2.2 Mechanistic considerations

As in the reactions with the S–S organic disulfides described in previous sections, the reaction is likely to be initiated by the attack of {CpCr(CO)₃} (**1A**) on the S–S bond of 5,5'-dithiobis(1-phenyl-1H-tetrazole), forming complex **4**. Scheme 2.2.2 shows the interaction of **4** with [CpCr(CO)₃]₂ to yield the polynuclear chromium complexes **5**, **6**, **25** and **26**, together with [CpCr(CO)₂]₂ (**23**), [CpCr(CO)₂]₂S (**24**) and Cr(SCN₄Ph)₃ (**7**).

The structural composition of **5**, **6**, **24**, **25** and **26** supports their formation from moieties, either discrete or quasi-associated, arising from the sequential cleavage of C–S, Cr–S, N–N and C–N bonds in **4**, as proposed in Chart 2.2.1; thus **5** was formed via a Cr-aminocarbyne through the interaction of CpCr(CO)₂ with a CN moiety **IIIA**, and subsequent combination with 4 molar equivalent of **IA** fragment and the triazenido moiety **IIIB**, with the loss of CO ligands. The direct interaction of 4 mole equivalents of fragment **IA** and the triazenido moiety **IIIB**, with the loss of a S atom and CO ligands would give **6**. In addition, the formation of **7** must have involved the loss of CO and Cp ligands from **4** with concomitant or subsequent intermolecular association, followed by bond dissociations via an intermediate such as “CpCr(η¹-STz)(η²-STz)”, a process previously described by Goh *et al.* in the production of Cr(S₂P(OR)₂)₃ in a reaction of bis(thiophosphoryl)disulfanes^{21,26} with **1** (Scheme 2.2.3) and that of Cr(S₂CNR₂)₃ in a reaction of tetralkylthiuram disulfides^{24,26} with **1**. It is clear that **1** plays a vital role in these transformations, via its incumbent monomer, {CpCr(CO)₃} (**1A**) derived from its facile dissociation in solution.⁵ The isolation of the cubane Cp₄Cr₄S₄ (**26**), the ultimate thermolysis product of [CpCr(CO)₂]₂S,^{17a} indicated that **1A**, a powerful thiophile, had abstracted a sulfur atom from **4**, probably in an initial step in the process. Based on previous findings of Goh and coworkers on the cothermolysis of **1** and

$\text{CpCr}(\text{CO})_2(\text{SCSN}(\text{C}_6\text{H}_4))$ (See Schemes 1.1.7 and 2.2.4),²⁵ a mechanism involving the aggregation of radicals was proposed here to rationalize the formation of products obtained at elevated temperatures (Chart 2.2.1). It was found that the formation of these polynuclear complexes only occurred at elevated temperatures.





2.2.3 Spectral features.

(i) $\text{CpCr}(\text{CO})_3(\text{SCN}_4\text{Ph})$ (**4**):

IR: The IR stretching frequencies for the CO ligands in the complexes **4** are found in the normal carbonyl region for terminal ligands.

NMR: The mononuclear complex **4** possesses a Cp resonance at δ 4.32 in the ¹H NMR spectrum.

FAB⁺-MS showed the molecular ion peak at m/z 378.

(ii) $\text{Cp}_4\text{Cr}_4\text{S}_2(\text{N}_3\text{Ph})(\text{CpCr}(\text{CO})_2\text{CN})$ (**5**):

IR: The CO stretching frequencies are observed at 1923 and 1854 cm^{-1} ; the $\nu(\text{N}=\text{N})$ are observed at 1401, 1203 and 1167 cm^{-1} .

NMR: The proton Cp resonance of the pentanuclear complex **5** is observed at δ 4.64, 4.93, 5.13 and 5.48 with relative intensity 1:1:2:1. It is consistent with the structure since Cr(1) and Cr(3) are equivalent, which results in a Cp proton shift at δ 5.13 double the intensity that of others.

FAB⁺-MS showed the molecular ion peak at m/z 850.

(iii) Cp₄Cr₄S₃(N₃Ph) (6):

IR: the $\nu(\text{N-N=N})$ are observed at 1430, 1277 and 1174 cm^{-1} .

NMR: The proton Cp resonance of the tetranuclear complex **6** is observed at δ 4.87 and 5.08 with relative intensity 1:3 respectively. It is consistent with the proposed structure since three of the chromium atoms that are bonded to three $\mu_3\text{-S}$ and one $\mu_3\text{-N}$ in the cubane are equivalent, hence resulting in a Cp proton shift at δ 5.08 that has three times the intensity of the other.

FAB⁺-MS showed the molecular ion peak at m/z 683.

(iv) Cr(SCN₄Ph)₃ (7):

IR: The IR spectrum did not give much information except for the absence of CO stretches.

NMR: There are no observable signals in 'normal' region of the ¹H NMR spectrum, indicative of paramagnetism.

FAB⁺-MS showed the molecular ion peak at m/z 583.

2.4.4. Crystallographic studies

(i) CpCr(CO)₃(SCN₄Ph) (4):

The ORTEP of **4** is depicted in Figure 2.2.1. Selected bond lengths and angles are listed in Table 2.2.1. The molecule possesses a four-legged piano-stool coordination at Cr, which is coordinated to a monodentate 5-mercapto(1-phenyl-1H-tetrazole) and three terminal CO ligands. The S(1)-C(4) bond length of 1.730(2) Å is within the range of the single C-S bonds and comparable to the C-S bond in complexes CpCr(CO)₃($\eta^1\text{-S}_2\text{CNR}_2$) (R = Me, Et, ^{*i*}Pr) reported by Goh *et al.* The bond length of N(2)-N(3) (1.290(3) Å) is shorter than N(1)-N(2) (1.346(3) Å) and N(3)-N(4) (1.368(3) Å) indicative of the N=N

double bond character. The C(4)-N(1) bond length is also within the range for C=N bonding. The Cr(1)-S(1)-C(4) angle is 107.92(7) indicative of a bent geometry. This complex is very similar to the iron analogue, $\text{CpFe}(\text{CO})_2(\text{SCN}_4\text{Ph})$ (**15**) reported in Section 2.4.

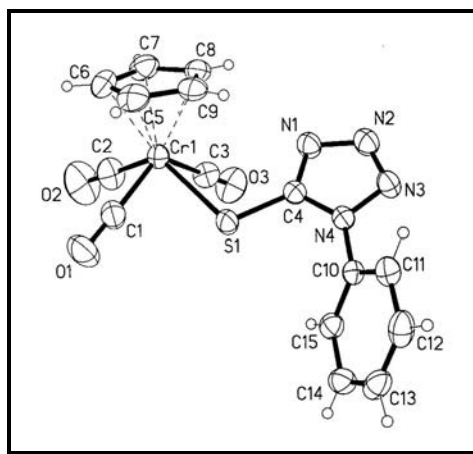


Figure 2.2.1. Molecular structure of $\text{CpCr}(\text{CO})_3(\text{SCN}_4\text{Ph})$ (**4**). Thermal ellipsoids are drawn at the 50% probability level.

Table 2.2.1. Selected bond distances (Å) and angles (deg) for **4**

Bond Distances (Å)			
Cr(1)-S(1)	2.4482(7)	S(1)-C(4)	1.730(2)
C(4)-N(1)	1.333(3)	C(4)-N(4)	1.346(3)
N(1)-N(2)	1.346(3)	N(2)-N(3)	1.290(3)
N(3)-N(4)	1.368(3)	N(4)-C(10)	1.425(3)
Bond Angles (deg)			
Cr(1)-S(1)-C(4)	109.40(8)		

(ii) **$\text{Cp}_4\text{Cr}_4\text{S}_2(\text{N}_3\text{Ph})(\text{CpCr}(\text{CO})_2\text{CN})$ (**5**):**

The ORTEP of **5** is depicted in Figure 2.2.2. Selected bond lengths and angles are listed in Table 2.2.2. A significant feature is the $\text{Cr}_4\text{S}_2\text{N}_2$ cube, in which all the four Cr corners are still attached to η^5 -Cp rings. The two μ_3 -bonding S(1) and S(4) is linked to

Cr(1), Cr(2), Cr(3) and Cr(4). The μ_3 -amino N(3) corner of the cube is singly-bonded (bond length 1.294(4) Å) to C(2), which itself is a metallo-carbyne, bonded to Cr(5). The triazenido ligand (N-N=N-) forms the last corner of the imperfect cube. The Cr-Cr distances have been found to be in the range 2.7031(9)–2.7653(9) Å for the cubane. The chromium-carbyne Cr(5)≡C(2) bond length of 1.748(4) Å compares favourably with the values of 1.735(4)–1.745(3) Å in the half-sandwich aminocarbyne complexes $\text{CpCr}(\text{CNR}_2)(\text{tBuNC})_2\text{X}$ (X = Br, tBuNC),⁸³ and 1.740(2) Å in $\text{CpCr}(\text{CO})_2(\text{CNMe}_2)$ (**12a**).²⁴ The bond length of N(2)-N(4) of 1.217(5) Å is significantly shorter than that of N(1)-N(2) of 1.397(5), which is slightly shorter than the range of N=N double bonds reported for a series of group 10 metal triazenido complexes of 1.26(3) – 1.28(6) Å.⁸⁴ However, the $\angle\text{NNN}$ in our cubane complex of 128.7(5)° was found to be much larger than the series of group 10 metal complexes (111(2)°- 116(2)°) mentioned earlier.

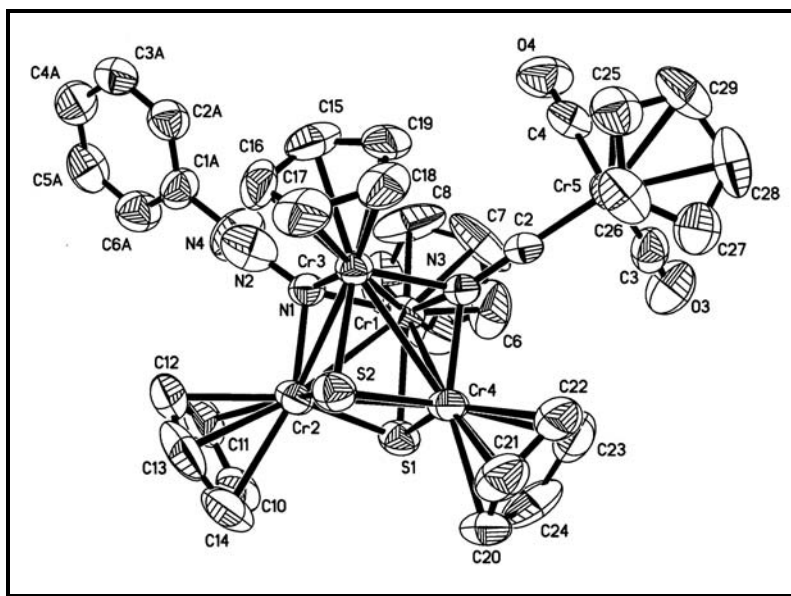


Figure 2.2.2. Molecular structure of $\text{Cp}_4\text{Cr}_4\text{S}_3(\text{N}_3\text{Ph})(\text{CpCr}(\text{CO})_2\text{CN})$ (**5**). Thermal ellipsoids are drawn at the 50% probability level.

Table 2.2.2. Selected bond distances (Å) and angles (deg) for **5**

Bond Distances (Å)			
Cr(1)-N(1)	1.957(3)	Cr(1)-N(3)	2.001(3)
Cr(1)-S(1)	2.2458(13)	Cr(1)-Cr(3)	2.7031(9)
Cr(1)-Cr(2)	2.7615(9)	Cr(1)-Cr(4)	2.7653(9)
Cr(2)-N(1)	1.962(3)	Cr(2)-S(2)	2.2457(13)
Cr(2)-S(1)	2.2533(13)	Cr(2)-Cr(3)	2.7256(9)
Cr(2)-Cr(4)	2.8123(10)	Cr(3)-N(1)	1.966(3)
Cr(3)-N(3)	2.006(3)	Cr(3)-S(2)	2.2445(12)
Cr(3)-Cr(4)	2.7986(9)	Cr(4)-N(3)	2.012(3)
Cr(4)-S(1)	2.2387(13)	Cr(4)-S(2)	2.2490(13)
Cr(5)-C(2)	1.748(4)	N(1)-N(2)	1.397(5)
N(2)-N(4)	1.217(5)	N(3)-C(2)	1.294(4)
N(4)-C(1A)	1.421(6)		
Bond Angles (deg)			
N(1)-Cr(1)-N(3)	94.22(13)	N(1)-Cr(1)-S(1)	96.90(10)
N(3)-Cr(1)-S(1)	98.00(9)	N(1)-Cr(2)-S(2)	98.46(10)
N(1)-Cr(2)-S(1)	96.51(10)	S(2)-Cr(2)-S(1)	100.82(5)
N(1)-Cr(3)-N(3)	93.77(13)	N(1)-Cr(3)-S(2)	98.37(10)
N(3)-Cr(3)-S(2)	96.71(9)	N(3)-Cr(4)-S(1)	97.88(9)
N(3)-Cr(4)-S(2)	96.38(9)	S(1)-Cr(4)-S(2)	101.17(5)
C(2)-Cr(5)-C(3)	88.08(19)	C(4)-Cr(5)-C(3)	93.9(2)
Cr(4)-S(1)-Cr(1)	76.14(4)	Cr(4)-S(1)-Cr(2)	77.52(4)
Cr(1)-S(1)-Cr(2)	75.73(4)	Cr(3)-S(2)-Cr(2)	74.75(4)
Cr(3)-S(2)-Cr(4)	77.04(4)	Cr(2)-S(2)-Cr(4)	77.46(4)
Cr(1)-N(1)-Cr(2)	89.61(14)	Cr(1)-N(1)-Cr(3)	87.10(14)
Cr(2)-N(1)-Cr(3)	87.88(13)	Cr(1)-N(3)-Cr(3)	84.86(13)
Cr(1)-N(3)-Cr(4)	87.12(12)	Cr(3)-N(3)-Cr(4)	88.29(12)
N(4)-N(2)-N(1)	128.7(5)	N(2)-N(4)-C(1A)	118.0(5)
N(3)-C(2)-Cr(5)	179.0(3)		

2.4.5. Conclusion.

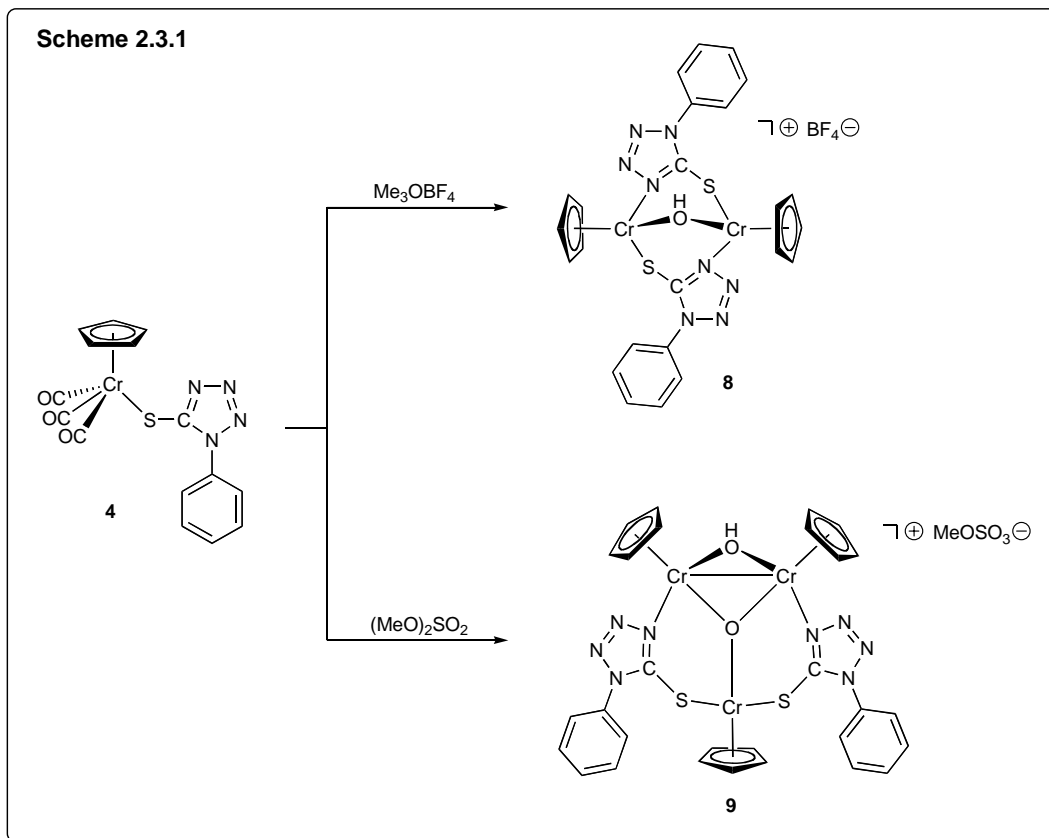
The homolytic S–S bond cleavage in 5,5'-dithiobis(1-phenyl-1H-tetrazole) (C₆H₅N₄CS)₂ by {CpCr(CO)₃} (**1A**) has provided a facile route to the cyclopentadienyl 5-mercapto(1-phenyl-1H-tetrazole) chromium complex CpCr(CO)₃(SCN₄Ph) (**4**). Further reaction of **4** with [CpCr(CO)₃]₂ (**1**) resulted in extensive cleavage of C–S, C–N, Cr–S, N–N bonds in the metal complex and tetrazole ring, giving fragments which assemble to form new polynuclear chromium compounds with novel structural features, viz. Cp₄Cr₄S₃(N₃Ph)(CpCr(CO)₂CN) (**5**), and Cp₄Cr₄S₃(N₃Ph) (**6**), together with the coordination complex Cr(SCN₄Ph)₃ (**7**). Most of the products formed in this reaction are diamagnetic since they result from radical coupling. However, some products e.g. complex **7**, are paramagnetic owing to the presence of Cr(III).

2.3 Reactions of $\text{CpCr}(\text{CO})_3(\eta^1\text{-STz})$ (**4**)

2.3.1 Reactions with methylating agents

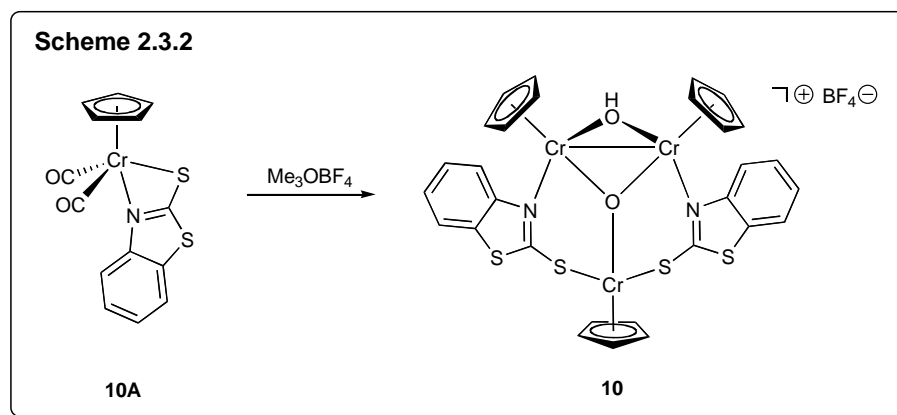
The reaction between $\text{CpCr}(\text{CO})_3(\text{STz})$ (**4**) and excess Me_3OBF_4 in toluene at ambient temperature was complete after 18 h. The colour of the reaction mixture had changed from deep purple to deep blue and the ^1H NMR spectrum indicated the absence of the starting material **4**. From this product solution was obtained $\text{Cp}_2\text{Cr}_2(\mu\text{-OH})(\mu\text{-}\eta^2\text{-SCN}_4\text{Ph})_2\text{BF}_4$ (**8**) (25%) (Scheme 2.3.1).

The reaction between $\text{CpCr}(\text{CO})_3(\text{STz})$ (**4**) and excess $(\text{MeO})_2\text{SO}_2$ in toluene at ambient temperature was also complete after 18 h, as indicated by similar colour change and the ^1H NMR spectrum as above. From the deep blue product solution, $\text{Cp}_3\text{Cr}_3(\mu_2\text{-OH})(\mu_3\text{-O})(\mu_2\text{-}\eta^2\text{-SCN}_4\text{Ph})_2(\text{CH}_3\text{OSO}_3)$ (**9**) (20%) was obtained (Scheme 2.3.1).

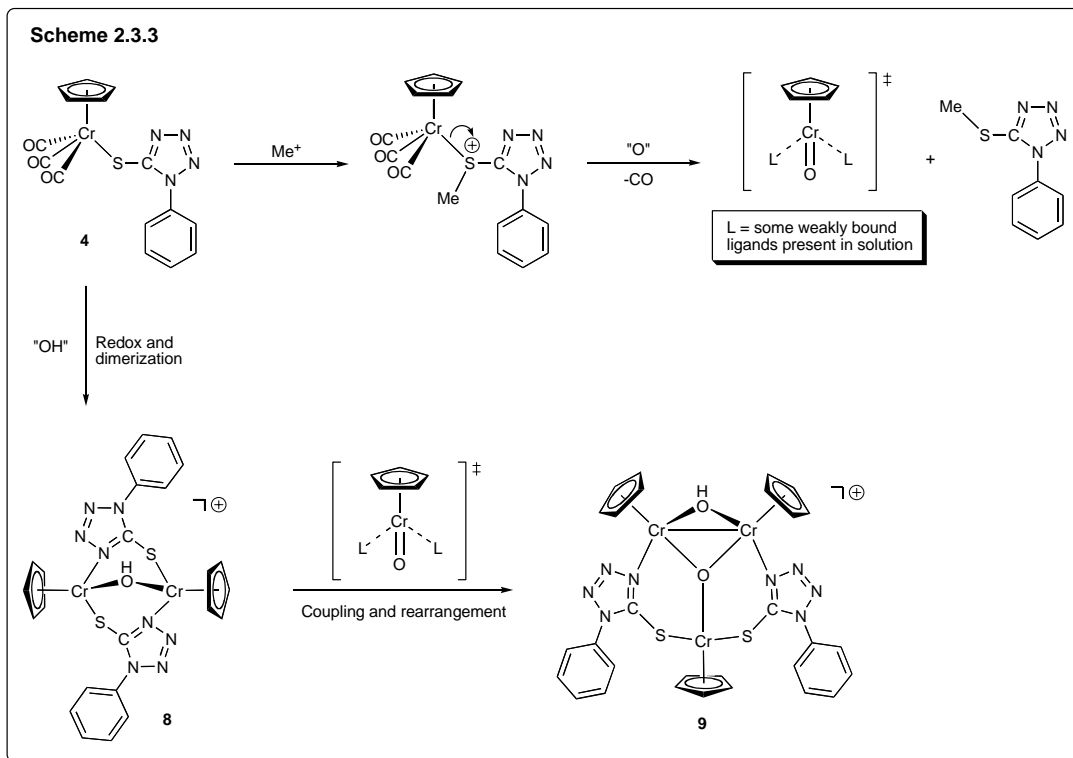


2.3.1.1 Products and reaction pathways

It is interesting to note that complex **9** is very similar to complex **10** obtained by a member of our research group from the reaction of the 2-mercaptobenzothiazole cyclopentadienylchromium complex **10A** with trimethyloxonium tetrafluoroborate (Scheme 2.3.2).⁸⁵

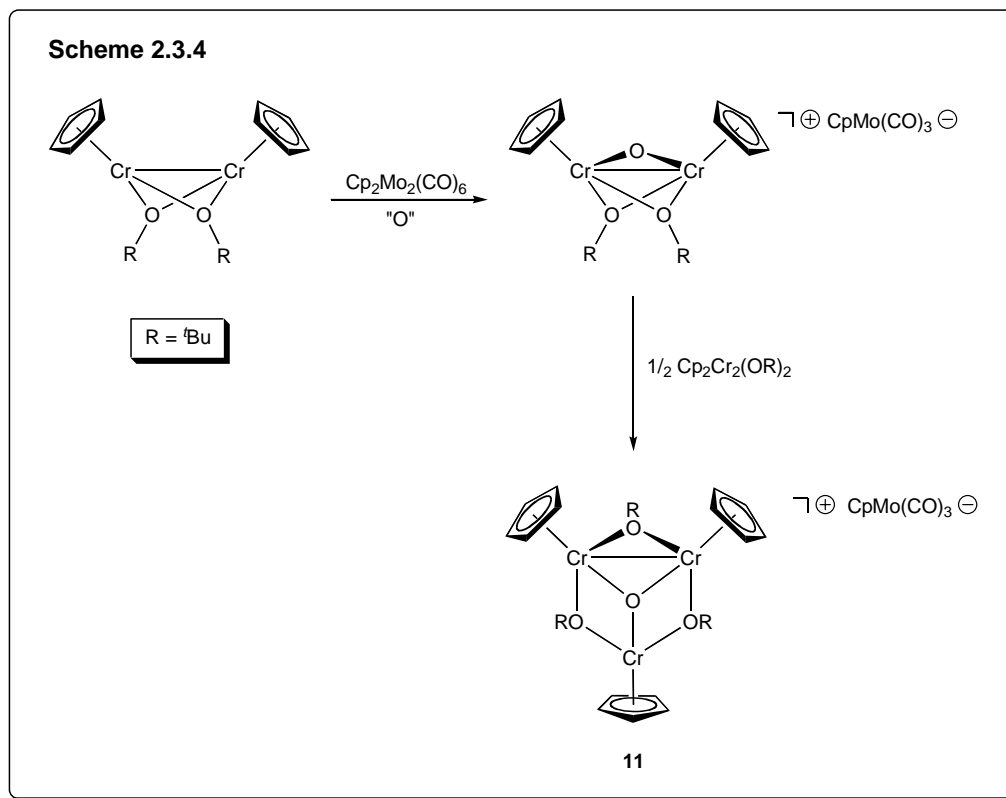


Based on the identification of the S-methylated derivative of the ligand, viz. MeSTz, from the mass spectrum of the product solution, mechanistic pathways shown in Scheme 2.3.3 are proposed. The binuclear complex, **8**, must have been formed via a dimerization of **4**, in which a redox reaction must have taken place concurrently. The inclusion of an OH-bridge was somewhat surprising and its origin could have been due to the water content present in the starting reagent. However, the fate of the H^+ was unknown, perhaps protonating $\text{CH}_3\text{OSO}_3^-$ to form $\text{CH}_3\text{OSO}_3\text{H}$, which was not detected. In another path, the methylating agent may have methylated the 5-mercaptotetrazole moiety on complex **4** resulting in the subsequent dissociation of the methylated organic molecule. The “naked” complex then picks up an oxygen atom, possibly from the CO in **4**, since it is coordinatively unsaturated and CpCr species being very oxophilic. The resulting intermediate must have been a very reactive species, which will in turn couple rapidly with **8** to form **9**. The total decarbonylation of **4** was to be expected since there is a formal oxidation of Cr(II) in **4** to Cr(III) in complex **8** and **9**. Cr(III) complexes are in general electron-deficient, and would therefore greatly reduce the stabilizing backbonding to the CO ligands, hence easily labilizing the terminal CO ligands. As far as I am aware, there is currently no known Cr(III) complexes with terminal CO ligands reported.



The binuclear complex, **8**, must have been formed via a dimerization of **4**, in which a redox reaction must have taken place concurrently. The inclusion of an OH-bridge was somewhat surprising and its origin could have been due to the water content present in the starting reagent. However, the fate of the H^+ was unknown, perhaps protonating $\text{CH}_3\text{OSO}_3^-$ to form $\text{CH}_3\text{OSO}_3\text{H}$, which was not detected. In another path, the methylating agent may have methylated the 5-mercaptotetrazole moiety on complex **4** resulting in the subsequent dissociation of the methylated organic molecule. The “naked” complex then picks up an oxygen atom, possibly from the CO in **4**, since it is coordinatively unsaturated and CpCr species being very oxophilic. The resulting intermediate must have been a very reactive species, which will in turn couple rapidly with **8** to form **9**.

This mechanistic pathway finds an analogy in Pasynskii's work for the formation of a similar μ_3 -oxo complex from a binuclear cation (**11**) with the inclusion of oxygen, proposed to have come from the CO ligand on $[\text{CpMo}(\text{CO})_3]_2$ (Scheme 2.3.4).⁸⁶



2.3.1.2 Product characterization

(i) $\text{Cp}_2\text{Cr}_2(\mu\text{-OH})(\mu\text{-}\eta^2\text{-SCN}_4\text{Ph})_2\text{BF}_4$ (**8**)

The infrared spectrum in KBr disc shows a broad and intense O-H band at 3413 cm^{-1} . No peaks are seen in the normal ^1H NMR region, indicative of paramagnetism, which was predictable since the complex contains two 15-electron chromium(III) centres. The FAB^+ -MS showed the molecular ion peak at m/z 605. The elemental analysis of the complex showed disappointing results due to its instability.

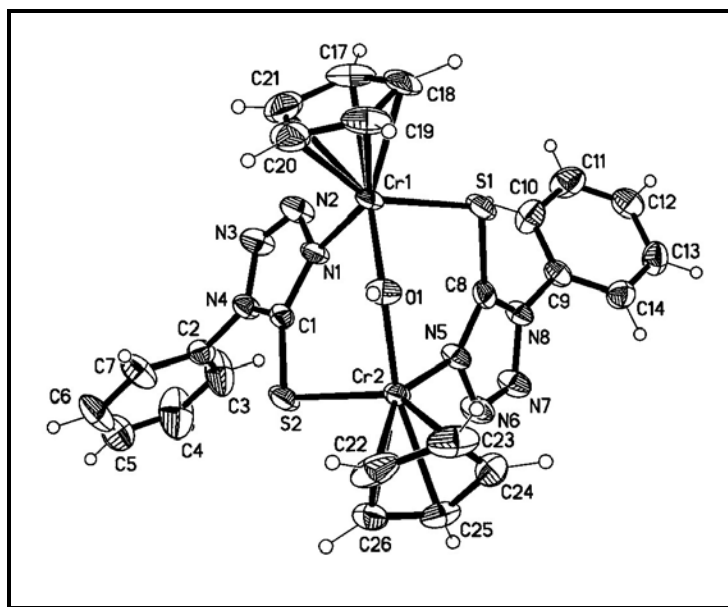


Figure 2.3.1. Molecular structure of $\text{Cp}_2\text{Cr}_2(\mu\text{-OH})(\mu\text{-}\eta^2\text{-SCN}_4\text{Ph})_2\text{BF}_4$ (**8**). Thermal ellipsoids are drawn at the 50% probability level.

The ORTEP of **8** is depicted in Figure 2.3.1. Selected bond lengths and angles are listed in Table 2.3.1. Each chromium centre possesses a three-legged piano-stool configuration, coordinated to two different bridging 5-mercaptotetrazole ligands, one via the S- while the other through the N-atoms, and a bridging OH ligand. The crystal packs in a triclinic space group P-1 and the asymmetric unit contains one titled cation, one BF_4^- , and one acetonitrile solvent molecule. The bridging OH between the two chromium atoms also shows a secondary hydrogen bonding to F(3) of the BF_4^- , at a distance of 2.755 Å for the O-F bond. In addition, the two bridging 5-mercaptotetrazole ligands and the two chromium centres forms an eight-membered buckered metallacycle (namely Cr(1), N(1), C(1), S(2), Cr(2), N(5), C(8) and S(1)), which includes two smaller six-membered sub-cycles (cycle A: Cr(1), N(1), C(1), S(2), Cr(2) and O(1); and cycle B:

Cr(2), N(5), C(8), S(1), Cr(1) and O(1)) when we take into account the bridging OH moiety. This is the first example of an anionic 5-mercaptotetrazole bridging complex.

Table 2.3.1. Selected bond lengths (Å) and angles (deg) for **8**

Bond lengths (Å)			
Cr(1)-O(1)	1.950(3)	Cr(1)-N(1)	2.090(3)
Cr(1)-S(1)	2.3978(12)	Cr(2)-O(1)	1.949(3)
Cr(2)-N(5)	2.085(3)	Cr(2)-S(2)	2.4031(11)
S(1)-C(8)	1.739(4)	S(2)-C(1)	1.734(4)
N(1)-C(1)	1.358(4)	N(5)-C(8)	1.361(5)
Bond angles (deg)			
O(1)-Cr(1)-N(1)	93.69(12)	O(1)-Cr(1)-S(1)	96.30(10)
N(1)-Cr(1)-S(1)	93.53(9)	O(1)-Cr(2)-N(5)	93.81(12)
O(1)-Cr(2)-S(2)	96.33(9)	N(5)-Cr(2)-S(2)	96.03(9)
C(8)-S(1)-Cr(1)	104.66(13)	C(1)-S(2)-Cr(2)	104.35(12)
Cr(2)-O(1)-Cr(1)	128.94(16)	C(1)-N(1)-Cr(1)	136.7(2)
C(8)-N(5)-Cr(2)	138.1(3)	N(1)-C(1)-S(2)	130.7(3)
N(5)-C(8)-S(1)	129.9(3)		

(ii) $\text{Cp}_3\text{Cr}_3(\mu_2\text{-OH})(\mu_3\text{-O})(\mu_2\text{-}\eta^2\text{-SCN}_4\text{Ph})_2(\text{CH}_3\text{OSO}_3)$ (9**)**

The infrared spectrum in KBr disc shows a broad and intense N-H band at 3254 cm^{-1} . The ^1H NMR spectrum shows no peaks in the normal region, indicative of paramagnetism, which was predictable since the complex consists of three 15-electron chromium(III) centres. The FAB⁺-MS showed the molecular ion peak at m/z 738. The elemental analysis of the complex showed disappointing results due to its instability.

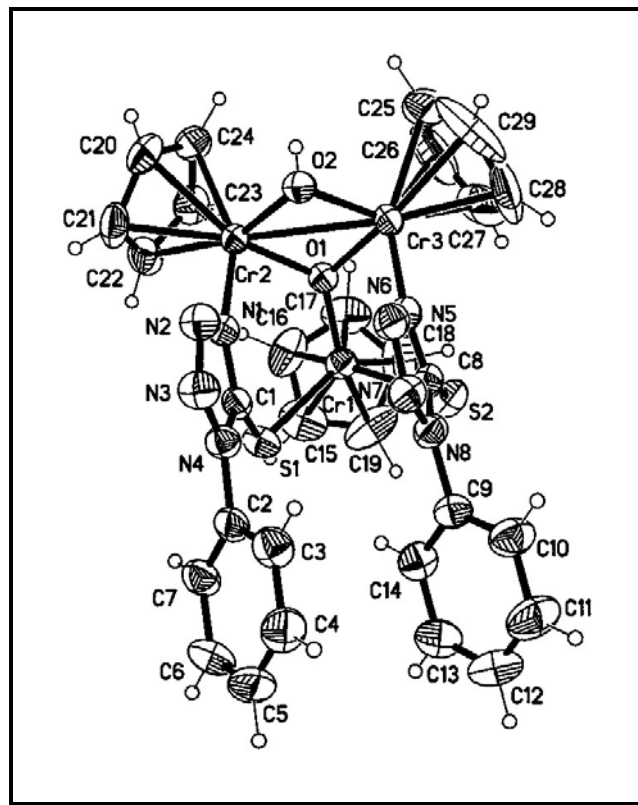


Figure 2.3.2. Molecular structure of $\text{Cp}_3\text{Cr}_3(\mu_2\text{-OH})(\mu_3\text{-O})(\mu_2\text{-}\eta^2\text{-SCN}_4\text{Ph})_2(\text{CH}_3\text{OSO}_3)$ (**9**). Thermal ellipsoids are drawn at the 50% probability level.

The ORTEP of **9** is depicted in Figure 2.3.2. Selected bond lengths and angles are listed in Table 2.3.2. The Cr(1) centre possesses a three-legged piano-stool configuration, coordinated to two bridging 5-mercaptotetrazole ligands, via the endocyclic thiolate S-atoms, and a μ_3 -bridging oxygen atom, O(1). The Cr(2) and Cr(3) centres each possesses a four-legged piano-stool configuration, coordinated to a bridging 5-mercaptotetrazole ligands, via the endocyclic N-atoms, a bridging OH ligand, a μ_3 -bridging oxygen atom, O(1), and a Cr-Cr bond at 2.8392(7) Å. The crystal packs in a triclinic space group P-1 and the asymmetric unit contains one titled cation, one anion MeOSO_3^- , and 2.85 acetonitrile solvent molecules. The two bridging 5-mercaptotetrazole ligands, the bridging OH and the two chromium centres form a ten-membered buckered metallacycle

(namely Cr(1), S(1), C(1), N(1), Cr(2), O(2), Cr(3), N(5), C(8) and S(2)), which includes two smaller six-membered sub-cycles (cycle A: Cr(1), S(1), C(1), N(1), Cr(2) and O(1); and cycle B: Cr(1), S(2), C(8), N(5), Cr(3) and O(1)) and a strained four-membered ring (cycle C: Cr(2), O(1), Cr(3) and O(2)) when we take into account the μ_3 -bridging oxygen atom, O(1). Similar to **8**, this is also the first example of an anionic 5-mercaptotetrazole bridging complex.

Table 2.3.2. Selected bond lengths (Å) and angles (deg) for **9**

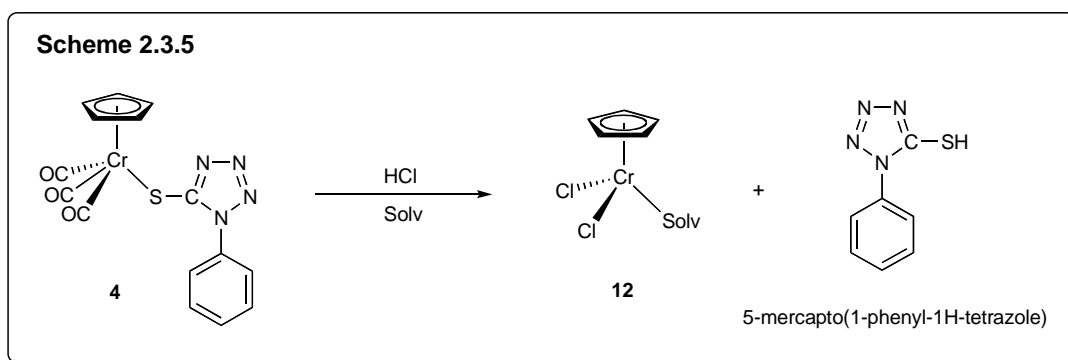
<i>Bond lengths (Å)</i>			
Cr(1)-O(1)	1.891(2)	Cr(1)-S(1)	2.4007(10)
Cr(1)-S(2)	2.4207(11)	Cr(2)-O(1)	1.914(2)
Cr(2)-O(2)	1.943(2)	Cr(2)-N(1)	2.061(3)
Cr(2)-Cr(3)	2.8392(7)	Cr(3)-O(1)	1.916(2)
Cr(3)-O(2)	1.936(2)	Cr(3)-N(5)	2.072(3)
S(1)-C(1)	1.712(3)	S(2)-C(8)	1.716(3)
N(1)-C(1)	1.331(4)	N(5)-C(8)	1.337(4)
<i>Bond angles (deg)</i>			
O(1)-Cr(1)-S(1)	97.00(7)	O(1)-Cr(1)-S(2)	96.96(7)
S(1)-Cr(1)-S(2)	96.49(3)	O(1)-Cr(2)-O(2)	84.66(10)
O(1)-Cr(2)-N(1)	91.54(9)	O(2)-Cr(2)-N(1)	90.58(10)
O(1)-Cr(2)-Cr(3)	42.18(6)	O(2)-Cr(2)-Cr(3)	42.85(7)
N(1)-Cr(2)-Cr(3)	95.84(7)	O(1)-Cr(2)-O(2)	84.81(10)
O(1)-Cr(3)-N(5)	88.96(10)	O(2)-Cr(3)-N(5)	93.05(11)
O(1)-Cr(3)-Cr(2)	42.12(6)	O(2)-Cr(3)-Cr(2)	43.06(7)
N(5)-Cr(3)-Cr(2)	95.75(7)	C(1)-S(1)-Cr(1)	109.44(10)
C(8)-S(2)-Cr(1)	100.00(10)	Cr(1)-O(1)-Cr(2)	131.31(11)
Cr(1)-O(1)-Cr(3)	128.50(11)	Cr(2)-O(1)-Cr(3)	95.70(10)
Cr(3)-O(2)-Cr(2)	94.08(11)	C(1)-N(1)-Cr(2)	130.7(2)
N(2)-N(1)-Cr(2)	121.19(19)	C(8)-N(5)-Cr(3)	124.6(2)
N(6)-N(5)-Cr(3)	127.6(2)		

2.3.1.3 Conclusion

The reactions of $\text{CpCr}(\text{CO})_3(\text{STz})$ (**4**) with trimethyloxonium tetrafluoroborate and dimethylsulfate gave unexpected results. The initial target of a simple methylation was unsuccessful but instead the reaction led to a series of interesting dinuclear and trinuclear chromium species and new reactivities. In both of the cases, the chromium centres exhibit strong affinity towards oxo-containing species where its source remains a mystery. It may be worthwhile to try to isolate the different products that exist in the solution mixture so as to provide us with a more complete mechanistic study into the deceitfully “simple” reaction.

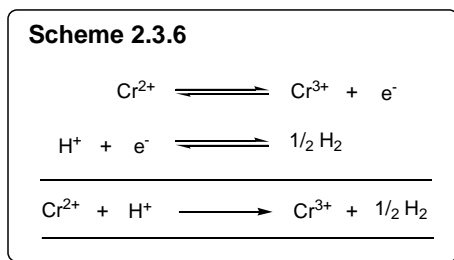
2.3.2 Reaction with hydrochloric acid

The reaction between $\text{CpCr}(\text{CO})_3(\text{STz})$ (**4**) and excess conc. HCl in toluene at ambient temperature was complete after 18 h. The colour of the reaction mixture had changed from magenta to deep green and the ^1H NMR spectrum indicated the absence of the starting material **4**. From this product solution was obtained $\text{CpCrCl}_2(\text{Solv})$ (**12**) and 5-mercapto(1-phenyl-1H-tetrazole) in moderate yields of 66% and 56% respectively (Scheme 2.3.5).



2.3.2.1 Products and reaction pathways

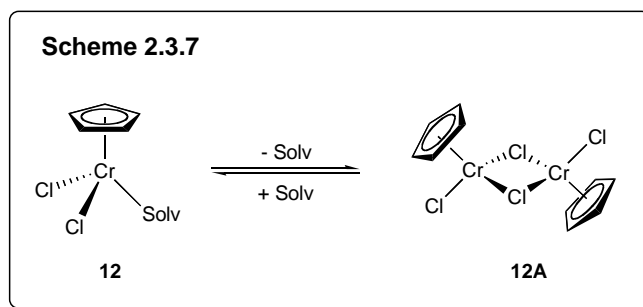
In this reaction, the HCl functions as both an acid and an oxidizing agent. It donates its proton to the thiopyridine moiety, and also oxidizes the chromium centre from an oxidation state of +2 to +3 by transferring its chloride. The relative participation of each of these roles are not known but are both crucial. The redox reaction is proposed to take the following half-equations:



In this reaction, two mole equivalents of HCl are required, one mole equivalent for the proton donation, and the second for oxidation. The transfer of the chlorides onto the chromium centre is an illustration of the “chlorophilicity” of chromium centres. The transfer is rather efficient and feasible due to the formation of the strong Cr-Cl bond, which is exothermic and provides an additional driving force for the reaction. The formation of such 15-electron Cr(III) open-shell complexes may be explained by two effects, namely excessive steric encumbering and electronic protection. Here in complex **12**, the achievement of a saturated configuration is impossible because inter-ligand van der Waals repulsions exceed the stabilization energy provided by the new bond(s) being formed. Cr(III), being highly charged and small in size may not be able to accommodate many big and bulky ligands in its coordination sphere.⁹² The liberated hydrogen was not detected.

The infrared spectrum of **12** in KBr disc was not informative and the ^1H NMR spectrum shows no peaks on the normal ^1H NMR range, which is indicative of

paramagnetism. This can be predicted since the complex consists of a 15-electron chromium (III) centre. The FAB^+ -MS shows an intense peak at m/z 188 indicating a loss of CH_3CN from the molecular ion, which is easily rationalized on the weak metal-solvent bond. In fact, in the absence of a coordinating solvent, dimerization could take place (Scheme 2.3.7).⁷⁹ However, due to the incompatible size differential between the radius of Cl^- (1.81 Å) and Cr^{3+} (0.69 Å), the Cr-Cr bond was excluded. This was apparent in the FAB^+ -MS spectrum, which shows a peak at m/z 376, corresponding to **12A**.



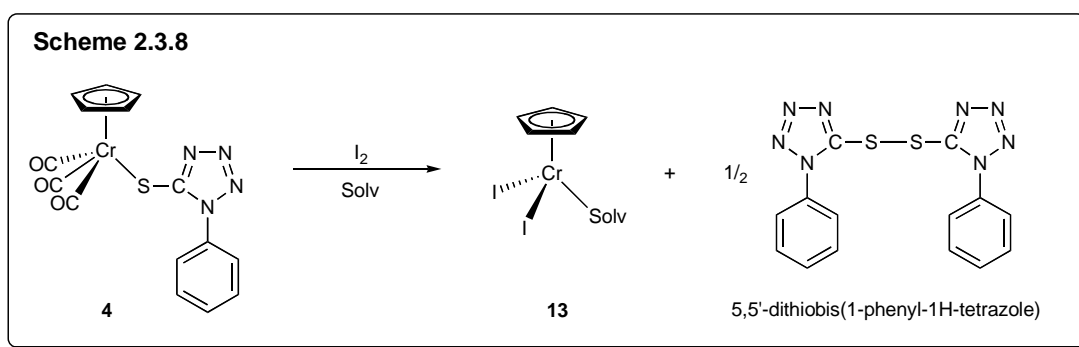
The molecule **12** possesses a three-legged piano-stool configuration at Cr, coordinated to an acetonitrile solvent molecule and two chloro ligands. This complex has been previously reported by Goh *et. al.*⁸⁷

2.3.2.2 Conclusion

The reaction of $\text{CpCr}(\text{CO})_3(\text{STz})$ (**4**) with HCl provide an insight to the reactivity of both the entities. HCl reacts as both an acid and an oxidant; **4** is shown to be an effective reducing agent and a rather “halophilic” moiety.

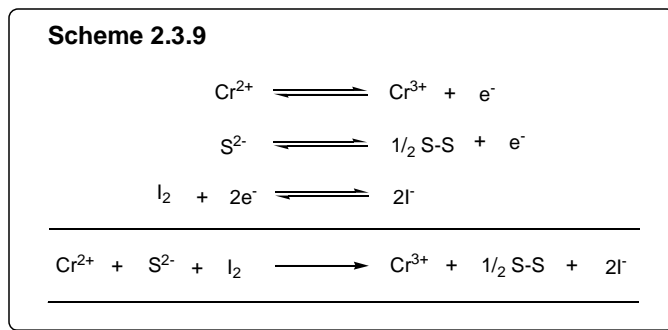
Reactions with iodine (oxidant)

The stoichiometric reaction between $\text{CpCr}(\text{CO})_3(\text{STz})$ (**4**) and iodine in toluene at ambient temperature was complete after 2 h, at which stage, the colour of the reaction mixture had changed from deep purple to deep green and ^1H NMR spectrum indicated the absence of any starting material **4**. From this product solution was obtained $\text{CpCrI}_2(\text{Solv})$ (**13**) (75%), along with the displaced ligand, 5,5'-dithiobis(1-phenyl-1H-tetrazole) (71%) in moderate yields (Scheme 2.3.8).



2.3.3.1 Products and reaction pathways

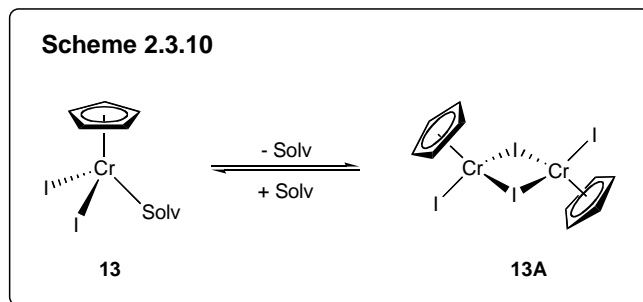
The reaction of $\text{CpCr}(\text{CO})_3(\text{STz})$ (**4**) with iodine resulted in a typical redox reaction. The chromium centre was oxidized from an oxidation state of +2 to +3 while the iodide was reduced from an oxidation state of 0 to -1. In addition, the bonded thiolate (5-mercapto(1-phenyl-1H-tetrazole)) was oxidized to a disulfide, which meant a formal oxidation state change from -2 to -1. The redox reaction can be represented by the following half-equations:



The inclusion of the iodides onto the chromium centre is an illustration of the “iodophilicity” of chromium centres. The transfer is rather efficient and feasible due to the formation of the strong Cr-I bond, which is exothermic and provides an additional driving force for the reaction. The iodine also causes an oxidation of the bound-thiolate to a disulfide. This is not unprecedented, and is a standard oxidation of thiolates to disulfide in many of the known protein synthesis. Therefore, in this reaction, the Cr(II) centre and the bound-thiolate sulfur each donates one electron to iodine, which is the sole source of electron acceptor. The formation of an open-shell complex, such as **13** may be rationalized as described in Section 2.3.2.1.

The infrared spectrum of **13** in KBr disc does not give much information. ^1H NMR spectrum shows no peaks in the ‘normal’ ^1H NMR range indicative of paramagnetism, again expected of a 15-electron chromium(III) centre, though recent literature gave a broad peak at *ca.* 270 ppm for the Cp protons of $\text{CpCrI}_2(\text{THF})$.⁷⁹ We did a similar scan and found a peak at *ca.* 260 ppm for $\text{CpCrI}_2(\text{CH}_3\text{CN})$. The FAB⁺-MS shows an intense peak at *m/z* 371, which corresponds to $[\text{M}^+ - \text{CH}_3\text{CN}]$ fragment, in agreement with facile loss of the weakly bound solvent molecule. In addition, the dimer peak at *m/z* 742 was also observed which indicated dimerization subsequent to solvent loss (Scheme 2.3.10).⁷⁹ As rationalized before for its chloro-analogue (See Section

2.3.2.1), the absence of a Cr-Cr bond in **13** was possibly due to the presence of the bulky bridging iodide anion.



The ORTEP of **13** is depicted in Figure 2.3.3. Selected bond lengths and angles are listed in Table 2.3.3. It should be noted that although this class of complex was documented, most of their X-ray structures were not reported. The molecule possesses a three-legged piano-stool configuration at Cr, coordinated to an acetonitrile solvent molecule and two iodo ligands. The chloro analogue **12** (See Figure 2.3.3) has been previously reported by Goh *et. al.*⁸⁷ The asymmetric unit contains half of the $\text{CpCrI}_2(\text{CH}_3\text{CN})$ molecule. The N(1)-C(1) bond length of 1.134(5) Å is within the range of the $\text{C}\equiv\text{N}$ bonds and the acetonitrile molecule is coordinated almost linearly to the chromium centre at 173.7(3)°. These data are comparable to the chloro-analogue **12** (Table 2.3.3).

Table 2.3.3. Comparison of selected bond lengths (Å) and angles (deg) for **12** and **13**

<i>Bond lengths (Å)</i>			
$\text{CpCrI}_2(\text{CH}_3\text{CN})$		$\text{CpCrCl}_2(\text{CH}_3\text{CN})$	
Cr(1)-I(1)	2.6587(5)	Cr(1)-Cl(1)	2.2849(11)
Cr(1)-I(1A)	2.6587(5)	Cr(1)-Cl(2)	2.2849(11)
Cr(1)-N(1)	2.040(4)	Cr(1)-N(1)	2.051(3)
N(1)-C(4)	1.125(6)	N(1)-C(1)	1.134(5)

Bond angles (deg)			
N(1)-Cr(1)-I(1)	93.90(7)	N(1)-Cr(1)-Cl(1)	94.29(10)
N(1)-Cr(1)-I(1A)	93.90(7)	N(1)-Cr(1)-Cl(2)	94.29(10)
I(1)-Cr(1)-I(1A)	100.52(2)	Cl(1)-Cr(1)-Cl(2)	
C(4)-N(1)-Cr(1)	172.9(4)	C(1)-N(1)-Cr(1)	173.7(3)
N(1)-C(4)-C(5)	179.3(5)	N(1)-C(1)-C(2)	179.9(6)

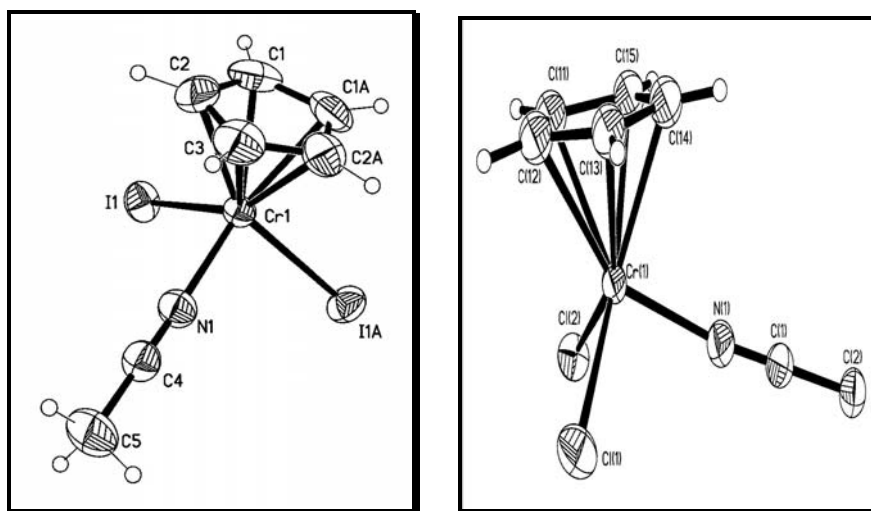


Figure 2.3.3. Molecular structure of $\text{CpCrI}_2(\text{CH}_3\text{CN})$ (**12**) (left) and $\text{CpCrCl}_2(\text{CH}_3\text{CN})$ (**13**) (right).

Thermal ellipsoids are drawn at the 50% probability level.

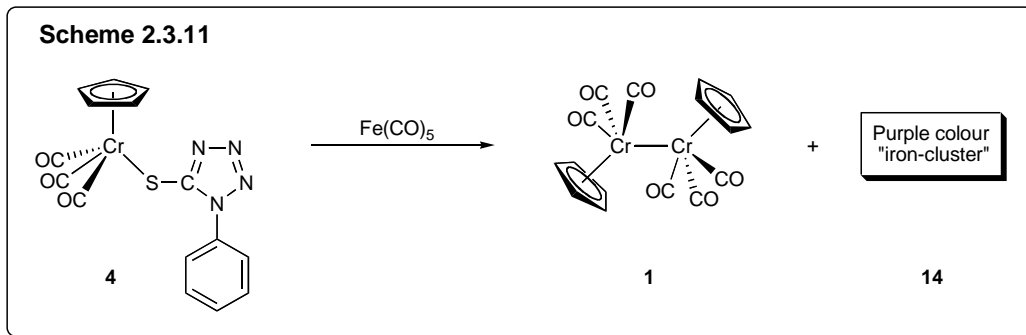
2.3.3.2 Conclusion

The products show that the reaction of $\text{CpCr}(\text{CO})_3(\text{STz})$ (**4**) with iodine results in a redox reaction. **4** is shown to be an effective reducing agent and an “iodophilic” moiety. The bonded thiolate moiety was found to be easily oxidized to the disulfide by iodine.

2.3.4 Reactions with iron pentacarbonyl

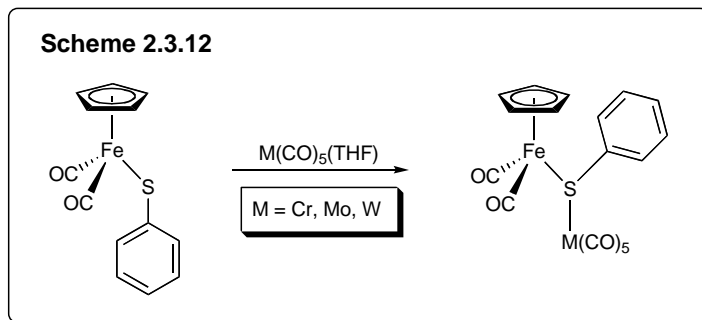
The reaction between $\text{CpCr}(\text{CO})_3(\text{STz})$ (**4**) and excess $\text{Fe}(\text{CO})_5$ in toluene at ambient temperature was complete after 18 h. The colour of the reaction mixture had changed from magenta to purplish-green and the ^1H NMR spectrum indicated the

absence of the starting material **4**. From this solution, **1** was obtained in 75% yield, along with moderate yield of an unknown purple solid **14**.

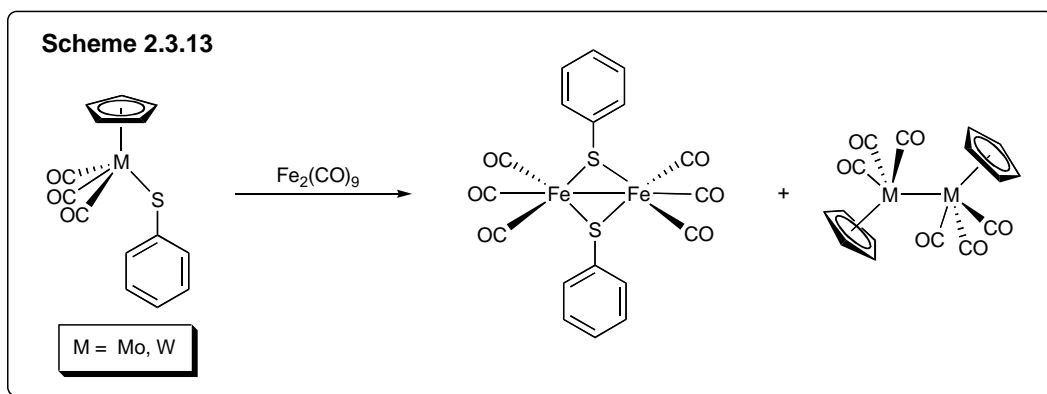


In the absence of a solid structural analysis due to poorly diffracting crystals, its characterization remains incomplete. Spectral data were inconclusive, viz. absence of CO bands in the infrared spectrum, presence of aromatic benzylic protons in the phenyl regions of the ^1H NMR spectrum and an FAB^+ -MS fragment of m/z 1207 that could not be rationalized.

Our initial aim was to examine the feasibility of coordinating an $\text{Fe}(\text{CO})_x$ fragment to either the thiolate sulfur or the endocyclic nitrogen atoms on the complex **4**. There is precedence for reactions,⁸⁸ which involves the coordination of metal-carbonyl complexes onto metal-thiolate complexes such as the one shown in Scheme 2.3.12.



Our reaction is very likely to be a ligand transfer reaction in which the complex **4** transfers its bonded 5-mercaptotetrazole fragment to the iron pentacarbonyl. In doing so, the $\{\text{CpCr(CO)}_3\}$ moiety becomes coordinatively unsaturated and therefore subsequently combines to form $[\text{CpCr(CO)}_3]_2$ (**1**). The iron pentacarbonyl may have undergone decarbonylation and aggregation to form a cluster-like structure with the inclusion of the tetrazole fragments. This postulation was made based on a high molecular mass fragment in the FAB-MS spectrum as well as preliminary elemental analysis. There is also a report on thiolate transfer from metallothiolates to iron carbonyl clusters by Shyu and coworkers (Scheme 2.3.13).⁸⁸ Thiolato ligand transfer is reported for a few cases, mainly from the early transition metals to the late transition metals. The reason may be due to the hard and soft mismatching of coordination hard metals to the soft thiolates.

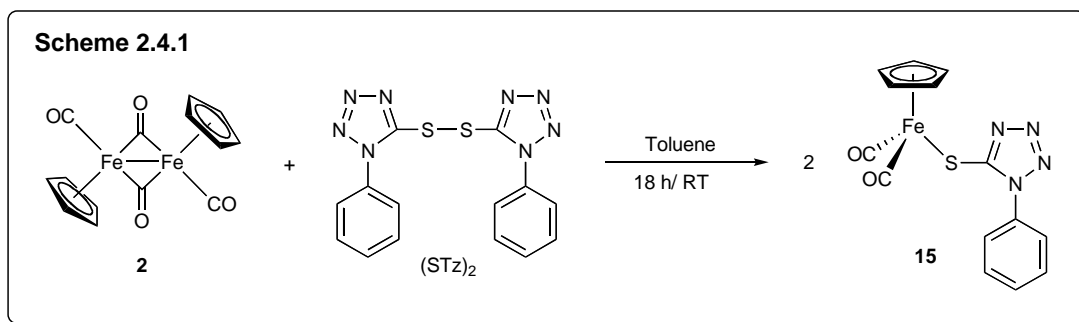


Thus, in the absence of a complete characterization of the purple product, the reaction of $\text{CpCr(CO)}_3(\text{STz})$ (**4**) with iron pentacarbonyl showed that iron carbonyl could not coordinate to the thiolate sulfur or the endocyclic nitrogen atoms.

2.4 The reaction of $[\text{CpFe}(\text{CO})_2]_2$ (**2**) with 5,5'-dithiobis(1-phenyl-1H-tetrazole) (STz)₂

2.1.1 Products and reaction pathways

The reaction between $[\text{CpFe}(\text{CO})_2]_2$ (**2**) and one mole equivalent of $(\text{STz})_2$ in toluene at ambient temperature produced a reddish-brown solution, from which red crystals of $\text{CpFe}(\text{CO})_2(\eta^1\text{-STz})$ (**15**) were obtained in 79% yield (Scheme 2.4.1).



The infrared spectrum of **15** in KBr disc shows two CO absorption bands (2034s, 1986s), indicating the presence of terminal carbonyls. The ^1H NMR spectrum shows the Cp (^1H) peak at δ 5.20 (s, 5H) and Ph (^1H) peaks at δ 7.50 – 7.73 (m, 5H). The ^{13}C NMR spectrum shows more peaks than expected probably due to decomposition over the period of scanning. The FAB⁺-MS showed the molecular ion peak at m/z 354. Elemental analysis was also consistent with our assignments.

2.4.1 Crystallographic studies

The ORTEP of **15** is depicted in Figure 2.4.1. Selected bond lengths and angles are listed in Table 2.4.1. The molecule possesses a three-legged piano-stool configuration

at Cr, which is coordinated to a monodentate STz organic fragment and two terminal CO ligands. The S(1)-C(3) bond length of 1.721(2) Å is within the range of the single C-S bonds. The bond length of N(2)-N(3) (1.290(3) Å) is shorter than N(1)-N(2) (1.365(3) Å) and N(3)-N(4) (1.357(3) Å) indicative of the N=N double bond character. The C(3)-N(1) bond length is also within the range for C=N bonding. The Fe(1)-S(1)-C(3) angle is 107.92(7) indicative of a bent geometry.

Table 2.4.1. Selected bond lengths (Å) and angles (deg) for **15**

Bond lengths (Å)			
Fe(1)-S(1)	2.2784(6)	S(1)-C(3)	1.721(2)
C(3)-N(1)	1.323(3)	C(3)-N(4)	1.356(3)
N(1)-N(2)	1.365(3)	N(2)-N(3)	1.290(3)
N(3)-N(4)	1.357(3)	N(4)-C(4)	1.428(3)
Bond angles (deg)			
Fe(1)-S(1)-C(3)	107.92(7)		

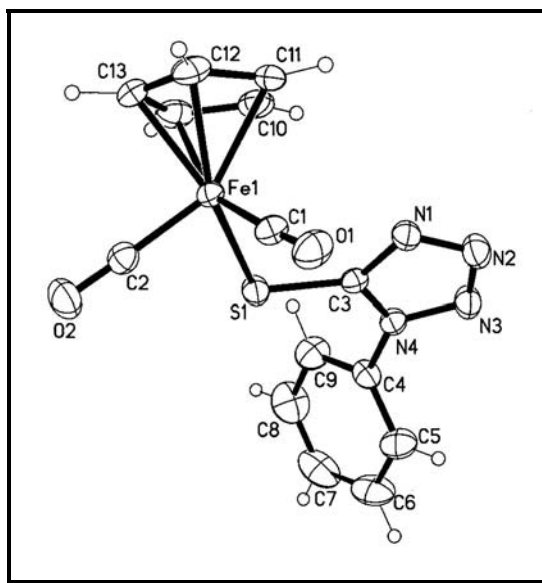
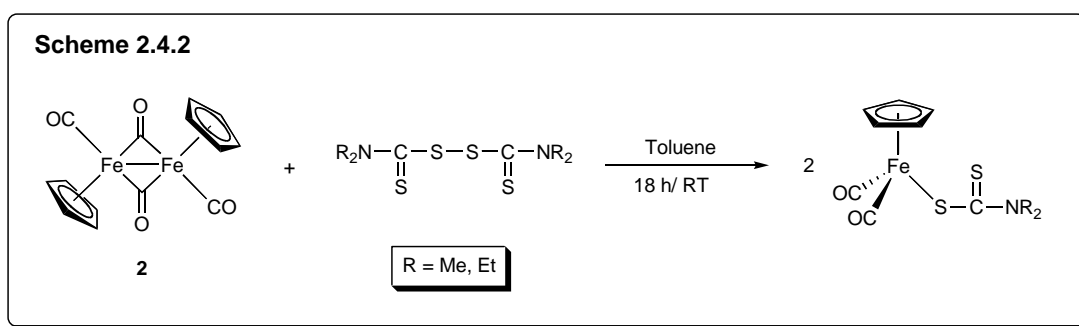


Figure 2.4.1. Molecular structure of CpFe(CO)₂(STz) (**15**). Thermal ellipsoids are drawn at the 50% probability level.

2 effects a similar reaction with tetraalkylthiuram disulfides, giving a S-S cleaved product, $\text{CpFe}(\text{CO})_2(\text{S}_2\text{CNR}_2)$ ($\text{R} = \text{Me}, \text{Et}$).⁸⁹ (Scheme 2.4.2). Compared to the similar reaction of **1**, this reaction is much more sluggish.²⁴ Similar relative rates were observed in the reaction of **1** and **2** with $(\text{STz})_2$ (Refer to Section 2.2.1). This can be rationalized on the bonding between the metal centres in the two complexes viz a long Cr-Cr bond in **1** and a shorter Fe-Fe bond with the bridging carbonyls in **2**.



2.4.3 Conclusion

The reaction of $[\text{CpFe}(\text{CO})_2]_2$ with 5,5'-dithiobis(1-phenyl-1H-tetrazole), $(\text{STz})_2$, provides a route to the 5-mercaptotetrazole (STz) cyclopentadienylchromium complexes in reasonably high yields. The coordination of the 5-mercaptotetrazole and Cp ligands, both uni-negatively charged, together with two neutral CO molecules confers a +2 oxidation state on Fe(1) atom. The organometallic complex obeys the 18-electron rule and is reasonably stable in the solid state, although decomposition occurred in solution.

These monodentate thiolate ligands are, in general, more reactive than their chelated counterparts and they usually exhibit reactivities not observed for their chelated counterparts. One very well-studied system is $\text{CpFe}(\text{CO})_2(\eta^1-\text{S}_2\text{CNR}_2)$ ($\text{R} = \text{Me}, \text{Et}$), which demonstrated exceptional high reactivity relative to $\text{CpFe}(\text{CO})(\eta^2-\text{S}_2\text{CNR}_2)$ ($\text{R} = \text{Me}, \text{Et}$).⁸⁹

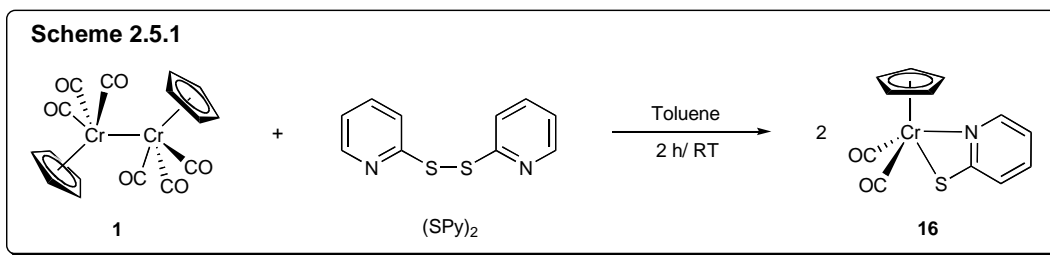
One of the initial aim in synthesizing CpFe(CO)₂(STz) was to compare its reactivity with the chromium analogue **4**, however, due to time constrains, this part of the project was not developed further.

2.5 The reaction of $[\text{CpCr}(\text{CO})_3]_2$ (**1**) with 2,2'-dithiodipyridine (SPy)₂

2.5.1 Products and reaction pathways

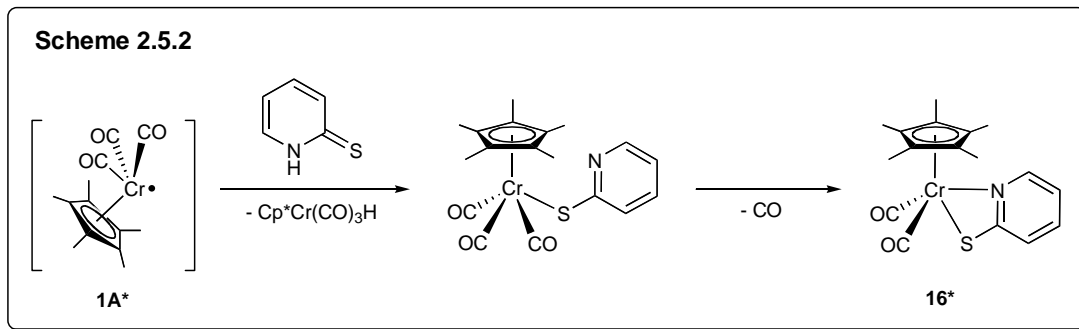
A facile reaction between $[\text{CpCr}(\text{CO})_3]_2$ (**1**) and one mole equivalent of $(\text{SPy})_2$ in toluene at ambient temperature produced a reddish-brown solution. From this solution, moderately high yields (72%) of brown crystals of $\text{CpCr}(\text{CO})_2(\eta^2\text{-SPy})$ (**16**) were obtained (Scheme 2.5.1).

The infrared spectrum of **16** in KBr disc shows two CO absorption bands (1950s, 1874s), indicating the presence of *cis* terminal carbonyls. The ^1H NMR spectrum shows the Cp (^1H) peak at δ 4.45 (s, 5H) and Py (^1H) peaks at δ 7.37 (d, $J = 6$ Hz, 1H); 6.48 (t, $J = 6$ Hz, 1H); 6.19 (d, $J = 6$ Hz, 1H); 5.97, (t, $J = 6$ Hz, 1H). The ^{13}C NMR indicated the presence of 8 types of carbons in their different environment. They are observed as, $\delta(\text{Cp})$ 94.2; $\delta(\text{Py})$ 116.1, 126.9, 135.0, 154.8 and 179.0; $\delta(\text{CO})$ 265.5 and 270.2. The FAB⁺-MS showed the molecular ion peak at m/z 283. Elemental analysis was also consistent with our assignments.



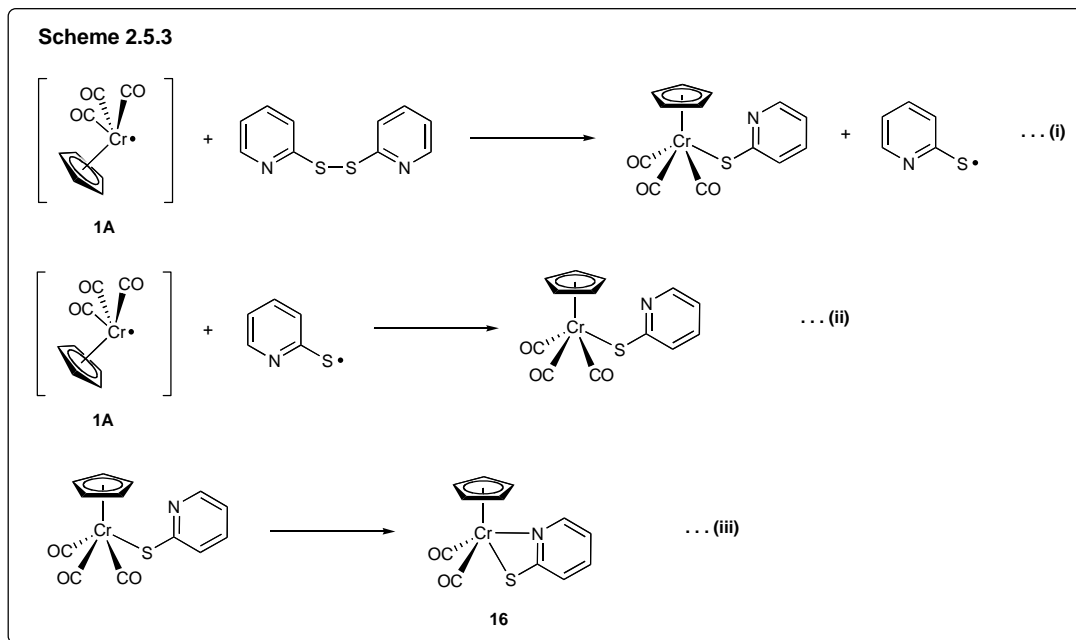
While this work was in progress, the Cp^* analogue, $\text{Cp}^*\text{Cr}(\text{CO})_2(\eta^2\text{-SPy})$ (**16***), as well as its monodentate precursor, $\text{Cp}^*\text{Cr}(\text{CO})_3(\eta^1\text{-SPy})$, was briefly reported by Hoff *et. al.* via the reaction of $[\text{Cp}^*\text{Cr}(\text{CO})_3]_2$ with pyridine thione (Scheme 2.5.2).⁸¹ It was

reported that $\text{Cp}^*\text{Cr}(\text{CO})_3(\eta^1\text{-SPy})$ readily converted to $\text{Cp}^*\text{Cr}(\text{CO})_2(\eta^2\text{-SPy})$ with the loss of a CO molecule, although there was no mention of their characterization.



Abrahamson and coworkers have previously demonstrated a reaction mechanism for the reaction of $[\text{CpW}(\text{CO})_3]_2$ with 2,2'-dithiodipyridine.⁶⁵ However, in these reactions, the monodentate species were obtained via the photolytic cleavage of the metal-dimers. Further chelation can then be induced using photochemical or thermal methods. In the reaction of **1** with $(\text{SPy})_2$, the transformation was so facile that the monodentate species, $\text{CpCr}(\text{CO})_3(\eta^1\text{-SPy})$, could not be isolated. The chelation effect provided sufficient entropic energy for the stabilization of the bidentate complex over the monodentate precursor. The precursor species may have been obtained if the reaction was carried out at a lower temperature. We have proposed a similar reaction mechanism as shown in Scheme 2.5.3 based on Abrahamson's proposition and Hoff's observation of the chelation process.

The much higher reactivity of **1** when compared with its W analogues is in agreement with the facile metal-metal bond dissociation in **1**, while in the W analogue requires photolytic or thermal activation.



2.5.2 Crystallographic studies

The ORTEP of **16** is depicted in Figure 2.5.1. Selected bond lengths and angles are listed in Table 2.5.1. The structure of **16** was found to be identical to those reported for the analogue complexes $\text{CpMo}(\text{CO})_2(\text{SPy})$ and $\text{CpW}(\text{CO})_2(\text{SPy})$.^{65,90} The molecule possesses a four-legged piano-stool configuration at Cr, coordinated to a bidentate thiopyridine and two CO ligands. The S(2)-C(2) bond length of 1.723(2) Å is within the range of the single C-S bonds of 1.55 – 1.81 Å.⁸² The thiopyridine ligand bite angle (N(1)-Cr(1)-S(2)) is 66.68(5)° while the S(2)-C(1)-N(1) angle is 109.36(16). These four atoms, namely Cr(1), C(1), N(1) and S(2) form a small strained four-membered metallacycle.

Table 2.5.1. Selected bond lengths (Å) and angles (deg) for **16**

Bond lengths (Å)			
Cr(1)-N(1)	2.0668(18)	Cr(1)-S(2)	2.4584(7)
S(2)-C(2)	1.723(2)	N(1)-C(2)	1.339(3)

N(1)-C(6)	1.343(3)	C(2)-C(3)	1.408(3)
C(3)-C(4)	1.369(4)	C(4)-C(5)	1.388(4)
C(5)-C(6)	1.374(3)		
Bond angles (deg)			
N(1)-Cr(1)-S(2)	66.68(5)	S(2)-C(1)-N(1)	109.36(16)

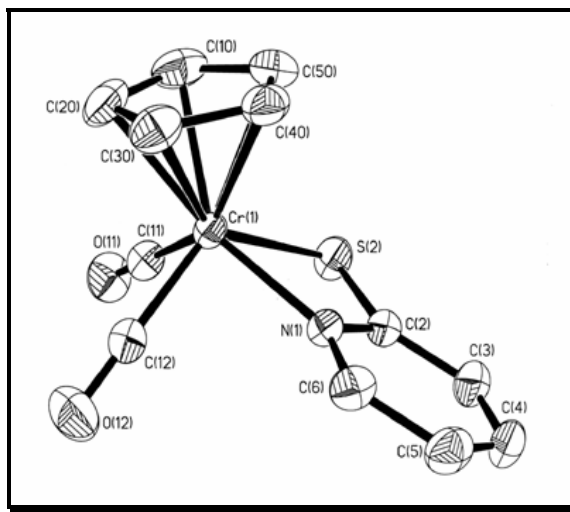


Figure 2.5.1. Molecular structure of $\text{CpCr}(\text{CO})_2(\text{SPy})$ (**16**). Thermal ellipsoids are drawn at the 50% probability level.

2.5.3 Conclusion

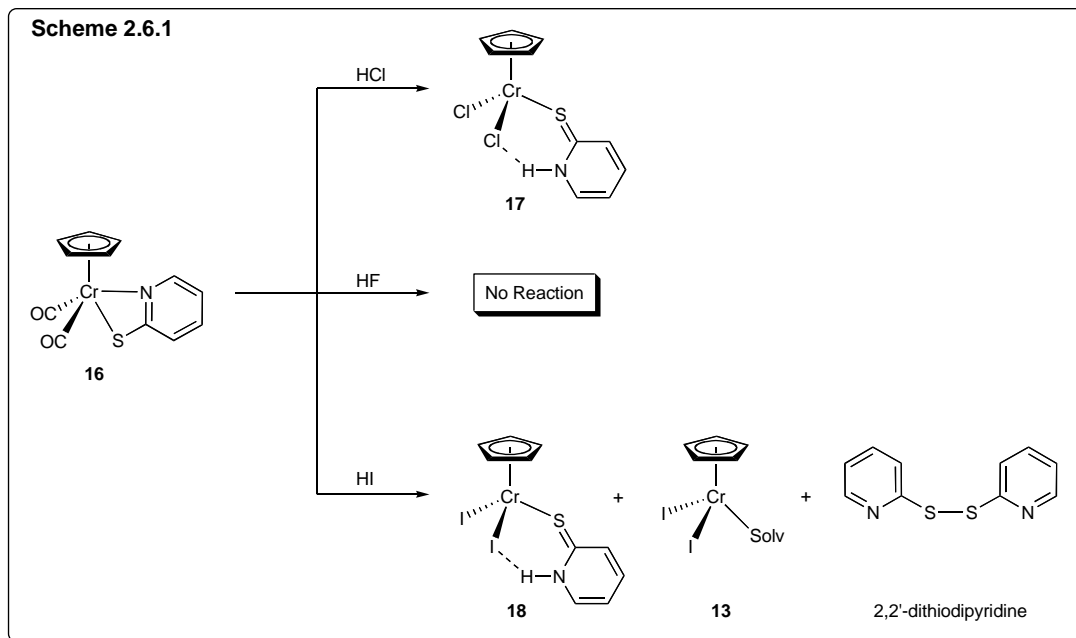
The reaction of $[\text{CpCr}(\text{CO})_3]_2$ with 2,2'-dithiodipyridine, $(\text{SPy})_2$, demonstrates the facile S–S homolytic bond cleavage by the 17-electron organometallic species **1A**, providing an efficient synthetic methodology for thiopyridine cyclopentadienyl chromium complexes. The coordination of the thiopyridine and Cp ligands, both uni-negatively charged, together with two neutral CO molecules confers a +2 oxidation state on Cr(1). The organometallic complex obeys the 18-electron rule and is reasonably stable in the solid state in the atmosphere.

2.6 Reactions of $\text{CpCr}(\text{CO})_2(\eta^2\text{-SPy})$ (**16**)

2.6.1 Reaction with HX (X = F, Cl, I)

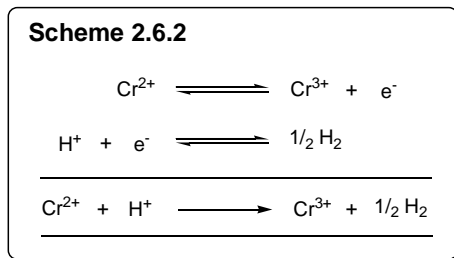
The reaction of $\text{CpCr}(\text{CO})_2(\text{SPy})$ (**16**) with excess HCl or HI in toluene at ambient temperature took 18 h for completion (Scheme 2.6.1). While the colour change in the HCl reaction was from dark brown to colourless, with the precipitation of a bluish-green oil, that of the HI reaction was from dark brown to deep green of a homogeneous solution. Both their ^1H NMR spectra indicated the absence of the starting material **16**. From the bluish-green oil was obtained an almost quantitative amount of $\text{CpCrCl}_2(\text{SPyH})$ (**17**) (90%) while the HI reaction mixture gave a mixture of $\text{CpCrI}_2(\text{Solv})$ (**13**) and $\text{CpCrI}_2(\text{SPyH})$ (**18**), together with 2,2'-dithiodipyridine.

The reaction between $\text{CpCr}(\text{CO})_2(\text{SPy})$ (**16**) and excess conc. HF in toluene at ambient temperature, however, was almost negligible even after four days, and there was no apparent change in the colour of the dark brown solution. Aliquots of the reaction mixture were withdrawn periodically and their ^1H NMR spectra checked. The ^1H NMR spectrum indicated presence of starting material **16**. From this solution, a quantitative amount of **16** was recovered via column chromatography (Scheme 2.6.1).



2.6.1.1 Products and reaction pathways

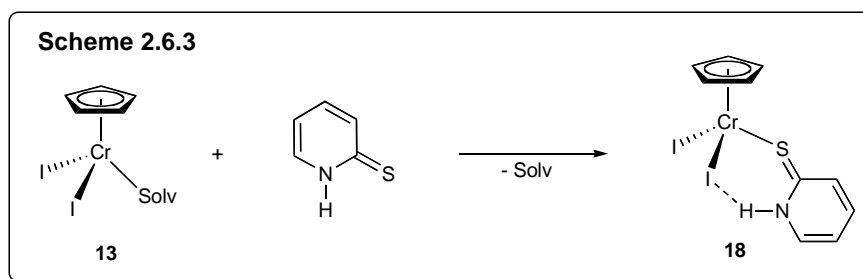
The study of the reaction of $\text{CpCr}(\text{CO})_2(\text{SPy})$ (**16**) with excess conc. HCl was intended to provide a comparison to a prior reaction with Cp_2ZrCl_2 in which **17** was obtained (Refer section 2.6.4). Here, the HCl functions as both an acid donating its proton to the thiopyridine moiety, and an oxidizing agent oxidizing the chromium centre from +2 to +3. The relative participation of each of these roles are not known but are both important. The redox reaction is proposed to take the following half-equations:



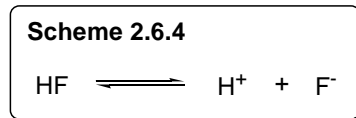
In this reaction, two mole equivalents of HCl are required, one mole equivalent for the proton donation, and the second for oxidation. The transfer of the chlorides onto

the chromium centre is an illustration of the “chlorophilicity” of chromium centres. The transfer is rather efficient and feasible due to the formation of the strong Cr-Cl bond, which is exothermic and provides an additional driving force for the reaction. The liberated hydrogen was not detected. The intact coordination of the SPyH on the chromium centre, in the presence of large amounts of the coordinating acetonitrile solvent molecules, was quite unexpected, and contrasting to the HCl reaction with $\text{CpCr}(\text{CO})_3(\text{STz})$ (**4**) in which the ligand was detached from the metal centre (Refer Section 2.3.2).

The reaction of $\text{CpCr}(\text{CO})_2(\text{SPy})$ (**16**) and excess HI was carried out in order to follow up a series of reactions involving haloacids HX. This reaction was, however, not very successful because the HI used had deteriorated and contain substantial amounts of I_2 . Here, we could detect the products for the reaction of **16** and iodine, namely **13** and 2,2'-dithiodipyridine (See Section 2.6.2 for discussion). In addition, there appears to be a new product, which contains the thiopyridine moiety, as indicated by the elemental analysis. The new product was formulated as $\text{CpCrI}_2(\text{SPyH})$ (**18**) based on its chloro-counterpart. Unfortunately, we have not been successful in the separation of **13** and **18** due to their similarity in solubility. In this reaction, the HI presumably functions as both an acid donating its proton to the thiopyridine moiety, and an oxidizing agent oxidizing the chromium centre from +2 to +3. The transfer is effected by the formation of the strong Cr-I bond, which is exothermic and provides an additional driving force for the reaction. One possible way of obtaining **18** may be to react **13** with 2-mercaptopyridine since the solvated complex may easily lose the coordinating solvent generating a vacant site for the inclusion of the incoming thio-ligand (Scheme 2.6.3). In doing so, we may compare the data obtained and gain a better insight into the HI reaction.



It was not totally surprising that the reaction of $\text{CpCr(CO)}_2(\text{SPy})$ (**16**) and excess HF did not proceed as expected, since HF is a poor proton donor, on the account of the extensive hydrogen bonding. Hence, the dissociation constant is high, and that meant that the protonating equilibrium of HF would lie very much to the left (Scheme 2.6.4).



This, of course, would also mean that the fluoride ions are not free to be transferred onto the chromium centre. Hence, the protonation of the thiopyridine moiety in **16** would very much be hindered and render the reaction successful.

2.6.1.2 Product characterization

(i) $\text{CpCrCl}_2(\text{SPyH})$ (**17**)

Its infrared spectrum in KBr disc shows a sharp and moderately strong N-H stretch at 3195 cm^{-1} . The ^1H NMR spectrum shows no peaks on the normal region, indicative of paramagnetism. This can be predicted since the complex consists of a 15-electron chromium(III) centre. The FAB^+ -MS shows the molecular ion peak at m/z 299. Elemental analysis was also consistent with our assignments.

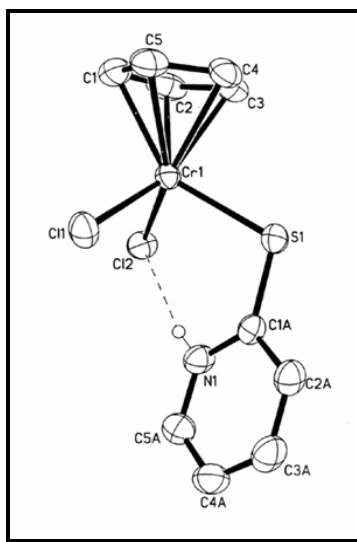


Figure 2.6.1. Molecular structure of $\text{CpCrCl}_2(\text{SPvH})$ (**17**). Thermal ellipsoids are drawn at the 50% probability level.

The ORTEP of **17** is depicted in Figure 2.6.1. Selected bond lengths and angles are listed in Table 2.6.1. The molecule possesses a three-legged piano-stool configuration at Cr, coordinated to a monodentate thiopyridine and two chloro ligands. It is noteworthy that there exists a hydrogen bond between Cl(2)-H-N(1) forming a stable pseudo-chelate six-membered ring, containing N(1), H, Cl(2), Cr(1), S(1) and C(1A) as illustrated in Figure 2.6.1.1. The nitrogen H atom was located and refined. The bond distance of N(1)-H(1A) and H(1A)...Cl(2) were found to be 0.81(3) Å and 2.39(3) Å respectively. The H-bonding interactions NH...Cl was not strong as judged by the N-Cl bond distance of 3.181(2) Å and the N(1)-H(1A)-Cl(2) bond angle was determined to be 169(2)°. The bond length of Cr(1)-Cl(2) (2.3157(6) Å) is slightly longer than that of Cr(1)-Cl(1) (2.2972(6) Å) due to its participation in the hydrogen bonding. The other reported complex having such a pseudo ring is $\text{Rh}_2\text{Cl}_2(\mu\text{-SPy})_2(\eta^1\text{-SPyH})_2(\text{CO})_2$, which was reported by Deeming and Meah.⁶⁶ The S(1)-C(1A) bond length of 1.726(2) Å is also comparable to 1.719(6) Å in this complex and is within the C=S bond length of 1.55 – 1.81 Å,⁸² perhaps due to the

backbonding from the metal centres. The bonding in the pyridine ring is almost delocalized as indicated by their bond lengths (Table 2.6.1).

Table 2.6.1. Selected bond lengths (Å) and angles (deg) for **17**

Bond lengths (Å)			
Cr(1)-Cl(1)	2.2972(6)	Cr(1)-Cl(2)	2.3157(6)
Cr(1)-S(1)	2.3830(6)	S(1)-C(1A)	1.726(2)
N(1)-C(5A)	1.340(3)	N(1)-C(1A)	1.346(3)
C(1A)-C(2A)	1.390(3)	C(2A)-C(3A)	1.364(4)
C(3A)-C(4A)	1.383(4)	C(4A)-C(5A)	1.355(4)
Bond angles (deg)			
Cl(1)-Cr(1)-Cl(2)	95.66(2)	Cl(1)-Cr(1)-S(1)	96.31(2)
Cl(2)-Cr(1)-S(1)	98.74(2)	C(1A)-S(1)-Cr(1)	108.47(7)
N(1)-C(1A)-C(2A)	116.4(2)	N(1)-C(1A)-S(1)	121.14(16)
C(2A)-C(1A)-S(1)	122.47(17)	C(3A)-C(2A)-C(1A)	120.4(2)
C(2A)-C(3A)-C(4A)	120.8(2)	C(5A)-C(4A)-C(3A)	118.3(2)
N(1)-C(5A)-C(4A)	119.9(2)		

(ii) $\text{CpCrI}_2(\text{SPyH})$ and $\text{CpCrI}_2(\text{Solv})$

The infrared spectrum in KBr disc shows a sharp and moderately strong N-H stretch at 3201 cm^{-1} . No signals are seen in the normal ^1H NMR region, indicative of paramagnetism, expected of 15-electron chromium(III) centres. The $\text{FAB}^+\text{-MS}$ shows the molecular ion peak at m/z 482 for $\text{CpCrI}_2(\text{SPyH})$. Elemental analysis of the mixture indicated the presence of a complex containing a thiopyridine moiety.

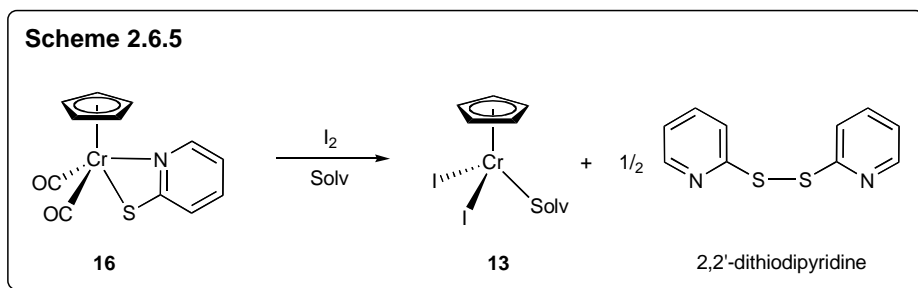
2.6.1.3 Conclusion

The reactions of $\text{CpCr}(\text{CO})_2(\text{SPy})$ (**16**) with various HX ($\text{X} = \text{F}, \text{Cl}, \text{I}$) provide an insight to the reactivity of both the entities. The inertness of HF was once again illustrated

by its reluctance to take part in the reaction with **16**, while both HCl and HI react in a similar fashion in a dual role of an acid as well as an oxidant; **16** is shown to be an effective reducing agent and a rather “halophilic” moiety. In this respect, we may be able to access a greater number of cyclopentadienylchromium(III) thio-containing complexes simply by the treatment of **16**-type of complexes with HX acids.

2.6.2 Reaction with iodine (oxidant)

The stoichiometric reaction between $\text{CpCr}(\text{CO})_2(\text{SPy})$ (**16**) and iodine in toluene at ambient temperature was complete after 2 h at which stage, the colour of the reaction mixture had changed from dark brown to deep green and the ^1H NMR spectrum indicated the absence of any starting material **16**. From this product solution was obtained a mixture of $\text{CpCrI}_2(\text{Solv})$ (**13**) in high yields (85%) along with the displaced ligand, 2,2'-dithiodipyridine, in 80% yield (Scheme 2.6.5).



2.6.2.1 Products and reaction pathways

The reaction of $\text{CpCr}(\text{CO})_2(\text{SPy})$ (**16**) with iodine resulted in a typical redox reaction. The chromium centre was oxidized from an oxidation state of +2 to +3 while the iodide reduced from an oxidation state of 0 to -1. In addition, the bonded thiolate (2-mercaptopyridine) was oxidized to a disulfide, which meant a formal oxidation state change from -2 to -1 (Refer to Section 2.3.3).

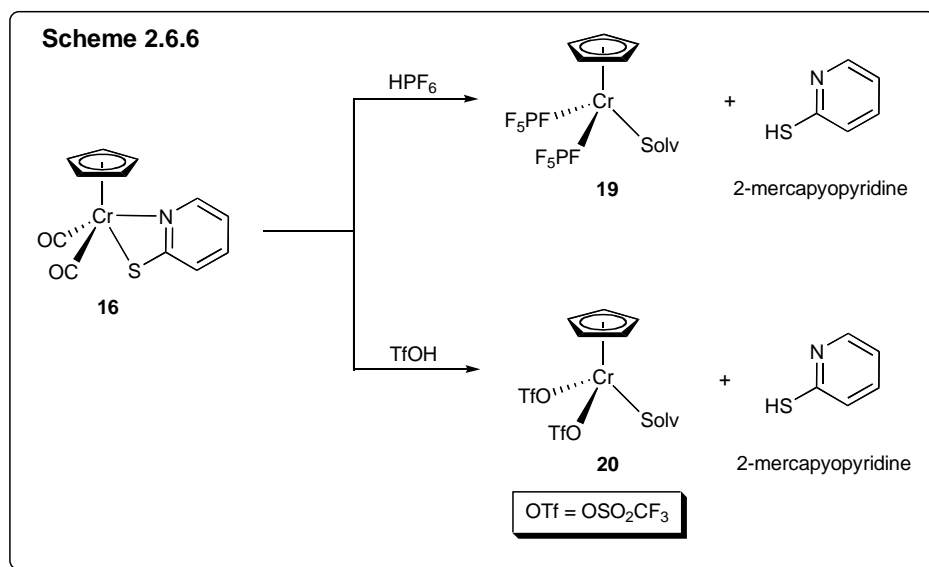
For a detailed mechanistic and crystallographic discussion on **13**, please refer to Section 2.3.3.

2.6.2.2 Conclusion

The reaction of $\text{CpCr}(\text{CO})_2(\text{SPy})$ (**16**) with iodine resulted in a redox reaction. **16** is shown to be an effective reducing agent and an “iodophilic” moiety. The bonded thiolate moiety was found to be easily oxidized to the disulfide by iodine.

2.6.3 Reaction with hexafluorophosphoric acid and triflic acid

As with the haloacids discussed above, the reaction of $\text{CpCr}(\text{CO})_2(\text{SPy})$ (**16**) with excess HPF_6 or TfOH in toluene at ambient temperature also required 18 h for completion. The colour of both the reaction mixtures changed from dark brown to deep green and their ^1H NMR spectrums indicated the absence of the starting material **16**. From these product solutions, moderate yields of $\text{CpCr}(\text{PF}_6)_2(\text{Solv})$ (**19**) (65%) and $\text{CpCr}(\text{OTf})_2(\text{Solv})$ (**20**) (50%) , along with 2-mercaptopyridine (70%, 60% respectively) were obtained.



2.6.3.1 Products and reaction pathways

The reaction of $\text{CpCr}(\text{CO})_2(\text{SPy})$ (**16**) with either HPF_6 or TfOH resembles that with HCl (Refer section 2.6.1), except that in this case, the ligand was detached from the chromium centre. In this reaction, both the acids still have a dual role to play, namely as a protonating acid and an oxidizing agent. (Refer to Section 2.6.1 for discussion).

In these reactions, two molar equivalents of acids are required, one mole for the proton donation, while the other as the oxidizing agent. The liberated hydrogen was not detected as in the case of HCl . The transfer of the PF_6^- anions onto the chromium centre illustrates the “halophilicity” of chromium centres while the transfer of a triflate anion shows the oxophilicity of the chromium centres. The transfers are rather efficient and feasible due to the formation of the strong Cr-F and Cr-O bonds, which are both exothermic and provide additional driving force for the individual reaction.

Because these complexes have been studied and documented, we have decided not to pursue in the investigation of these reactions and complexes any further.⁷⁹

2.6.3.2 Spectral characterization

(i) $\text{CpCr}(\text{PF}_6)_2(\text{CH}_3\text{CN})$ (19)

Its infrared spectrum in KBr disc does not give much information and the ^1H NMR spectrum shows no peaks in the normal ^1H NMR range indicative of paramagnetism, expected of a 15-electron chromium (III) centre. The compound, $\text{CpCr}(\text{PF}_6)_2(\text{CH}_3\text{CN})$, was reported to exhibit a broad peak at *ca.* 300 ppm for the Cp protons.⁷⁹ The FAB^+ -MS showed an intense peak at m/z 407, which corresponds to $[\text{M}^+ - \text{CH}_3\text{CN}]$ fragment, in agreement with facile loss of the weakly-bound solvent molecule.

(ii) $\text{CpCr}(\text{OTf})_2(\text{CH}_3\text{CN})$ (20)

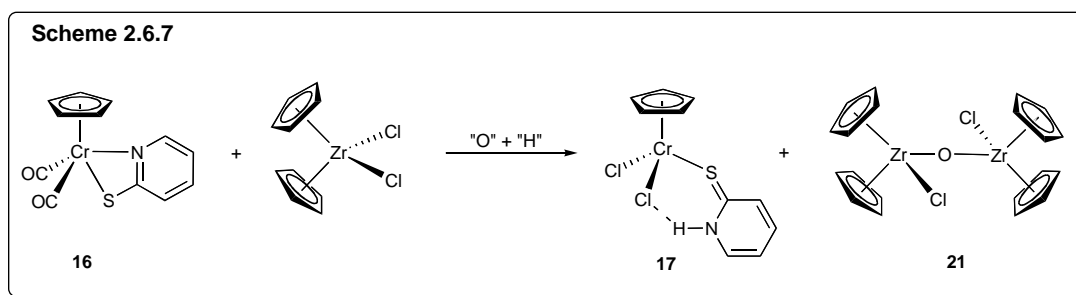
Its infrared spectrum in KBr disc again does not give much information and the ^1H NMR spectrum shows no peaks in the normal ^1H NMR range indicative of paramagnetism, expected of a 15-electron chromium(III) centre. The compound, $\text{CpCr}(\text{OTf})_2(\text{CH}_3\text{CN})$, was reported to exhibit a broad peak at *ca.* 313 ppm for the Cp protons while the corresponding THF analogue, $\text{CpCr}(\text{OTf})_2(\text{THF})$, exhibit a broad peak at *ca.* 314 ppm for the Cp protons.⁷⁹ The FAB^+ -MS showed an intense peak at m/z 415, which corresponds to $[\text{M}^+ - \text{CH}_3\text{CN}]$ fragment, in agreement with facile loss of the weakly-bound solvent molecule.

2.6.3.3 Conclusion

The reactions of $\text{CpCr}(\text{CO})_2(\text{SPy})$ (16) with HPF_6 or TfOH showed that the CpCr-moiety is very halo- and oxophilic and is an effective reducing agent.

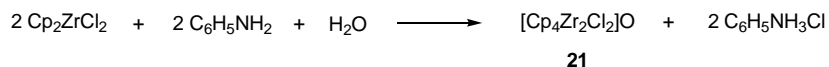
2.6.4 Reaction with dicyclopentadienylzirconium dichloride

The reaction between $\text{CpCr}(\text{CO})_2(\text{SPy})$ (**16**) and Cp_2ZrCl_2 in toluene at ambient temperature was quite sluggish and was only ca. 50% complete after 24 h. The ^1H NMR spectrum indicated the presence of starting material **16** which was recovered in 46%. The residue after extracting **16**, yielded a mixture of $[\text{Cp}_4\text{Zr}_2\text{Cl}_2]\text{O}$ (**21**) and $\text{CpCrCl}_2(\text{SPyH})$ (**17**), which could not be separated physically.



2.6.4.1 Products and reaction pathways

In an attempt to synthesize heterobimetallic complex, possibly bridged by the chloro or SPy ligands, $\text{CpCr}(\text{CO})_2(\text{SPy})$ (**16**) was reacted with two mole equivalents of Cp_2ZrCl_2 in toluene. However, no heterobimetallic species was observed. From the products, it is clear that the chromium fragment has reacted as a capable chloride-abstracting agent forming $\text{CpCrCl}_2(\text{SPyH})$ (**17**). In fact, a redox reaction must have taken place; however, the detailed mechanism remained elusive. The Cr atom is oxidized from +2 in **16** to +3 in **17** but the zirconium moiety's redox status remained unknown. The source of the oxygen and proton was also a mystery although it was thought to be from the solvent used. In spite of this, we note that all solvents were stringently dried prior to use. Previous studies showed that $[\text{Cp}_4\text{Zr}_2\text{Cl}_2]\text{O}$ (**21**) could be synthesized as follows (Scheme 2.6.8).⁹¹

Scheme 2.6.8

The transfer of the chlorides onto the chromium centre is an illustration of the “chlorophilicity” of chromium centres. The transfer is rather efficient and feasible due to the formation of the strong Cr-Cl bond, and the unexpected formation of the Zr-O bond, which are both exothermic, providing additional driving force for the reaction.

2.6.4.2 Spectral characterization**(i) $\text{CpCrCl}_2(\text{SPyH})$ (17)**

Please refer to Section 2.6.1.2 (i).

(ii) $[\text{Cp}_4\text{Zr}_2\text{Cl}_2]\text{O}$ (21)

Its infrared spectrum in KBr disc again does not give much information.

The ^1H NMR spectrum shows a Cp peak at δ 6.02 as reported. The FAB⁺-MS showed an intense peak at m/z 415, which corresponds to $[\text{M}^+ - \text{CH}_3\text{CN}]$ fragment. (Please refer to Ref. 91 for more details).

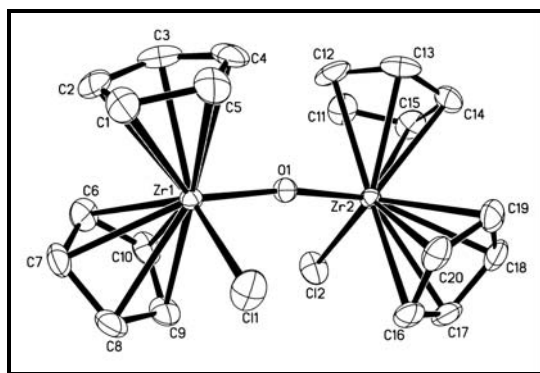


Figure 2.6.2. Molecular structure of $[\text{Cp}_4\text{Zr}_2\text{Cl}_2]\text{O}$ (21). Thermal ellipsoids are drawn at the 50% probability level.

The ORTEP of **21** is depicted in Figure 2.6.2. Selected bond lengths and angles are listed in Table 2.6.2. The geometry around both the zirconium atoms are approximately tetrahedral. Each of them is coordinated to a chloro, a μ₂-bridging oxo and two cyclopentadienyl ligands. Reid and coworkers determined the crystal structure of **21** having a monoclinic crystal system,⁹¹ while in our case, it was found to be trigonal. The different solvents and temperature of crystallization probably cause the difference. The pair of bond lengths of Zr(1)-Cl(1) and Zr(2)-Cl(2), and of Zr(1)-O(1) and Zr(2)-O(1) are very similar. The molecule is almost symmetrical about the plane perpendicular to the Zr(1)-O(1)-Zr(2) bond. The Zr(1)-O(1)-Zr(2) bond angle of 171.27(13) indicates a bent geometry between the zirconium atoms and a sp³ hybridized oxygen atom.

Table 2.6.2. Selected bond lengths (Å) and angles (deg) for **21**

Bond lengths (Å)			
Zr(1)-Cl(1)	2.4708(11)	Zr(2)-Cl(2)	2.4726(11)
Zr(1)-O(1)	1.944(3)	Zr(2)-O(1)	1.945(3)
Bond angles (deg)			
Cl(1)-Zr(1)-O(1)	97.02(9)	Cl(2)-Zr(2)-O(1)	97.04(9)
Zr(1)-O(1)-Zr(2)	171.27(13)		

2.6.4.3 Conclusion

The reactions of CpCr(CO)₂(SPy) (**16**) with Cp₂Zr₂Cl₂ once again showed that the CpCr-moiety is an efficient halide abstractor as well as an effective reducing agent.

Chapter 3: Experimental

3.1 General procedures.

All reactions were carried out using conventional Schlenk techniques under an inert atmosphere of nitrogen or under argon in an M. Braun Labmaster 130 Inert Gas System. All solvents were dried over sodium/benzophenone and distilled before use. Silica gel (Merck Kieselgel 60, 230-400 Mesh) was dried at 140 °C overnight before chromatographic use.

NMR spectra were measured on a Bruker 300 MHz FT NMR spectrometer (^1H at 300.14 MHz and ^{13}C at 75.43 MHz); ^1H and ^{13}C chemical shifts were referenced to residual C_6H_6 in C_6D_6 , CHCl_3 in CDCl_3 or CH_2DCN in CD_3CN .

IR spectra in nujol mulls or KBr pellet were measured in the range 4000-400 cm^{-1} on a BioRad FTS-165 FTIR instrument.

Mass spectra were obtained on a Finnigan Mat 95XL-T spectrometer.

Elemental analyses were performed by the Microanalytical Laboratory in the Chemistry Department of the National University of Singapore.

$[\text{CpCr}(\text{CO})_3]_2$ (**1**) was synthesised as described in the literature.³

X-ray diffraction analysis was done on a Siemens SMART diffractometer with a CCD Area Detector using MoK_α radiation. The crystals were mounted on quartz fibres. X-ray data were collected on a Siemens SMART diffractometer, equipped with a CCD detector, using MoK_α radiation (λ 0.71073 Å). The data was corrected for Lorentz and polarisation effects with the SMART suite of programs and for absorption effects with

SADABS. Structure solution and refinement were carried out with the SHELXTL suite of programs. The structure was solved by direct methods to locate the heavy atoms, followed by difference maps for the light non-hydrogen atoms.

3.2 The reaction of $[\text{CpCr}(\text{CO})_3]_2$ (**1**) with 2,5-dimercapto-1,3,4-thiadiazole (DMcTH₂)

3.2.1 At ambient temperature

A deep red solution mixture was obtained instantaneously when green solids of $[\text{CpCr}(\text{CO})_3]_2$ (**1**) (80 mg, 0.20 mmol) and yellow solids of 2,5-dimercapto-1,3,4-thiadiazole (DMcTH₂) (30.0 mg, 0.20 mmol) were dissolved in toluene (7 mL). The mixture was stirred at RT for 30 min. The resultant deep red product solution was concentrated to ca. 2 mL and loaded on to a silica gel column (2 x 10 cm) prepared in n-hexane. Elution gave 4 fractions: (i) a yellowish-green eluate in n-hexane (10 mL), which yielded green crystals of $\text{CpCr}(\text{CO})_3\text{H}$ (**22**) (ca. 22 mg, 0.06 mmol, 30% yield), identified by its colour characteristics and Cp resonance (¹H) in benzene-*d*₆ at δ -5.61 and 4.06 and its FAB⁺-MS molecular ion peak at *m/z* 202; (ii) a deep green eluate in toluene (7 mL), which on concentration gave deep green crystals (ca. 18 mg), the proton NMR spectrum of which showed a 2:1 molar mixture of $[\text{CpCr}(\text{CO})_2]_2$ (**23**) (ca. 6 mg, 0.02 mmol, 4% yield) and $[\text{CpCr}(\text{CO})_2]_2\text{S}$ (**24**) (ca. 12 mg, 0.03 mmol, 8% yield) at $\delta(\text{Cp})$ 4.24 and 4.36, respectively; (iii) a reddish-brown eluate in ether (10 mL), which yielded red crystals of $\text{CpCr}(\text{CO})_3(\text{DMcTH})$ (**3**) (ca. 40 mg, 0.11 mmol, 28% yield); (iv) a deep green eluate in acetonitrile (5 mL) which yielded a deep green oil of an uncharacterizable compound (ca. 20 mg). An immovable dirty green band (ca. 1 mm thick) was left on the column.

Data for 3. IR (KBr, cm^{-1}): $\nu(\text{N-H stretch})$ 3099s; $\nu(\text{sp}^2\text{-C-H stretch})$ 3097w and 3088w; $\nu(\text{C}\equiv\text{O stretch})$ 2034s, 1954s and 1890s; $\nu(\text{other bands})$ 1626m, 1469m, 1428m,

1384m, 1343m, 1268m, 1094s, 1048s, 1017s, 820vs, 769w, 707m, 666w, 606m, 579m and 517m. ^1H NMR (300MHz, 300 K, C_6D_6): δ 4.00 (s, 5 H, C_5H_5); δ 8.93 (s, 1 H, NH). A ^{13}C NMR spectrum is not available owing to instability in solution. In addition, the elemental analysis of the complex also showed disappointing results due to its instability. ESI⁺-MS: m/z 350 [M^+ , $\text{C}_{10}\text{H}_6\text{CrN}_2\text{O}_3\text{S}_3$]; FAB⁺-MS: m/z 351 [$\text{M}+\text{H}$, $\text{C}_{10}\text{H}_7\text{CrN}_2\text{O}_3\text{S}_3$]⁺, 266 [$\text{M}-3\text{CO}$]⁺, 182 [$\text{C}_{10}\text{H}_{10}\text{Cr}$]. High resolution FAB⁺-MS: m/z 350.9016 ([$\text{M}+\text{H}$]⁺, calcd m/z 350.9024). **3** is highly unstable and readily converts to a dirty green insoluble solid (**R1**) even under inert atmosphere at ambient temperature. The elemental analysis of which possessed an empirical formula $\text{C}_{8.34}\text{H}_{8.45}\text{N}_{1.55}\text{S}_{2.36}\text{Cr}$, *i.e.* in the proximity of $[\text{C}_5\text{H}_5\text{CrS}_3\text{C}_2\text{N}_2\text{H}]_n$, indicative of a polymeric form of **3** with loss of CO.

3.2.2 At 90 °C

A deep red solution mixture was obtained instantaneously when green solids of $[\text{CpCr}(\text{CO})_3]_2$ (**1**) (40 mg, 0.10 mmol) and yellow solids of DMcTH₂ (7.5 mg, 0.05 mmol) were dissolved in toluene (7 mL). The deep red mixture was heated at 90 °C for 2 h. ^1H NMR spectrum of the reaction mixture showed similar product composition as that obtained for ambient temperature. However, the amount of the insoluble dirty green solid obtained was significantly increased at 90 °C. The unreacted **1** was degraded to the triply bonded chromium dimer, $[\text{CpCr}(\text{CO})_2]_2$ (**23**), under thermolytic condition. This reaction was not pursued further due to the indifference.

3.2.3 NMR tube reactions

(i) Reaction of $[\text{CpCr}(\text{CO})_3]_2$ with 2,5-dimercapto-1,3,4-thiadiazole

A deep red mixture of $[\text{CpCr}(\text{CO})_3]_2$ (**1**) (4 mg, 0.01 mmol) and DMcTH₂ (2 mg, 0.01 mmol) in benzene-*d*₆ (0.5 ml) in a 5-mm NMR tube was manually shaken up for 10 min, and then its proton NMR spectrum scanned and subsequently monitored at intervals (15 min, 30 min, 1 h and 2 h). The integral ratios of the Cp resonances of the products were estimated.

(ii) Degradation of $\text{CpCr}(\text{CO})_3(\text{DMcTH})$ at different concentrations

Three red solutions of $\text{CpCr}(\text{CO})_3(\text{DMcTH})$ (**3**) at different concentrations (0.04 molL⁻¹, 0.02 molL⁻¹, 0.01 molL⁻¹) were prepared from a stock solution (14 mg, 0.04 mmol in 1.0 mL benzene-*d*₆). The three samples were manually shaken up, and kept cool at 0 °C before their proton NMR spectra were scanned. The integral ratios of the Cp resonances of the products were estimated.

3.2.4 Crystal structure analyses.

Diffraction-quality crystals of **3** were obtained as air-sensitive bright red plate-like crystals from solutions in toluene layered with hexane after 4 days at -30 °C.

3.3 The reaction of $[\text{CpCr}(\text{CO})_3]_2$ (**1**) with 5,5'-dithiobis(1-phenyl-1H-tetrazole) (**STz**)₂

3.3.1 At -30 °C

A deep green solution of **1** (40 mg, 0.10 mmol) in 2 mL THF was added to a solution of 5,5'-dithiobis(1-phenyl-1H-tetrazole) (35 mg, 0.10 mmol) in 2 mL THF in a test tube, the magenta mixture was immediately kept at -30 °C. After 4 days, bright red rhombic-shaped crystals of $\text{CpCr}(\text{CO})_3(\eta^1\text{-SCN}_4\text{Ph})$ (**4**) (60 mg, 0.16 mmol, 79%) was obtained.

Data for 4. IR [KBr, cm^{-1}] $\nu(\text{CO})$ 2044s, 1937s, 1894s; $\nu(\text{N-N=N})$ 1275m; $\nu(\text{C-S})$ 696s, 685s, 627s. $\nu(\text{other bands})$ 1597m, 1500s, 1459w, 1428m, 1388msh, 1369s, 1313w, 1228m, 1173w, 1091m, 1040w, 1016m, 915w, 852s, 764s, 580s, 507s. $^1\text{H NMR}$ (300 MHz, 300 K, C_6D_6): δ 4.32 (s, 5 H, C_5H_5); δ 7.63, 7.66 (m, 5 H, C_6H_5). The $^{13}\text{C NMR}$ experiment could not be done owing to the instability of the complex. Anal. Calcd for $\text{C}_{15}\text{H}_{10}\text{CrN}_4\text{O}_3\text{S}$: C, 47.6; H, 2.7; N, 14.8%. Found: C, 47.9; H, 2.9; N, 14.6. FAB⁺-MS: m/z 379 [$\text{M}^+\text{+H}$, $\text{CpCr}(\text{CO})_3(\text{SCN}_4\text{Ph})$], 351 [$\text{M}^+\text{-CO}$, $\text{CpCr}(\text{CO})_2(\text{SCN}_4\text{Ph})$], 294 [$\text{M}^+\text{-3CO}$ $\text{CpCr}(\text{SCN}_4\text{Ph})$], 219 [$\text{CpCr}(\text{SCN}_4)$], 136 [$(\text{CN}_4)_2$], 69 [CN_4].

3.3.2 At ambient temperature

$[\text{CpCr}(\text{CO})_3]_2$ (**1**) (40 mg, 0.10 mmol) and 5,5'-dithiobis(1-phenyl-1H-tetrazole) (35 mg, 0.10 mmol) were dissolved in toluene (5 mL). A deep magenta mixture was

immediately obtained and stirred at RT for 30 min. The resultant deep magenta product solution was filtered to remove some purple residue (**R2**) (40 mg). Concentration of the filtrate to 2 mL followed by addition of *n*-hexane (*ca.* 2 mL) and subsequent overnight cooling at - 30 °C gave air-sensitive bright red crystals of $\text{CpCr}(\text{CO})_3(\eta^1\text{-SCN}_4\text{Ph})$ (**4**). (25 mg, 0.07 mmol, 33% yield), identified by its colour characteristics and Cp resonance (^1H) in benzene- d_6 at δ 4.32 and its FAB^+ -MS molecular ion peak at m/z 379. **4** was found to convert quantitatively to the insoluble purple powder after stirring for 24 h or when the solution was heated at high temperatures.

Data for R2. IR (KBr, cm^{-1}): $\nu(\text{N-H stretch})$ 3099s; $\nu(\text{sp}^2\text{-C-H stretch})$ 3101w and 3068w; No $\text{C}\equiv\text{O}$ stretch; $\nu(\text{other bands})$ 1634mb, 1597m, 1499s, 1463w, 1432w, 1375s, 1322m, 1302w, 1268s, 1093s, 1049s, 1018s, 916w, 822s, 760s, 688s, 613w, 560m and 471m. ^1H NMR and ^{13}C NMR spectra were not available because the complex is an insoluble solid. The elemental analyses: C, 47.9; H, 2.9; N, 14.6; S, 11.6; Cr, 12.7, could not be rationalized.

3.3.3 Cothermolysis of $\text{CpCr}(\text{CO})_3(\text{SCN}_4\text{Ph})$ with $[\text{CpCr}(\text{CO})_3]_2$ at 90 °C

A dark brown mixture of $[\text{CpCr}(\text{CO})_3]_2$ (**1**) (80 mg, 0.20 mmol) and $\text{CpCr}(\text{CO})_3(\text{SCN}_4\text{Ph})$ (**X**) (76 mg, 0.20 mmol) in toluene (7 mL) was stirred at 90 °C for 2 h. The resultant blackish-brown reaction mixture was concentrated to *ca.* 3 mL and filtered to remove some blackish-green precipitate (**R3**) (40 mg). The filtrate was then loaded onto a silica gel column (2.5 × 15 cm) prepared in *n*-hexane. Elution gave seven fractions: (i) a bright green eluate in *n*-hexane (15 mL), ^1H NMR spectrum of which showed a 4:1 molar mixture of $[\text{CpCr}(\text{CO})_2]_2$ (**23**) and $[\text{CpCr}(\text{CO})_2]_2\text{S}$ (**24**) equivalent to

24 mg and 6 mg, 0.07 mmol and 0.02 mmol, 34% and 8% respectively; (ii) a grayish-green eluate in n-hexane/toluene (1:1, 5 mL), which on concentration gave $\text{Cp}_4\text{Cr}_4\text{S}_4$ (**26**) (10 mg, 0.02 mmol, 17%); (iii) a brown eluate in n-hexane/toluene (1:2, 5 mL), which yielded brown crystals of $\text{Cp}_4\text{Cr}_4\text{S}_3(\text{N}_3\text{Ph})(\text{CpCr}(\text{CO})_2\text{CN})$ (**5**) (3 mg, 3.5 μmol , 4%); (iv) a dark brown eluate in toluene (5 mL), which yielded brown crystals of $\text{Cp}_4\text{Cr}_4\text{S}_3(\text{N}_3\text{Ph})$ (**6**) (5 mg, 7.3 μmol , 7%); (v) a deep green eluate in toluene/ether (5 mL), which yielded green crystals of an unknown (3 mg); (vi) a dirty green eluate in THF (5 mL), which on concentration gave black-green crystals of $\text{Cp}_4\text{Cr}_4\text{S}_2\text{O}_2$ (**25**) (5 mg, 0.01 mmol, 9%); (vii) a navy blue eluate in methanol (10 mL), which yielded blue crystals of $\text{Cr}(\text{SCN}_4\text{Ph})_3$ (**7**) (3 mg, 5.1 μmol , 1%). A deep purplish-blue band remained unmoved on top of the column.

Data for R3. IR [KBr, cm^{-1}] $\nu(\text{sp}^2\text{-C-H})$ 3108s; $\nu(\text{other bands})$ 1628m, 1595m, 1499s, 1460w, 1411m, 1380s, 1318m, 1246m, 1176w, 1092m, 1055m, 1023m, 916w, 824s, 763s, 688s, 571s, 513w. $^1\text{H NMR}$ (300 MHz, 300 K, C_6D_6): δ 5.10 (s, 15 H, C_5H_5), 4.84 (s, 5 H, C_5H_5); 7.42-7.72 (m, 5 H, C_6H_5). The elemental analyses: C, 44.8; H, 3.6; N, 13.1; S, 9.87, could not be rationalized. $\text{FAB}^+\text{-MS}$ shows a largest m/z at 914 and a most intense peak at 698, both of which were not assignable.

Data for 5. IR [KBr, cm^{-1}] $\nu(\text{CO})$ 1923s, 1854s; $\nu(\text{N-N=N})$ 1401m, 1203m, 1167m; $\nu(\text{C-N})$ 1030sb; $\nu(\text{other bands})$ 1656m, 1584m, 1474m, 802s. $^1\text{H NMR}$ (300 MHz, 300 K, C_6D_6): δ 4.64 (s, 5 H, C_5H_5), 4.93 (s, 5 H, C_5H_5), 5.13 (s, 10 H, C_5H_5), 5.48 (s, 5 H, C_5H_5); 7.42-7.72 (m, 5 H, C_6H_5). The $^{13}\text{C NMR}$ experiment and the elemental

analyses could not be done because of insufficient material available. FAB⁺-MS: m/z 850 [M^+ , $\text{Cp}_4\text{Cr}_4\text{S}_3(\text{N}_3\text{Ph})(\text{CpCr}(\text{CO})_2\text{CN})$].

Data for 6. IR [KBr, cm^{-1}] $\nu(\text{N-N=N})$ 1431m, 1278w, 1175s; $\nu(\text{C-N})$ 1009b; $\nu(\text{other bands})$ 3074w, 3026w, 1685w, 1651m, 1600vs, 1508w, 1488w, 1385w, 1363w, 1317w, 1257w, 1121m, 1074m, 1009s, 942w, 918w, 901w, 874w, 839s, 806vs, 766s, 721m, 697s, 639m. ^1H NMR (300 MHz, 300 K, C_6D_6): δ 5.08 (s, 15 H, C_5H_5), 4.87 (s, 5 H, C_5H_5); 7.42-7.72 (m, 5 H, C_6H_5). The ^{13}C NMR experiment and the elemental analyses could not be done because of insufficient material available. FAB⁺-MS: m/z 683 [M^+ , $\text{Cp}_4\text{Cr}_4\text{S}_3(\text{N}_3\text{Ph})$].

Data for 7. IR spectrum shows the absence of CO stretches. ^1H NMR shows no peaks indicative of paramagnetism. The elemental analyses could not be done due to shortage of complex. FAB⁺-MS: m/z 583 [M^+ , $\text{Cr}(\text{SCN}_4\text{Ph})_3$].

3.3.4 Crystal structure analyses

Diffraction-quality crystals of $\text{CpCr}(\text{CO})_3(\eta^1\text{-SCN}_4\text{Ph})$ (**4**) were obtained as bright red rhombic-shaped crystals from solutions in toluene layered with hexane after 4 days at -30 °C. Brown rhombic crystals of $\text{Cp}_4\text{Cr}_4\text{S}_3(\text{N}_3\text{Ph})(\text{CpCr}(\text{CO})_2\text{CN})$ (**5**) were obtained from solutions in toluene layered with hexane after 7 days at -30 °C. Diffraction quality black-green crystals of $\text{Cp}_4\text{Cr}_4\text{S}_2\text{O}_2$ (**25**) were obtained from a solution of THF layered with n-hexane after 3 days at -30 °C.

3.4 Reactions of $\text{CpCr}(\text{CO})_3(\eta^1\text{-STz})$ (**4**)

3.4.1 Reaction with trimethyloxonium tetrafluoroborate

To a deep magenta solution of $\text{CpCr}(\text{CO})_3(\eta^1\text{-SCN}_4\text{Ph})$ (**4**) (38 mg, 0.10 mmol) in toluene (7 mL) was added trimethyloxonium tetrafluoroborate, $(\text{CH}_3)_3\text{OBF}_4$ in excess (30 mg, 0.20 mmol) at 0 °C. The reaction mixture was stirred at 0 °C for 30 min followed by 18 h at RT. The deep purple solution obtained was evacuated to dryness and the residue redissolved in CH_3CN and filtered through a frit. The filtrate was concentrated to *ca.* 2 mL and diethyl ether (*ca.* 2 mL) added. Subsequent cooling to -30 °C overnight gave colourless crystals of the excess unreacted $(\text{CH}_3)_3\text{OBF}_4$. Removal of this followed by further cooling at -30 °C for 2 days gave air-sensitive deep blue crystals of $\text{Cp}_2\text{Cr}_2(\mu\text{-OH})(\mu\text{-}\eta^2\text{-SCN}_4\text{Ph})_2\text{BF}_4$ (**8**) (15 mg, 0.02 mmol, 25% yield).

Data for 8. IR (KBr, cm^{-1}): $\nu(\text{O-H})$ 3413 sb. $\nu(\text{C-H})$ 3114m. $\nu(\text{other bands})$ 1630w, 1596m, 1498s, 1460w, 1431m, 1380s, 1331s, 1237m, 1123s, 1084vs, 1050s, 1017s, 824s, 762s, 686s, 617m, 588m and 565m. $^1\text{H NMR}$ shows no peaks in the normal region, indicative of paramagnetism. In addition, the elemental analysis of the complex also showed disappointing results, perhaps due to its instability. $\text{FAB}^+\text{-MS}$: m/z 605 [M^+ , $\text{Cp}_2\text{Cr}_2(\text{OH})(\text{SCN}_4\text{Ph})_2$], 588 [$\text{M}^+\text{-OH}$, $\text{Cp}_2\text{Cr}_2(\text{SCN}_4\text{Ph})_2$]. $\text{FAB}^-\text{-MS}$: m/z 87 [BF_4^-].

3.4.2 Reaction with dimethylsulfate

To a deep magenta solution of $\text{CpCr}(\text{CO})_3(\eta^1\text{-SCN}_4\text{Ph})$ (**4**) (38 mg, 0.10 mmol) in toluene (7 mL) was added dimethylsulfate, $(\text{CH}_3\text{O})_2\text{SO}_2$ in large excess (100 μL) at 0 °C.

The reaction mixture was stirred at 0 °C for 30 min followed by 18 h at RT. The deep blue solution obtained was evacuated to dryness to remove the unreacted methylating reagent and solvent. The residue was redissolved in CH_3CN and filtered through a frit. The filtrate was concentrated to *ca.* 2 mL and diethyl ether (*ca.* 2 mL) added. Subsequent cooling to -30 °C overnight gave air-sensitive deep purple crystals of $\text{Cp}_3\text{Cr}_3(\mu_2\text{-OH})(\mu_3\text{-O})(\mu_2\text{-}\eta^2\text{-SCN}_4\text{Ph})_2(\text{CH}_3\text{OSO}_3)$ (**9**) (15 mg, 0.02 mmol, 20% yield).

Data for 9. IR (KBr, cm^{-1}): $\nu(\text{O-H})$ 3254 sb. $\nu(\text{C-H})$ 3104m. $\nu(\text{other bands})$ 1633wb, 1595m, 1498s, 1461w, 1426w, 1380s, 1321s, 1262s, 1246s, 1208s, 1090m, 1056s, 1007s, 825s, 763s, 747s, 695s, 606m, 563s and 430w. $^1\text{H NMR}$ shows no peaks in the normal region, indicative of paramagnetism. In addition, the elemental analysis of the complex also showed disappointing results, perhaps due to its instability. $\text{FAB}^+\text{-MS}$: m/z 738 [M^+ , $\text{Cp}_3\text{Cr}_3(\text{OH})(\text{O})(\text{SCN}_4\text{Ph})_2$], 605 [M^+ - CpCrO , $\text{Cp}_2\text{Cr}_2(\text{OH})(\text{SCN}_4\text{Ph})_2$], 588 [M^+ - CpCrOOH , $\text{Cp}_2\text{Cr}_2(\text{SCN}_4\text{Ph})_2$]. $\text{FAB}^-\text{-MS}$: m/z 111 [$\text{CH}_3\text{OSO}_3^-$].

3.4.3 Reaction with HCl

To a deep magenta solution of $\text{CpCr}(\text{CO})_3(\eta^1\text{-SCN}_4\text{Ph})$ (**4**) (38 mg, 0.10 mmol) in toluene (7 mL) was added hydrochloric acid in large excess (1.0 mL, 1.0 molL^{-1}) at 0 °C. The reaction mixture was stirred at 0 °C for 30 min followed by 18 h at RT. The bluish-green oil obtained was evacuated to dryness to remove the excess acid and solvent, and the residue was extracted with *n*-hexane/toluene (2:1) to remove any organic product, which was characterized as 5-mercapto(1-phenyl-1H-tetrazole), $\text{HSCN}_4\text{C}_6\text{H}_5$ (10 mg, 0.06 mmol, 56%) via $^1\text{H NMR}$ spectrum and EI-MS. The organometallic product was dissolved in CH_3CN , and filtered through a frit but no residue was observed. The resultant

solution was concentrated to *ca.* 2 mL and diethylether (*ca.* 2 mL) added. Subsequent cooling to $-30\text{ }^\circ\text{C}$ overnight gave some air-sensitive microcrystalline green crystals of $\text{CpCrCl}_2(\text{CH}_3\text{CN})$ (**12**) (15 mg, 0.06 mmol, 66% yield).

Data for 12. ^1H NMR shows no peaks in the normal region, indicative of paramagnetism. FAB⁺-MS and ESI⁺-MS analysis did not show the M⁺ peak but an x-ray diffraction procedure revealed the structure of this solvated complex. Because this class of complexes has been reviewed, we have chosen not to investigate the product and reaction further.

3.4.4 Reaction with iodine

To a deep magenta solution of $\text{CpCr}(\text{CO})_3(\eta^1\text{-SCN}_4\text{Ph})$ (**4**) (38 mg, 0.10 mmol) in toluene (7 mL) was added iodine crystals (25 mg, 0.10 mmol) at $0\text{ }^\circ\text{C}$. The reaction mixture was stirred at $0\text{ }^\circ\text{C}$ for 30 min followed by 2 h at RT. The deep green solution obtained was evacuated to dryness and the residue was extracted with *n*-hexane/toluene (2:1) to remove any organic product which was characterized as 5,5'-dithiobis(1-phenyl-1H-tetrazole) (25 mg, 0.07 mmol, 71%) via ^1H NMR spectrum and EI-MS. The organometallic remnant was dissolved in CH_3CN and filtered through a frit, but no residue was observed. The resultant solution was concentrated to *ca.* 2 mL and diethyl ether (*ca.* 2 mL) added. Subsequent cooling to $-30\text{ }^\circ\text{C}$ overnight gave air-sensitive green crystals of $\text{CpCrI}_2(\text{CH}_3\text{CN})$ (**13**) (31 mg, 0.07 mmol, 75% yield).

Data for 13. ^1H NMR shows no peaks in the normal region, indicative of paramagnetism. FAB⁺-MS: *m/z* 742 [$2\text{M}^+ - 2\text{CH}_3\text{CN}$, $(\text{CpCrI}_2)_2$], 371 [$\text{M}^+ - \text{CH}_3\text{CN}$,

CpCrI_2], 254 [I₂], 182 [Cp₂Cr]. An x-ray diffraction procedure revealed the structure of this solvated complex. Because this class of complexes has been reviewed, we have chosen not to investigate the product and reaction further.

3.4.5 Reaction with iron pentacarbonyl

To a deep magenta solution of $\text{CpCr}(\text{CO})_3(\eta^1\text{-SCN}_4\text{Ph})$ (**4**) (38 mg, 0.10 mmol) in toluene (7 mL) was added iron pentacarbonyl in large excess (1.0 mL) at 0 °C. The reaction mixture was stirred at 0 °C for 30 min followed by 18 h at RT. The dark green solution obtained was evacuated to dryness to remove the excess iron pentacarbonyl and solvent. The green mixture contains some purple residue which was filtered and analysed. The green filtrate was gave $[\text{CpCr}(\text{CO})_3]_2$ (15 mg, 0.04 mmol, 75% yield) diagnosed via its IR and ¹H NMR spectral characteristics reported in the literature.^{3,5} The purple residue (**14**) obtained (15 mg) was dissolved in THF (*ca.* 2 mL) and *n*-hexane (*ca.* 2 mL) added. Subsequently cooled to -30 °C. Deep purple microcrystalline crystals were obtained after 7 days.

Data for 14. IR (KBr, cm⁻¹): $\nu(\text{C-H})$ 3106w, 3070w. $\nu(\text{other bands})$ 1624wb, 1597m, 1498s, 1460w, 1429w, 1380s, 1322s, 1303s, 1239m, 1208s, 1089m, 1052m, 1021m, 914w, 819s, 761s, 692s, 607m and 569m. ¹H NMR shows only some peaks in the phenyl region. The elemental analysis was found to be: C, 44.5; H, 2.9; N, 22.3; S, 11.7%. FAB⁺-MS: *m/z* 1027.

3.4.6 Crystal structure analyses

Diffraction-quality single crystals were obtained as follows: $\text{Cp}_2\text{Cr}_2(\mu\text{-OH})(\mu\text{-}\eta^2\text{-SCN}_4\text{Ph})_2\text{BF}_4$ (**8**) as deep blue rhombus from a solution of acetonitrile layered with toluene after 2 days at $-30\text{ }^\circ\text{C}$; $\text{Cp}_3\text{Cr}_3(\mu_2\text{-OH})(\mu_3\text{-O})(\mu_2\text{-}\eta^2\text{-SCN}_4\text{Ph})_2(\text{CH}_3\text{OSO}_3)$ (**9**) as dark purple rhombus from a solution of acetonitrile layered with toluene after 1 day at $-30\text{ }^\circ\text{C}$; $\text{CpCrCl}_2(\text{CH}_3\text{CN})$ (**12**) and $\text{CpCrI}_2(\text{CH}_3\text{CN})$ (**13**) as dark bluish-green needles from a solution of acetonitrile layered with toluene after 1 day at $-30\text{ }^\circ\text{C}$.

3.5 The reaction of $[\text{CpFe}(\text{CO})_2]_2$ (**2**) with 5,5'-dithiobis(1-phenyl-1H-tetrazole) (**STz**)₂

3.5.1 At ambient temperature

A deep brown solution of $[\text{CpFe}(\text{CO})_2]_2$ (**2**) (105 mg, 0.30 mmol) and 5,5-dithio(1-phenyl-1H-tetrazole) (105 mg, 0.30 mmol) in toluene (5 mL) was stirred at ambient temperature for 18 h. An orangish-brown mixture was obtained. The resultant mixture was filtered, but no residue was observed. Concentration of the filtrate to *ca.* 2 mL and n-hexane (*ca.* 2 mL) added gave air-sensitive bright red crystals of $\text{CpFe}(\text{CO})_2(\eta^1\text{-SCN}_4\text{Ph})$ (**15**) (85 mg, 0.24 mmol, 80.0% yield) after 2 h at -30°C .

Data for 15. IR (KBr, cm^{-1}): $\nu(\text{aromatic C-H})$ 3122m, 3095m. $\nu(\text{CO})$ 2034s and 1986s. $\nu(\text{other bands})$ 1594w, 1497s, 1427w, 1367s, 1271m, 1228m, 1082w, 1018w, 845m, 748m, 689s, 679m, 603s, 571s, 544s. $^1\text{H NMR}$ (300MHz, 300 K, CD_3CN): δ 5.20 (s, 5 H, C_5H_5); δ 7.50-7.73 (m, 5 H, C_6H_5). Anal. Calcd for $\text{C}_{14}\text{H}_{10}\text{FeN}_4\text{O}_2\text{S}$: C, 47.46; H, 2.82; N, 15.82; S, 9.04%. Found: C 47.85; H, 2.81; N, 15.90; S, 9.15%. FAB⁺-MS: *m/z* 709.0 [2M^+ ; $\text{Cp}_2\text{Fe}_2(\text{CO})_4(\text{SCN}_4\text{Ph})_2$], 652.0 [$2\text{M}^+-2\text{CO}$; $\text{Cp}_2\text{Fe}_2(\text{CO})_2(\text{SCN}_4\text{Ph})_2$], 587.0 [$2\text{M}^+-2\text{CO}-\text{Cp}$; $\text{CpFe}_2(\text{CO})_2(\text{SCN}_4\text{Ph})_2$], 355.0 [M^+ ; $\text{CpFe}(\text{CO})_2(\text{SCN}_4\text{Ph})$], 299.0 [M^+-2CO ; $\text{CpFe}(\text{SCN}_4\text{Ph})$], 270.0 [$\text{CpFe}(\text{SCN}_2)$], 136.0 [$(\text{CN}_4)_2$].

3.5.2 Crystal structure analysis

Diffraction-quality crystals were obtained as air-sensitive bright red rhombic crystals from solutions in toluene layered with hexane after 2 h at -30 °C.

3.6 The reaction of $[\text{CpCr}(\text{CO})_3]_2$ (**1**) with 2,2'-dithiodipyridine (SPy)₂

3.6.1 At ambient temperature

A deep green mixture of $[\text{CpCr}(\text{CO})_3]_2$ (**1**) (45 mg, 0.11 mmol) and 2,2'-dithiodipyridine (24.5 mg, 0.11 mmol) in toluene (5 mL) was stirred at ambient temperature for 1.5 h. The resultant reddish-brown mixture was filtered, but no residue was observed. Concentration of the filtrate to ca. 1 mL and n-hexane (ca. 1 mL) added gave air-stable dark brown crystals of $\text{CpCr}(\text{CO})_2(\text{SPy})$ (**16**) (45 mg, 0.016 mmol, 72 % yield) after 2 h at -30 °C.

Data for 16. IR (KBr, cm^{-1}): $\nu(\text{aromatic C-H})$ 3117w; $\nu(\text{C=N})$ 2364w, 2343w; $\nu(\text{C}\equiv\text{O})$ 1950s, 1874s; $\nu(\text{other bands})$ 1584m, 1541m, 1449m, 1412m, 1261m, 1153m, 1137m, 1062w, 1013w, 852m, 825s, 744s, 631m, 567s, 524m, 464m. $^1\text{H NMR}$ (300 MHz, 300 K, C_6D_6): δ 4.44 (s, 5 H, C_5H_5); δ 7.37 (d, $J = 6$ Hz, 1 H, Py); 6.48 (t, $J = 6$ Hz, 1 H, Py); 6.20 (d, $J = 6$ Hz, 1 H, Py); 5.97 (t, $J = 6$ Hz, 1 H, Py). $^{13}\text{C NMR}$ (75 MHz, 300 K, C_6D_6): δ 94.2 (s, C_5H_5); δ 116.1, 126.9, 135.0, 154.8 and 179.0 (s, Py); δ 265.5 and 270.2 (s, CO). Anal. Calcd for $\text{C}_{12}\text{H}_9\text{CrNO}_2\text{S}$: C, 50.8; H, 3.2; N, 4.9; S, 11.3%. Found: C, 51.0; H, 3.1; N, 4.8; S, 11.1%. FAB⁺-MS: m/z 283 [M^+ , $\text{CpCr}(\text{CO})_2(\text{SPy})$], 227 [$\text{CpCr}(\text{SPy})$], 195 [$\text{CpCr}(\text{Py})$], 162 [$\text{Cr}(\text{SPy})$].

3.6.2 Crystal structure analysis

Diffraction-quality crystals were obtained as dark brown rhombic crystals from solutions in toluene layered with hexane after 2 h at -30 °C. An IR spectrum of the crystals shows that the compound is stable in the atmosphere for days.

3.7 Reactions of $\text{CpCr}(\text{CO})_2(\eta^2\text{-SPy})$ (**16**)

3.7.1 Reaction with HX (X = F, Cl, I)

(i) Reaction with HF

To a dark brown solution of $\text{CpCr}(\text{CO})_2\text{SPy}$ (**16**) (28 mg, 0.10 mmol) in toluene (7 mL) was added conc. hydrofluoric acid in excess (1.0 mL) at 0 °C. The reaction mixture was stirred at 0 °C for 30 min followed by 4 days at RT. Aliquots of the reaction mixture were withdrawn periodically and their ^1H NMR were checked. This showed no change for 4 days of reaction had occurred.

(ii) Reaction with HCl

To a dark brown solution of $\text{CpCr}(\text{CO})_2\text{SPy}$ (**16**) (57 mg, 0.20 mmol) in toluene (7 mL) was added conc. hydrochloric acid in large excess (1.0 mL) at 0 °C. The reaction mixture was stirred at 0 °C for 30 min followed by 18 h at RT. The bluish-green oil obtained was evacuated to dryness to remove the excess acid and solvent. The residue was redissolved in CH_3CN and filtered through a frit. The filtrate was concentrated to *ca.* 2 mL and diethylether (*ca.* 2 mL) added. Subsequent cooling to -30 °C overnight gave air-sensitive bluish-green crystals of $\text{CpCrCl}_2(\text{SPyH})$ (**17**) (54 mg, 0.17 mmol, 90% yield).

(iii) Reaction with HI

To a dark brown solution of $\text{CpCr}(\text{CO})_2\text{SPy}$ (**16**) (57 mg, 0.20 mmol) in toluene (7 mL) was added conc. hydroiodic acid in large excess (1.0 mL) at 0 °C. The reaction mixture was stirred at 0 °C for 30 min followed by 18 h at RT. The deep green solution obtained was evacuated to dryness to remove the excess acid

and solvent. It was then extracted with toluene to remove the excess HI before redissolved in CH_3CN and filtered through a frit. The filtrate was concentrated to *ca.* 2 mL and diethylether (*ca.* 2 mL) added. Subsequent cooling to $-30\text{ }^\circ\text{C}$ overnight gave a mixture of air-sensitive green crystals of $\text{CpCrI}_2(\text{CH}_3\text{CN})$ (**13**) and $\text{CpCrI}_2(\text{SPyH})$ (**18**).

Data for 17. ^1H NMR shows no peaks in the normal region, indicative of paramagnetism. IR (KBr, cm^{-1}): $\nu(\text{N-H})$ 3429 sb. $\nu(\text{C-H})$ 3128w, 3074w, 3041w, 3015w. $\nu(\text{other bands})$ 2367w, 2336w, 1583s, 1513m, 1374m, 1260ws, 1158w, 1126s, 1018w, 1007w, 819s, 754s, 485w and 448w. ^1H NMR shows no peaks indicative of paramagnetism. Anal. Calcd for $\text{C}_{10}\text{H}_{10}\text{CrCl}_2\text{NS}$: C, 40.1; H, 3.3; N, 4.7; S, 10.7%. Found: C, 39.6; H, 3.5; N, 5.1; S, 11.2%. FAB⁺-MS: m/z 298 [$\text{M}^+\text{-H}$, $\text{CpCrCl}_2(\text{SPy})$], 263 [$\text{CpCrCl}(\text{SPy})$], 227 [$\text{CpCr}(\text{SPy})$], 195 [$\text{CpCr}(\text{Py})$], 112 [HSPy+H].

Data for 13 and 18.⁷⁹ Because this mixture cannot be separated, we probe the spectroscopic properties as a mixture. IR (KBr, cm^{-1}): $\nu(\text{N-H stretch})$ 3201m; $\nu(\text{sp}^2\text{-C-H stretch})$ 3110m, 3079m, 3022; $\text{C}\equiv\text{O}$ stretch is not observed; $\nu(\text{C=C})$ 1608s; $\nu(\text{C-N})$ 1584vs; $\nu(\text{other bands})$ 1507s, 1439m, 1370m, 1281w, 1262w, 1227w, 1161m, 1133s, 1097w, 1033w, 997m, 821s, 752m, 725s, 621w, 477m, 447m. ^1H NMR shows no peaks in the normal region, indicative of paramagnetism. The elemental analysis of the sample: C, 20.3; H, 2.1; N, 3.8; S, 6.0%. The ratio of N:S is approximately one indicating the presence of the thiopyridine moiety which consists of one N- and S-atom each. FAB⁺-MS: m/z 482 [M^+ , $\text{CpCrI}_2(\text{SPyH})$], 355 [$\text{M}^+\text{-I}$, $\text{CpCrI}(\text{SPyH})$], 244 [CpCrI], 227 [CpCrSPy].

3.7.2 Reaction with iodine

To a dark brown solution of CpCr(CO)₂SPy (**16**) (57 mg, 0.20 mmol) in toluene (7 mL) was added iodine crystals (51 mg, 0.20 mmol) at 0 °C. The reaction mixture was stirred at 0 °C for 30 min for 2 h at RT. The deep green solution obtained was evacuated to dryness and was then extracted with *n*-hexane/toluene (2:1) to remove any organic products, which was characterized as 2,2'-dithiodipyridine (35 mg, 0.16 mmol, 80%) via ¹H NMR spectrum and EI-MS. The organometallic remnant was dissolved in CH₃CN and filtered through a frit but no residue was observed. The filtrate was concentrated to *ca.* 2 mL and diethylether (*ca.* 2 mL) added. Subsequent cooling to -30 °C overnight gave air-sensitive green crystals of CpCrI₂(CH₃CN) (**13**) (70 mg, 0.17 mmol, 85% yield).

Data for 13.⁷⁹ Please refer to section 3.4.5.

3.7.3 Reaction with hexafluorophosphoric acid and triflic acid

(i) Reaction with hexafluorophosphoric acid

To a dark brown solution of CpCr(CO)₂SPy (**16**) (28 mg, 0.10 mmol) in toluene (7 mL) was added conc. HPF₆ acid in large excess (1.0 mL) at 0 °C. The reaction mixture was stirred at 0 °C for 30 min for 18 h at RT. The deep green solution obtained was evacuated to dryness to remove the excess acid and was then extracted with *n*-hexane/toluene (2:1) to remove any organic product, which was characterized as 2-thiopyridine (PySH) (8 mg, 0.07 mmol, 70%) via ¹H NMR spectrum and EI-MS. The organometallic remnant was dissolved in CH₃CN and filtered through a frit but no residue was observed. The filtrate was concentrated

to *ca.* 2 mL and diethylether (*ca.* 2 mL) added. Subsequent cooling to -30 °C overnight gave some air-sensitive microcrystalline green crystals of CpCr(PF₆)₂(CH₃CN) (**19**) (29 mg, 0.06 mmol, 65% yield).

(ii) Reaction with triflic acid

To a dark brown solution of CpCr(CO)₂SPy (**16**) (28 mg, 0.10 mmol) in toluene (7 mL) was added conc. HOSO₂CF₃ in large excess (1.0 mL) at 0 °C. The reaction mixture was stirred at 0 °C for 30 min for 18 h at RT. The deep green solution obtained was evacuated to dryness to remove the excess acid and was then extracted with *n*-hexane/toluene (2:1) to remove any organic product, which was characterized as 2-thiopyridine (PySH) (7 mg, 0.06 mmol, 60%) via ¹H NMR spectrum and EI-MS. The organometallic remnant was dissolved in CH₃CN and filtered through a frit but no residue was observed. The filtrate was concentrated to *ca.* 2 mL and diethylether (*ca.* 2 mL) added. Subsequent cooling to -30 °C overnight gave some air-sensitive microcrystalline green crystals of CpCr(OSO₂CF₃)₂(CH₃CN) (**20**) (23 mg, 0.05 mmol, 50% yield).

Data for 19. ¹H NMR shows no peaks in the normal region, indicative of paramagnetism. FAB⁺-MS: *m/z* 407 [M-CH₃CN, C₅H₅CrF₆P]⁺, 145 [PF₆]. Because this class of complexes has been reviewed, we have chosen not to pursue the product and the reaction further.⁷⁹

Data for 20. ¹H NMR shows no peaks in the normal region, indicative of paramagnetism. FAB⁺-MS: *m/z* 415 [M- CH₃CN, C₇H₅CrF₆O₆S₂]⁺, 149 [OSO₂CF₃].

Because this class of complexes has been reviewed, we have chosen not to pursue the product and the reaction further.⁷⁹

3.7.4 Reaction with dicyclopentadienylzirconium dichloride

A reddish-brown mixture of $\text{CpCr}(\text{CO})_2(\text{SPy})$ (**16**) (28 mg, 0.10 mmol) and Cp_2ZrCl_2 (30 mg, 0.10 mmol) in toluene (5 mL) was stirred at ambient temperature for 24 h. The resultant black solution mixture was evacuated to dryness. Extraction by the addition of n-hexane gave a brown fraction. This was diagnosed as unreacted $\text{CpCr}(\text{CO})_2(\text{SPy})$ (**16**) (13 mg, 0.05 mmol, 46 % yield) via its colour characteristics and Cp resonance in benzene- d_6 . ^1H NMR (300MHz, 300 K, C_6D_6): δ 4.44 (s, 5 H, C_5H_5) and its FAB^+ -MS molecular ion peak at m/z 283. The remaining mixture was washed with more n-hexane and then evacuated to dryness. The residue was dissolved in acetonitrile (ca. 2 mL) and additional diethylether (ca. 2 mL) was added. Subsequent standing at -30°C for 2 days gave a mixture of colourless and bluish-green crystals of $[\text{Cp}_2\text{ZrCl}_2]\text{O}$ (**21**) and $\text{CpCrCl}_2(\text{SPyH})$ (**17**). Separation of the mixture was unfruitful, however the bulk ^1H NMR spectrum confirms the presence of **21**.

Data for 21. ^1H NMR (300MHz, 300 K, C_6D_6): δ 6.02 (s, 5 H, C_5H_5). ESI^+ -MS: m/z 783 [M^+ , $\text{C}_{10}\text{H}_{10}\text{Zr}_2\text{Cl}_2\text{O}$]; FAB^+ -MS: m/z 784 [$\text{M}+\text{H}$, $\text{C}_{10}\text{H}_{11}\text{Zr}_2\text{Cl}_2\text{O}$]⁹⁰

Data for 17. ^1H NMR shows no peaks in the normal region, indicative of paramagnetism. IR (KBr, cm^{-1}): $\nu(\text{N-H})$ 3429 sb. $\nu(\text{C-H})$ 3128w, 3074w, 3041w, 3015w. $\nu(\text{other bands})$ 2367w, 2336w, 1583s, 1513m, 1374m, 1260ws, 1158w, 1126s, 1018w, 1007w, 819s, 754s, 485w and 448w. ^1H NMR shows no peaks present indicative of

paramagnetism. FAB⁺-MS: m/z 298 [$\text{M}^+\text{-H}$, $\text{CpCrCl}_2(\text{SPy})$], 263 [$\text{CpCrCl}(\text{SPy})$], 227 [$\text{CpCr}(\text{SPy})$], 195 [$\text{CpCr}(\text{Py})$], 112 [$\text{HSPy}+\text{H}$]. The elementary analysis could not be carried out because of the difficulty in separating the mixtures of crystals. However, we have overcome this problem by simply reacting $\text{CpCr}(\text{CO})_2\text{SPy}$ with HCl (Please refer to section 3.7.1 (ii)).

3.7.5 Crystal structure analyses

Diffraction-quality crystals of $[\text{Cp}_2\text{ZrCl}]_2\text{O}$ (**21**) and $\text{CpCrCl}_2(\text{SPyH})$ (**17**) were obtained as colourless crystals and bluish-green needles from solutions in acetonitrile layered with diethylether after 3 days at $-30\text{ }^\circ\text{C}$.

Chapter 4 References

- 1 (a) Hoff, C. D. *Coord. Chem. Rev.* **2000**, 206-207, 451. (b) Torraca, K. E. *Coord. Chem. Rev.* **2000**, 206-207, 451. (c) Stiegman, A. E.; Tyler, D. R. *Comments Inorg. Chem.* **1986**, 5, 215.
- 2 (a) Tyler, D. R. *Acc. Chem. Res.* **1991**, 24, 325. (b) Tyler, D. R. *J. of Chem. Edu.* **1997**, 74, 668. (c) Meyer, T. J.; Caspar, J. V. *Chem. Rev.* **1985**, 85, 187. (d) Stiegman, A. E.; Tyler, D. R. *Coord. Chem. Rev.* **1985**, 63, 217. (e) Morris, M. J. *Comprehensive Organometallic Chemistry*; Pergamon: New York, **1995**, 7, 402.
- 3 (a) King, R. B.; *Organomet. Synth.* **1965**, 1, 109. (b) Keppie, S. A.; Lappert, M. F. *J. Chem. Soc. A* **1971**, 3216. (c) Hackett, P.; O'Neill, P. S.; Manning, A. R. *J. Chem. Soc. Dalton Trans.* **1974**, 1625. (d) Manning, A. R.; Hackett, P.; Birdwhistell, R.; Soye, P. *Organomet. Synth.* **1990**, 28, 148.
- 4 (a) Baird, M. C. *Chem. Rev.* **1988**, 88, 1217. (b) Tyler, D. R. *Prog. Inorg. Chem.* **1988**, 36, 125.
- 5 Adams, R. D.; Collins, D. E.; Cotton, F. A. *J. Am. Chem. Soc.* **1974**, 96, 749.
- 6 McLain, S. J. *J. Am. Chem. Soc.* **1988**, 110, 643.
- 7 (a) Madach, T.; Vahrenkamp, H. *Z. Naturforsch. B.* **1978**, 33b, 1310. (b) Rieger, P. H. *Coord. Chem. Rev.* **1994**, 135, 203.
- 8 (a) Goh, L. Y.; Lim, Y. Y. *J. Organomet. Chem.* **1991**, 402, 209. (b) Goh, L. Y.; Khoo, S. K.; Lim, Y. Y. *J. Organomet. Chem.* **1990**, 399, 115.
- 9 (a) Halpern, J. *Pure Appl. Chem.* **1986**, 58, 575. (b) Kochi, J. K. *Organometallic Mechanisms and Catalysis*, Academic Press, New York, 1978.

- 10 Gonzalez, A. A.; Hoff, C. D. *Inorg. Chem.* **1989**, *28*, 4295.
- 11 Ju, T. D.; Lang, R. F.; Roper, G. C.; Hoff, C. D. *J. Am. Chem. Soc.* **1996**, *118*, 5328.
- 12 Capps, K. B.; Bauer, A.; Ju, T. D.; Hoff, C. D. *Inorg. Chem.* **1999**, *38*, 6130.
- 13 Ju, T. D.; Capps, K. B.; Lang, R. F.; Roper, G. C.; Hoff, C. D. *Inorg. Chem.* **1997**, *36*, 614.
- 14 Cooley, N. A.; Watson, K. A.; Fortier, S.; Baird, M. C.; *Organometallics* **1986**, *5*, 2563.
- 15 (a) Goh, L. Y.; D'aniello Jr., M. J.; Slater, S; Muetterties, E. L.; Tavanaiepour, I.; Chang, M. I.; Fredrich, M. F.; Day, V. W. *Inorg. Chem.* **1979**, *18*, 192. (b) Cooley, N. A.; MacConnachie, P. T. F.; Baird, M. C. *Polyhedron* **1988**, *7*, 1965. (c) O'Callaghan, K. A. E.; Brown, S. J.; Page, J. A.; Baird, M. C. *Organometallics* **1991**, *10*, 3119.
- 16 Hackett, P.; O'Neill, P. S.; Manning, A. R. *J. Chem. Soc. Dalton Trans.* **1974**, 1625.
- 17 (a) Goh, L. Y. *Coord. Chem. Rev.* **1999**, *185-186*, 257 and references therein. (b) Goh, L. Y.; Chen, W.; Wong, R. C. S.; K. Karaghiosoff. *Organometallics* **1995**, *14*, 3886. (c) Goh, L. Y.; Chen, W.; Wong, R. C. S. *Organometallics* **1999**, *18*, 306. (d) Goh, L. Y.; Chen, W.; Wong, R. C. S. *Chem. Commun.* **1999**, 1481. (e) Sekar, P.; Umbarkar, S.; Scheer, M.; Voigt, A.; Kirmse, R. *Eur. J. Inorg. Chem.* **2000**, 2585.
- 18 (a) Goh, L. Y.; Tay, M. S.; Mak, T. C. W.; Wang, R.-J. *Organometallics* **1992**, *11*, 1711. (b) Goh, L. Y.; Tay, M. S.; Lim, Y. Y.; Mak, T. C. W.; Zhou, Z.-Y. *J. Chem. Soc., Dalton Trans.* **1992**, 1239. (c) Goh, L. Y.; Tay, M. S.; Chen, W. *Organometallics* **1994**, *13*, 1813.
- 19 (a) Goh, L. Y.; Wong, R. C. S.; Sinn, E. *Chem. Comm.* **1990**, 1484. (b) Goh, L. Y.; Wong, R. C. S.; Sinn, E. *Organometallics* **1993**, *12*, 888.

- 20 (a) Goh, L. Y.; Chen, W.; Wong, R. C. S. *Angew. Chem., Int. Ed. Engl.* **1993**, *32*, 1728; (b) Goh, L. Y.; Chen, W.; Wong, R. C. S.; Karaghiosoff, K. *Organometallics* **1995**, *14*, 3886.
- 21 (a) Goh, L. Y.; Leong, W. K.; Leung, P.-H.; Weng, Z.; Haiduc, I. *J. Organomet. Chem.*, **2000**, *607*, 64. (b) Goh, L. Y.; Weng, Z.; Leong, W. K.; Haiduc, I. Lo, K. M.; Wong R. C. S. *J. Organomet. Chem.*, **2001**, *631*, 67.
- 22 Goh, L. Y.; Weng, Z.; Leong, W. K.; Vittal, J. J.; Haiduc, I. *Organometallics* **2002**, *21*, 5287.
- 23 (a) Weng, Z.; Leong, W. K.; Vittal, J. J.; Goh, L. Y. *Organometallics* **2003**, *22*, 1645. (b) Weng, Z.; Leong, W. K.; Vittal, J. J.; Goh, L. Y. *Organometallics* **2003**, *22*, 1657.
- 24 (a) Goh, L. Y.; Weng, Z.; Leong, W. K.; Leung, P. H. *Angew. Chem. Int. Ed.* **2001**, *40*, 3236. (b) Goh, L. Y.; Weng, Z.; Leong, W. K.; Leung, P. H. *Organometallics* **2002**, *21*, 4398. (c) Goh, L. Y.; Weng, Z.; Hor, T. S. Andy; Leong, W. K. *Organometallics* **2002**, *21*, 4408.
- 25 Goh, L. Y.; Weng, Z.; Leong, W. K. Vittal, J. J. *J. Am. Chem. Soc.* **2002**, *124*, 8804.
- 26 Weng, Z.; Goh, L. Y. *Acc. Chem. Res.* **2004**, *37*, 187.
- 27 (a) Ray, P; Gupta, J. *J. Indian Chem. Soc.* **1935**, *12*, 308. (b) Majumdar, A. K. *J. Indian Chem. Soc.* **1942**, *19*, 396. (c) Pnevmticakis, G. A.; Statnis, E. C. *Chem. Ind. (London)* **1963**, 1240.
- 28 (a) Evva, F.; Wiss, Z. *Photogr., Photophys. Photochem.* **1967**, *60*, 145. (b) Nagasawa, M. U.S. Pat. 3268347 (Cl 106-115) Aug. 13, **1966**.
- 29 (a) Emelius, H. J.; Hass, A.; Sheppard, N. *J. Chem. Soc.* **1963**, 3168. (b) Thorn, G. D. *Can. J. Chem.* **1960**, *38*, 1493.

- 30 Mura, P.; Olby, B. G.; Robinson, S. D. *Inorg. Chim. Acta* **1985**, *97*, 45.
- 31 Tannai, H.; Tsuge, K.; Sasaki, Y.; Hatozaki, O.; Oyama, N. *J. Chem. Soc. Dalton Trans.* **2003**, 2353.
- 32 (a) Wilton-Ely, J. D. E. T.; Schier, A.; Schmidbaur, H. *Organometallics* **2001**, *20*, 1895. (b) Wilton-Ely, J. D. E. T.; Schier, A.; Mitzel, N. W.; Schmidbaur, H. *Inorg. Chem.* **2001**, *40*, 6266.
- 33 Castano, M. V.; Plasencia, M. M.; Macias, A.; Casas, J. S.; Sordo, J.; Castellano, E. *J. Chem. Soc. Dalton Trans.* **1989**, 1409.
- 34 Castano, M. V.; Sanches, A.; Casas, J. S.; Sordo, J.; Castellano, E. *Inorg. Chim. Acta* **1992**, *201*, 83.
- 35 Ma, C.; Li, F.; Jiang, Q.; Zhang, R. *J. Organomet. Chem.* **2004**, *689*, 96.
- 36 Gajendragad, M. R.; Agarwala, U. *Aust. J. Chem.* **1975**, *28*, 763.
- 37 Domazetis, G.; Magee, R. J.; James, B. D. *J. Inorg. Nucl. Chem.* **1981**, *43*, 1351.
- 38 (a) Bladin, J. A. *Chem. Ber.* **1885**, *18*, 1544. (b) Yamaguchi, K.; Ohsawa, A.; Kaihoh, T.; Itoh, T. *Acta Cryst.* **1990**, *C46*, 1161.
- 39 Butler, R. N. *Comprehensive Heterocyclic Chemistry*; Pergamon Press, **1984**, *4.13*, p 834.
- 40 (a) Nomiya, K.; Yamamoto, S.; Noguchi, R.; Yokoyama, H.; Kasuga, N. C.; Ohya, K.; Kato, C. *J. Inorg. Biochem.* **2003**, *95*, 208. (b) Nomiya, K.; Noguchi, R.; Ohya, K.; Tsuda, K.; Oda, M. *J. Inorg. Biochem.* **2000**, *78*, 363.
- 41 Brodie, A. M. H. *J. Steroid Biochem. & Mol. Biol.* **1994**, *49*, 281.
- 42 (a) Bhandari, S.; Mahon, M. F.; Molloy, K. C.; Palmer, J. S.; Sayers, S. F. *J. Chem. Soc. Dalton Trans.* **2000**, 1053. (b) Bhandari, S.; Mahon, M. F.; Molloy, K. C. *J. Chem. Soc. Dalton Trans.* **1999**, 1951. (c) Bhandari, S.; Mahon, M. F.; McGinley, J.

- G.; Molloy, K. C.; Roper, C. E. *J. Chem. Soc. Dalton Trans.* **1998**, 3425. (d) Bethel, P. A.; Hill, M. S.; Mahon, M. F.; Molloy, K. C. *J. Chem. Soc. Perkin Trans. I* **1999**, 3507. (e) Hill, M. S.; Mahon, M. F.; Molloy, K. C. *J. Chem. Soc. Dalton Trans.* **1996**, 1857. (f) Goodger, A.; Hill, M.; Mahon, M. F.; McGinley, J. G.; Molloy, K. C. *J. Chem. Soc. Dalton Trans.* **1996**, 847. (g) Hill, M.; Mahon, M. F.; McGinley, J. G.; Molloy, K. C. *J. Chem. Soc. Dalton Trans.* **1996**, 835.
- 43 Alam, M. M.; Watanabe, A.; Ito, O. *Int. J. Chem. Kinet.* **1996**, 28(6), 405.
- 44 Kim, Y.-J.; Han, J.-T.; Kang, S.; Han, W. S.; Lee, S. W. *J. Chem. Soc. Dalton Trans.* **2003**, 3357.
- 45 Banbury, F. A.; Davidson, M. G.; Martin, A.; Raithby, P. R.; Snaith, R.; Verhorevoort, K. L.; Wright, D. S. *J. Chem. Soc. Chem. Commun.* **1992**, 1152.
- 46 Parimal, P.; Kamalaksha, Nag. *Inorg. Chem.* **1987**, 26, 2969.
- 47 Cea-Olivares, R.; Jiménez-Sandoval, O.; Espinosa-Pérez, G.; Silvestru, C. *J. Organomet. Chem.* **1994**, 484, 33.
- 48 Nöth, H.; Beck, W.; Burger, K. *Eur. J. Inorg. Chem.* **1998**, 93.
- 49 (a) Power, A. I. *Coord. Chem. Rev.* **1969**, 4, 463. (b) Butler, R. N. *Adv. Heterocycl. Chem.* **1977**, 21, 323. (c) Palenik, G. J. *Acta Crystallogr.* **1963**, 16, 596.
- 50 Bhandari, S.; Frost, C. G.; Hague, C. E.; Mahon, M. F.; Molloy, K. C. *J. Chem. Soc. Dalton Trans.* **2000**, 663.
- 51 John, E. O.; Willett, R. D.; Scott, B.; Kirchmeier, R. L.; Shreeve, J. M. *Inorg. Chem.* **1989**, 28, 893.
- 52 Zhou, X. G.; Zhang, L. X.; Huang, Z. E.; Cai, R. F.; Huang X. Y. *Synth. & Reactivity in Inorg. and Metal-Org. Chem.* **2000**, 30(5), 965.

- 53 (a) Palazzi, A.; Stagni, S.; Bordoni, S.; Monari, M.; Selva, S. *Organometallics* **2002**, *21*, 3774. (b) Palazzi, A.; Stagni, S.; Selva, S.; Monari, M. *J. Organomet. Chem.* **2003**, *669*, 135.
- 54 (a) Deeth, R. J.; Molloy, K. C.; Mahon, M. F.; Whittaker, S. *J. Organomet. Chem.* **1992**, *430*, 25. (b) Bravo, J.; Cordero, M. B.; Casas, J. S.; Sánchez, A.; Sordo, J.; Castellano, E. E.; Zukerman-Schpector, J. *J. Organomet. Chem.* **1994**, *482*, 147.
- 55 Yélamos, C. Gust, K. R.; Baboul, A. G.; Heeg, M. J.; Schlegel, H. B.; Winter, C. H. *Inorg. Chem.* **2001**, *40*, 6451.
- 56 Cea-Olivares, R.; Jiménez-Sandoval, O.; Espinosa-Pérez, G.; Silvestru, C. *Polyhedron* **1994**, *13(19)*, 2809.
- 57 Bravo, J.; Cordero, M. B.; Casas, J. S.; Castaño, M. V.; Sánchez, A.; Sordo, J. *J. Organomet. Chem.* **1996**, *513*, 63.
- 58 (a) Lieber, E.; Rao, C. N. R.; Pillaj, C. N.; Ramachandran, J.; Hites, R.D. *Can. J. Chem.* **1958**, *36*, 801. (b) Könnecke, R.; Lippmann, E.; Kleinpeter, E. *Z. Chem.* **1975**, *15*, 402. (c) Ellis, B.; Griffith, P. J. *Spectrochim. Acta* **1966**, *22*, 205.
- 59 Yoshihito, O.; Naomi, K.; Kenji, H.; Kiyoshi, Z. *Anal. Sci.* **2000**, *16*, 659.
- 60 Mosca et al. *A Guide to Preventive Cardiology for Woman* **1999**, 1751.
- 61 James, B. D.; Magee, R. J.; Patalinghug W. C.; Skelton, B. W.; White, A. H. *J. Organomet. Chem.* **1994**, *467*, 51.
- 62 Daly, W. H.; Evenson, T. S. *Polymer* **2000**, *41*, 5063.
- 63 Diaz, C.; Spodine, E.; Moreno, Y.; Arancibia, A. *Bol. Soc.Chil. Quim.* **2000**, *45(2)*, 317.
- 64 Moran, D.; Sukcharoenphon, K.; Puchta, R.; Schaefer III, H. F.; Schleyer, P. v. R.; Hoff, C. D. *J. Org. Chem.* **2002**, *67*, 9061.

- 65 Brandenburg, K. L.; Heeg, M. J.; Abrahamson, H. B. *Inorg. Chem.* **1987**, *26*, 1064.
- 66 Deeming, A. J.; Nafees Meah, M. N.; Dawes, H. M.; Hursthouse, M. B. *J. Organomet. Chem.* **1986**, *299*, C25.
- 67 Ciriano, M. A.; Viguri, F.; Pérez-Torrentz, J. J.; Lahoz, F. J.; Oro, L. A.; Tiripicchio, A.; Tiripicchio Camellini, M. *J. Chem. Soc. Dalton Trans.* **1989**, 25.
- 68 Yamamoto, J. H.; Yoshida, W.; Jensen, C. *Inorg. Chem.* **1991**, *31*, 1353.
- 69 Yu, P.; Hiang, L.; Zhuang, B. *Acta Crystallogr.* **1994**, *C50*, 1191.
- 70 Ciriano, M. A.; Pérez-Torrentz, J. J.; Viguri, F.; Lahoz, F. J.; Oro, L. A.; Tiripicchio, A.; Tiripicchio Camellini, M. *J. Chem. Soc. Dalton Trans.* **1990**, 1493.
- 71 Deeming, A. J.; Hardcastle, K. I.; Karim, M. *Inorg. Chem.* **1992**, *31*, 4792.
- 72 Lu, X. L.; Vittal, J. J.; Tiekink, E. R. T.; Goh, L. Y.; Hor, T. S. A. *J. Organomet. Chem.* **2004**, ASAP Article.
- 73 Weinmann, D. J.; Abrahamson, H. B. *Inorg. Chem.* **1987**, *26*, 3034.
- 74 (a) Deeming, A. J.; Vaish, R. *J. Organomet. Chem.* **1993**, *460*, C8. (b) Hardcastle, K. I.; Cockerton, B. R.; Deeming, A. J.; Karim, M. *J. Chem. Soc. Dalton Trans.* **1992**, 1607.
- 75 (a) Rejoan, A.; Cais, M. *Prog. Coord. Chem.* **1968**, 32. (b) Miyake, A.; Kondo, H. *Angew. Chem.* **1968**, *80*, 663; *Angew. Chem., Int. Ed. Engl.* **1968**, *7*, 631. (c) Wrighton, M. S.; Schroeder, M. A. *J. Am. Chem. Soc.* **1973**, *95*, 5764. (d) Pustarnakova, G. F.; Solianikov, V. M.; Denisov, E. T. *Izv. Akad. Nauk. SSSR, Ser. Khim.* **1975**, 547.
- 76 Parshall, G. W. *Homogeneous Catalysis*; Wiley: New York, **1980**; p 49.
- 77 Theopold, K. H. *Acc. Chem. Res.* **1990**, *23*, 263.

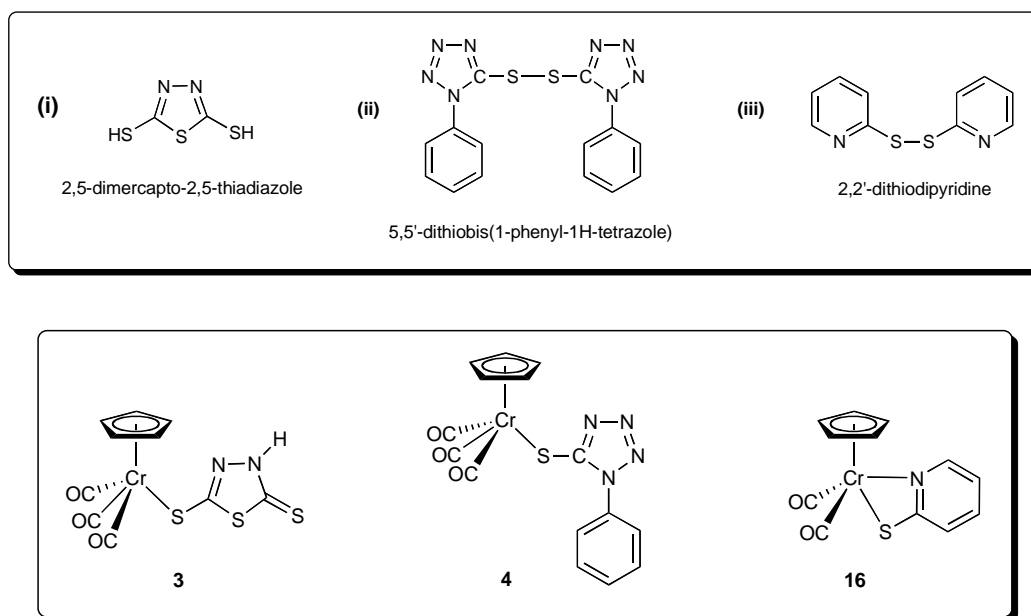
- 78 (a) Richeson, D. S.; Mitchell, J. F.; Theopold, K. H. *J. Am. Chem. Soc.* **1987**, *109*, 5868. (b) Richeson, D. S.; Mitchell, J. F.; Theopold, K. H. *Organometallics* **1989**, *8*, 2570.
- 79 (a) Köhler, F. H.; Lachmann, J.; Müller, G.; Zeh, H.; Brunner, H.; Pfauntsch, J.; Wachter, J. *J. Organomet. Chem.* **1989**, *365*, C15. (b) Bräunlein, B.; Köhler, F. H.; Strauß, W.; Zeh, H. *Z. Naturforsch.* **1995**, *50b*, 1739.
- 80 (a) Rojas, R.; Valderrama, M.; Garland, M. T. *J. Organomet. Chem.* **2004**, *689*, 293. (b) Gallant, A. J.; Smith, K. M.; Patrick, B. O. *J. Chem. Soc. Chem. Commun.* **2002**, 2914. (c) Danopoulos, A. A.; Wilkinson, G.; Sweet, T. K. N.; Hursthouse, M. B. *J. Chem. Soc. Dalton Trans.* **1996**, 271.
- 81 Sukcharoenphon, K.; Ju, T. D.; Abboud, K. A.; Hoff, C. D. *Inorg. Chem.* **2002**, *41*, 6769.
- 82 Pauling, L. *The Nature of the Chemical Bond*; Ithaca, New York, **1960**.
- 83 Filippou, A. C.; Lungwitz, B. G.; Wanniger, K. M. A.; Herdtweck, E. *Angew. Chem. Int. Ed. Engl.* **1995**, *34*, 924.
- 84 (a) Bombieri, G.; Immirzi, A.; Toniolo, L. *Inorg. Chem.* **1976**, *15*, 2428. (b) Immirzi, A.; Bombieri, G.; Toniolo, L. *J. Organomet. Chem.* **1976**, *118*, 355. (c) Bombieri, G.; Immirzi, A.; Toniolo, L. *Transition Met. Chem.* **1976**, *1*, 130. (d) Brown, L. D.; Ibers, J. A. *Inorg. Chem.* **1976**, *11*, 2794.
- 85 Kuan, S. L.; Goh, L. Y. Unpublished work.
- 86 Nefedov, S. E.; Pasynskii, A. A.; Eremenko, I. L.; Orazsakhmatov, B.; Ellert, O. G.; Novotortsev, V. M. *J. Organomet. Chem.* **1990**, *385*, 277.
- 87 Goh, L. Y.; Hambley, T. W. *J. Organomet. Chem.* **1990**, *395*, 269.
- 88 Hossain, M. M.; Lin, H.-M.; Shyu, S.-G. *Eur. J. Inorg. Chem.* **2001**, 2655.

- 89 Catheline, D.; Román, E.; Astruc, D. *Inorg. Chem.* **1984**, *23*, 4508.
- 90 Shi, Y.; Cheng, G.; Lu, S.; Guo, H.; Wu, Q.; Huang, X.; Hu, N. *J. Organomet. Chem.* **1993**, *455*, 115.
- 91 Reid, A. F.; Shannon, J. S.; Swan, J. M.; Wailes, P. C. *Aust. J. Chem.* **1965**, *18*, 173.
- 92 Poli, R. *J. Organomet. Chem.* **2004**, ASAP Article. (*New addition made after the first submission of thesis*)

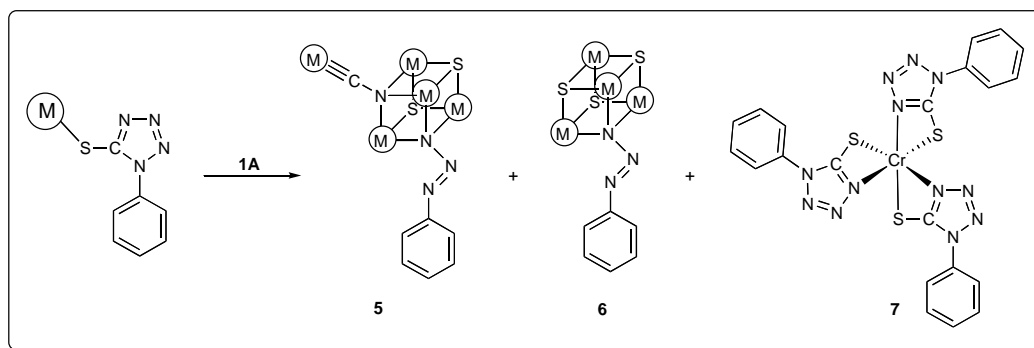
Chapter 5 Conclusion

5.1 Conclusion

The 17-electron organometallic radical $\{\text{CpCr}(\text{CO})_3\}$ (**1A**) has demonstrated a remarkable ability in the scission of a variety of non-metal–non-metal and chromium–non-metal bonds. Cleavage of S–H, S–S, C–S, C–N, N–N and Cr–S bonds in organic substrates and in cyclopentadienyl chromium complexes, accompanied by rearrangement and aggregation, has generated a variety of organometallics compounds. Thus cleavage of the S–H and S–S bonds in 2,5-dimercapto-1,3,4-thiadiazole (DMcTH₂), 5,5'-dithiobis(1-phenyl-1H-tetrazole) (STz)₂, (C₆H₅N₄CS)₂ and 2,2'-dithiodipyridine, (SPy)₂ gave complexes containing thiolate ligands shown in structures **3**, **4** and **16** respectively.



Some structurally interesting complexes such as the aminocarbonyne-cubane complex $\text{Cp}_4\text{Cr}_4\text{S}_3(\text{N}_3\text{Ph})(\text{CpCr}(\text{CO})_2\text{CN})$ (**5**), the triazenido-cubane complex $\text{Cp}_4\text{Cr}_4\text{S}_3(\text{N}_3\text{Ph})$ (**6**) and the coordination complex $\text{Cr}(\text{SCN}_4\text{Ph})_3$ (**7**) have been isolated from the ring opening of ligated 5-mercapto(1-phenyl-1H-tetrazole) ligand.



The reactivity of **4** and **16** towards various substrates, such as methylating agents, haloacids, and oxidizing agents, display some unexpectedly interesting results, e.g. the formation of the first cationic mercaptotetrazole binuclear and trinuclear complexes **8** and **9** with methylating agents and complex **17** from reaction with haloacids. These reactions give an insight on the thio-, oxo- and “halo”-philicity of the cyclopentadienylchromium species.

The reaction of $[\text{CpFe}(\text{CO})_2]_2$ (**2**) with $(\text{STz})_2$ yields the mercapto(1-phenyl-1H-tetrazole) complex $\text{CpFe}(\text{CO})_2(\eta^1\text{-STz})$ (**15**), a close analogue of **4**. Such monodentate thiolate complexes should, in principle, exhibit high reactivity behaviour. However, due to time constraints, this part of the investigation was not carried out.

These findings may have important inference for the investigations of the reactivity of related chromium and other transition metal complexes.

Appendix 1. Data collection and processing parameters.

complexes	3	4	5	8
formula	C ₁₀ H ₆ CrN ₂ O ₃ S ₃	C ₁₅ H ₁₀ CrN ₄ O ₃ S	C ₃₅ H ₃₀ Cr ₅ N ₃ O ₂ S ₂	C ₂₆ H ₂₄ BCr ₂ F ₄ N ₉ OS ₂
<i>M_r</i>	350.35	378.33	848.74	733.49
temp, K	223(2)	223(2)	223(2)	223(2)
cryst size, mm	0.20 × 0.12 × 0.08	0.30 × 0.24 × 0.10	0.30 × 0.18 × 0.16	0.38 × 0.38 × 0.10
cryst system	Triclinic	Triclinic	Monoclinic	Triclinic
space group	P1	P1	P2 ₁ /n	P-1
<i>a</i> , Å	10.131(3)	6.6121(3)	9.7392(8)	9.4536(14)
<i>b</i> , Å	11.514(3)	11.3626(5)	20.3415(16)	10.9489(17)
<i>c</i> , Å	13.555(3)	12.2539(5)	16.9235(13)	16.161(3)
<i>α</i> , deg	90.587(8)	110.150(2)	90	82.378(3)
<i>β</i> , deg	104.534(6)	104.495(2)	96.921(2)	84.912(3)
<i>γ</i> , deg	115.999(6)	101.065(2)	90	77.518(3)
<i>V</i> , Å ³	1362.5(6)	796.64(6)	3328.3(5)	1615.7(4)
<i>Z</i>	4	2	4	2
density, Mg m ⁻³	1.708	1.577	1.694	1.508
abs. coeff, mm ⁻¹	1.301	0.870	1.744	0.862
<i>F</i> (000)	704	384	1716	744
<i>θ</i> range for data collection	1.57 to 25.00	1.88 to 30.08	1.57 to 28.74	1.92 to 27.50
index ranges	-12 ≤ <i>h</i> ≤ 11, -10 ≤ <i>k</i> ≤ 13, -16 ≤ <i>l</i> ≤ 16	-9 ≤ <i>h</i> ≤ 8, -15 ≤ <i>k</i> ≤ 16, -17 ≤ <i>l</i> ≤ 17	-11 ≤ <i>h</i> ≤ 13, -27 ≤ <i>k</i> ≤ 25, -21 ≤ <i>l</i> ≤ 17	-12 ≤ <i>h</i> ≤ 12, -14 ≤ <i>k</i> ≤ 14, -20 ≤ <i>l</i> ≤ 20
no. of reflns collected	7934	6773	21123	20040
indep reflns	4783	4576	7881	7288
max. and min. transmission	0.9031 and 0.7809	0.8959 and 0.7199	0.8040 and 0.6941	0.9188 and 0.7355
no. of data/restraints/params	4783 / 2 / 351	4576 / 0 / 257	7881 / 0 / 424	7288 / 0 / 411
final <i>R</i> indices [<i>I</i> > 2σ(<i>I</i>)] ^{a, b}	R1 = 0.0443, wR2 = 0.1135	R1 = 0.0501, wR2 = 0.1059	R1 = 0.0577, wR2 = 0.0998	R1 = 0.0701, wR2 = 0.1474
<i>R</i> indices (all data)	R1 = 0.1256, wR2 = 0.1313	R1 = 0.0677, wR2 = 0.1137	R1 = 0.1006, wR2 = 0.1103	R1 = 0.0947, wR2 = 0.1572
goodness-of-fit on <i>F</i> ^{2 c}	0.945	0.989	1.012	1.133
large diff peak and hole, e ⁻³	0.567 and -0.439	0.511 and -0.310	0.649 and -0.330	1.001 and -0.475

$$^a R = (\sum |F_o| - |F_c|) / \sum |F_o| \quad ^b wR2 = [(\sum \omega |F_o| - |F_c|)^2 / \sum \omega |F_o|^2]^{1/2} \quad ^c \text{GoF} = [(\sum \omega |F_o| - |F_c|)^2 / (N_{\text{obs}} - N_{\text{param}})]^{1/2}$$

Appendix 1. (continued)

complexes	9	13	15	16
formula	C ₂₉ H ₂₆ Cr ₃ N ₈ O ₂ S ₂ . {CH ₃ SO ₄ }.2.85{CH ₃ CN}	C ₇ H ₈ CrI ₂ N	C ₁₄ H ₁₀ FeN ₄ O ₂ S	C ₁₂ H ₉ CrNO ₂ S
<i>M_r</i>	966.80	411.94	354.17	283.28
temp, K	223(2)	223(2)	223(2)	223(2)
cryst size, mm	0.30 × 0.28 × 0.14	0.46 × 0.36 × 0.12	0.50 × 0.10 × 0.10	0.36 × 0.24 × 0.18
cryst system	Triclinic	Orthorhombic	Monoclinic	Monoclinic
space group	P-1	Pnma	P2 ₁ /c	P2 ₁ /c
<i>a</i> , Å	11.634(2)	8.5634(13)	6.8300(5)	12.7123(4)
<i>b</i> , Å	13.358(2)	9.9415(15)	7.2529(6)	7.4752(2)
<i>c</i> , Å	15.740(3)	13.102(2)	29.221(2)	12.6061(4)
<i>α</i> , deg	109.677(3)	90	90	90
<i>β</i> , deg	109.671(3)	90	95.627(10)	100.4610(10)
<i>γ</i> , deg	92.603(3)	90	90	90
<i>V</i> , Å ³	2133.7(6)	1115.40(3)	1440.56(19)	1178.01(6)
<i>Z</i>	2	4	4	4
density, Mg m ⁻³	1.505	2.453	1.633	1.597
abs. coeff, mm ⁻¹	0.954	0.651	1.203	1.134
<i>F</i> (000)	991	748	720	576
<i>θ</i> range for data collection	1.48 to 27.50	2.57 to 27.48	1.40 to 27.49	3.18 to 28.28
index ranges	-15 ≤ <i>h</i> ≤ 15, -17 ≤ <i>k</i> ≤ 17, -20 ≤ <i>l</i> ≤ 20	-11 ≤ <i>h</i> ≤ 10, -12 ≤ <i>k</i> ≤ 11, 0 ≤ <i>l</i> ≤ 22	-8 ≤ <i>h</i> ≤ 8, -7 ≤ <i>k</i> ≤ 9, -37 ≤ <i>l</i> ≤ 37	-16 ≤ <i>h</i> ≤ 16, 0 ≤ <i>k</i> ≤ 9, 0 ≤ <i>l</i> ≤ 16
no. of reflns collected	27766	7320	9495	19518
indep reflns	9757	1337	3268	2868
max. and min. transmission	0.8780 and 0.7628	0.5090 and 0.1538	0.8892 and 0.5845	0.8219 and 0.6856
no. of data/restraints/params	9757 / 4 / 540	1337 / 0 / 60	3268 / 0 / 199	2868 / 0 / 190
final <i>R</i> indices [<i>I</i> > 2σ(<i>I</i>)] ^{a, b}	<i>R</i> 1 = 0.0543, w <i>R</i> 2 = 0.1445	<i>R</i> 1 = 0.0244, w <i>R</i> 2 = 0.0579	<i>R</i> 1 = 0.0422, w <i>R</i> 2 = 0.1017	<i>R</i> 1 = 0.0443, w <i>R</i> 2 = 0.1091
<i>R</i> indices (all data)	<i>R</i> 1 = 0.0707, w <i>R</i> 2 = 0.1538	<i>R</i> 1 = 0.0264, w <i>R</i> 2 = 0.0590	<i>R</i> 1 = 0.0472, w <i>R</i> 2 = 0.1051	<i>R</i> 1 = 0.0518, w <i>R</i> 2 = 0.1138
goodness-of-fit on <i>F</i> ^{2 c}	1.061	1.104	1.136	1.065
large diff peak and hole, e Å ⁻³	0.723 and -0.540	0.650 and -0.855	0.846 and -0.348	0.775 and -0.224

$$^a R = (\sum |F_o| - |F_c|) / \sum |F_o|. \quad ^b wR2 = [(\sum w|F_o| - |F_c|)^2 / \sum w|F_o|^2]^{1/2}. \quad ^c GoF = [(\sum w|F_o| - |F_c|)^2 / (N_{obs} - N_{param})]^{1/2}$$

Appendix 1. (continued)

complexes	17	21
formula	C ₁₀ H ₁₀ Cl ₂ CrNS	C ₂₀ H ₂₀ Zr ₂ Cl ₂ O
<i>M_r</i>	299.15	529.70
temp, K	243(2)	243(2)
cryst size, mm	0.40 × 0.12 × 0.02	0.38 × 0.16 × 0.10
cryst system	Monoclinic	Trigonal
space group	P2 ₁ /c	P3(1)
<i>a</i> , Å	8.3745(6)	7.8804(3)
<i>b</i> , Å	6.6935(5)	7.8804(3)
<i>c</i> , Å	21.7625(17)	27.8842(16)
<i>α</i> , deg	90	90
<i>β</i> , deg	99.440(2)	90
<i>γ</i> , deg	90	120
<i>V</i> , Å ³	1203.37(16)	1499.63(12)
<i>Z</i>	4	3
density, Mg m ⁻³	1.651	1.760
abs. coeff, mm ⁻¹	1.532	1.315
<i>F</i> (000)	604	786
<i>θ</i> range for data collection	1.90 to 27.49	2.19 to 27.50
index ranges	-10 ≤ <i>h</i> ≤ 10, -8 ≤ <i>k</i> ≤ 8, -21 ≤ <i>l</i> ≤ 28	-10 ≤ <i>h</i> ≤ 9, -6 ≤ <i>k</i> ≤ 10, -36 ≤ <i>l</i> ≤ 31
no. of reflns collected	8101	10409
indep reflns	2755	4408
max. and min. transmission	0.9700 and 0.5793	0.8798 and 0.6350
no. of data/restraints/params	2755 / 0 / 176	4408 / 1 / 226
final <i>R</i> indices [<i>I</i> > 2σ(<i>I</i>)] ^{a, b}	R1 = 0.0324, wR2 = 0.0729	R1 = 0.0269, wR2 = 0.0627
<i>R</i> indices (all data)	R1 = 0.0400, wR2 = 0.0760	R1 = 0.0286, wR2 = 0.0633
goodness-of-fit on F ² ^c	1.067	1.069
large diff peak and hole, e Å ⁻³	0.420 and -0.232	0.400 and -0.263

$$^a R = (\sum |F_o| - |F_c|) / \sum |F_o|, \quad ^b wR2 = [(\sum w|F_o| - |F_c|)^2 / \sum w|F_o|^2]^{1/2}, \quad ^c \text{GoF} = [(\sum w|F_o| - |F_c|)^2 / (N_{\text{obs}} - N_{\text{param}})]^{1/2}$$